

# Important Notice

This copy may be used only for the purposes of research and private study, and any use of the copy for a purpose other than research or private study may require the authorization of the copyright owner of the work in question. Responsibility regarding questions of copyright that may arise in the use of this copy is assumed by the recipient.

THE UNIVERSITY OF CALGARY

**SEISMIC IMAGING OF A NON-EMERGENT THRUST FRONT  
IN THE FALLEN TIMBER CREEK AREA,  
SOUTHERN ALBERTA FOOTHILLS**

by

Chakrit Sukaramongkol

A THESIS

SUBMITTED TO THE FACULTY OF GRADUATE STUDIES  
IN PARTIAL FULFILLMENT OF THE REQUIREMENTS FOR THE  
DEGREE OF MASTER OF SCIENCE

DEPARTMENT OF GEOLOGY AND GEOPHYSICS

CALGARY, ALBERTA

JULY, 1993

© Chakrit Sukaramongkol 1993

THE UNIVERSITY OF CALGARY  
FACULTY OF GRADUATE STUDIES

The undersigned certify that they have read, and recommend to the Faculty of Graduate Studies for acceptance, a thesis entitled "Seismic Imaging of a Non-Emergent Thrust Front in the Fallen Timber Creek Area, Southern Alberta Foothills" submitted by Chakrit Sukaramongkol in partial fulfillment of the requirements for the degree of Master of Science.



---

Supervisor, Dr. D. C. Lawton,  
Department of Geology and Geophysics



---

Dr. R. J. Brown,  
Department of Geology and Geophysics



---

Dr. D. A. Spratt  
Department of Geology and Geophysics



---

Dr. S. E. Franklin  
Department of Geography

June 25, 1993

## **ABSTRACT**

Reflection seismic data, acquired across the leading edge of the Alberta Foothills in the Fallen Timber Creek region, have been processed and interpreted to show geometries of frontal structures in the Triangle Zone. The Triangle Zone comprises an antiformal stack of Upper Cretaceous rocks that has been advanced into the foreland basin between upper and lower detachments. A pop-up structure located east of the current antiformal stack indicates the presence of layer-parallel shortening in this region and is interpreted to represent an early stage of the development of a new antiformal stack.

Seismic modelling shows that later undulating events in the seismic sections is attributed to lateral velocity variations within the Triangle Zone. Further modelling analyses indicate that far offsets can be detrimental in stacking. Therefore, the key to optimally image the Triangle Zone is to use small offsets with small shot intervals in data acquisition.

## **Acknowledgements**

I would like to express my sincere appreciation to Dr. D. C. Lawton, my academic advisor, who introduced me to the Geophysics discipline and provided great inspiration. I will never forget the support, guidance and invaluable suggestions he provided throughout this study. I wish to thank Petrel Robertson Ltd., Calgary for donating reflection seismic data to this project and Eric Gallant of the CREWES Project for his assistance in building the physical model. Also I would like to thank the staff of the CREWES project for their technical support during my work.

I benefited greatly from discussions with many people in the Department of Geology and Geophysics, particularly Gregory S. Soule, Kelly Hrabí, Donald Easley, Gerardo Quiroga-Goode, Taiwan Chen, Zandong Sun, Ye Zheng and Dr. D. A. Spratt. Special thanks also go to Gregory S. Soule for providing me with a surface geology map in the study area and for sharing his curiosity and knowledge of the Triangle Zone. I thank Armin Schafer for his assistance in running the P-SV binning program and Mark Lane for editing an early version of Chapter 3 (Seismic Data Processing) in this thesis.

I would like to acknowledge the following people who extended their generosity to me during my stay in Canada: Keith Edwards for comfortable accommodation during my first few months in Calgary as well as for his assistance in generating synthetic seismograms used in this thesis; Jim and Bev Cowley for the Canadian-style Thai Foods and for my first experience in skiing; and lastly Gerd Eichele for sharing the memory about Thailand in "Thai Sa-On" with me.

This study was financially supported by the Canadian International Development Agency (CIDA).

## Table of Contents

|   |     |
|---|-----|
| Approval Page .....   | ii  |
| Abstract .....  | iii |
| Acknowledgements .....  | iv  |
| Table of Contents .....                                       | v   |
| List of Tables .....  | ix  |
| List of Figures .....   | x   |
| Chapter 1 - INTRODUCTION .....                                | 1   |
| 1.1 Triangle Zones .....                                      | 1   |
| 1.2 Converted Waves (P-SV).....                               | 9   |
| 1.3 Objectives and Structure of the Thesis .....              | 10  |
| 1.4 Geophysical and Geological Data used in this Thesis ..... | 11  |
| 1.4.1 Conventional Seismic data .....                         | 11  |
| 1.4.2 Synthetic Seismic Data .....                            | 12  |
| 1.4.3 Well-Log Data.....                                      | 12  |
| 1.4.4 Surface Geology.....                                    | 12  |
| 1.5 Software used in this Research .....                      | 12  |
| Chapter 2 - GEOLOGY .....                                     | 14  |
| 2.1 Study Area.....   | 14  |
| 2.2 Stratigraphy .....  | 15  |
| 2.2.1 Cambrian .....  | 15  |
| 2.2.2 Devonian .....  | 15  |
| 2.2.3 Mississippian.....                                      | 17  |
| 2.2.4 Jurassic .....  | 17  |
| 2.2.5 Cretaceous .....  | 17  |

|  |    |
|--|----|
| 2.2.5.1 Blairmore Group .....                                  | 17 |
| 2.2.5.2 Blackstone Formation .....                             | 18 |
| 2.2.5.3 Cardium Formation .....                                | 18 |
| 2.2.5.4 Wapiabi Formation .....                                | 19 |
| 2.2.5.5 Brazeau Formation .....                                | 19 |
| 2.2.6 Tertiary .....   | 19 |
| 2.3 Surface Geology .....                                      | 20 |
| Chapter 3 - SEISMIC DATA PROCESSING .....                      | 23 |
| 3.1 Introduction .....   | 23 |
| 3.2 Seismic Reflection Data .....                              | 23 |
| 3.3 Preprocessing .....  | 24 |
| 3.3.1 Demultiplexing and Preliminary Editing .....             | 24 |
| 3.3.2 Geometry .....   | 27 |
| 3.4 Prestack Processing .....                                  | 27 |
| 3.4.1 Refraction Statics and Datum Elevation Corrections ..... | 27 |
| 3.4.2 First-Break Muting .....                                 | 29 |
| 3.4.3 Band-Pass and Notch Filtering .....                      | 30 |
| 3.4.4 Predictive (Gapped) Deconvolution .....                  | 30 |
| 3.4.5 Gain .....   | 32 |
| 3.4.6 Data Sorting .....                                       | 34 |
| 3.4.7 Velocity Analysis .....                                  | 35 |
| 3.4.8 Normal-Moveout (NMO) Correction .....                    | 35 |
| 3.4.9 Surface-Consistent Residual Statics Corrections .....    | 36 |
| 3.4.10 Dip-Moveout (DMO) Correction .....                      | 38 |
| 3.4.11 Stacking .....  | 41 |
| 3.5 Poststack Processing .....                                 | 44 |
| 3.5.1 Migration .....  | 44 |

|   |     |
|---|-----|
| 3.5.1.1 Finite-Difference Migration .....                             | 44  |
| 3.5.1.2 Phase-Shift Migration .....                                   | 45  |
| 3.5.1.3 Stolt ( <i>f-k</i> ) Migration .....                          | 46  |
| 3.5.2 Coherency Filter .....  | 47  |
| 3.5.3 Offset-Limited Stack .....                                      | 47  |
| Chapter 4 - SEISMIC INTERPRETATION .....                              | 57  |
| 4.1 Introduction .....  | 57  |
| 4.2 Seismic Correlation and Interpretation .....                      | 57  |
| 4.2.1 The Upper and Lower Detachments .....                           | 67  |
| 4.2.2 Antiformal Stack .....  | 68  |
| 4.2.3 Pop-Up Structure .....  | 68  |
| 4.2.4 Evolution of the Pop-Up Structure .....                         | 71  |
| 4.2.5 Rock Sequences Overlying and Underlying the Triangle Zone ..... | 76  |
| 4.3 An Alternative Interpretation of the Triangle Zone Geometry ..... | 78  |
| 4.4 Cross-Section Balancing .....                                     | 78  |
| 4.5 Discussion .....  | 83  |
| Chapter 5 - SEISMIC MODELLING .....                                   | 86  |
| 5.1 Introduction .....  | 86  |
| 5.2 Numerical Seismic Modelling .....                                 | 87  |
| 5.2.1 Background .....  | 87  |
| 5.2.2 Model Construction and Physical Parameters .....                | 88  |
| 5.2.3 Normal-Incidence Ray Tracing .....                              | 91  |
| 5.2.4 Discussion .....  | 94  |
| 5.2.5 Offset Ray Tracing .....  | 98  |
| 5.2.5.1 P-P Modelling .....   | 99  |
| 5.2.5.1.1 Dip-Moveout (DMO) Correction .....                          | 106 |
| 5.2.5.1.2 Offset-Limited Stack .....                                  | 108 |

|   |     |
|---|-----|
| 5.2.5.2 Discussion .....                          | 111 |
| 5.2.5.3 P-SV Modelling .....                      | 113 |
| 5.2.5.4 Discussion .....                          | 118 |
| 5.3 Physical Seismic Modelling .....              | 121 |
| 5.3.1 Background .....                            | 121 |
| 5.3.2 Model Construction and Data Collection..... | 122 |
| 5.3.3 Results and Discussion.....                 | 124 |
| Chapter 6 - CONCLUSIONS AND RECOMMENDATIONS ..... | 131 |
| References .....                                  | 135 |

## **List of Tables**

|   |    |
|---|----|
| Table 2.1. Table of Formations in the Foothills and Front ranges, west of Calgary ..... | 15 |
| Table 3.1. Field Acquisition Parameters .....   | 24 |
| Table 5.1. Physical parameters of the numerical model shown in Figure 5.1 .....         | 88 |

## List of Figures

|  |    |
|--|----|
| FIG. 1.1. Generalized structural geometry of the Triangle Zone .....   | 2  |
| FIG. 1.2. Schematic cross-section of the Triangle Zone near Edson .....  | 5  |
| FIG. 1.3. Triangle Zone evolution according to Jones (1982) .....  | 6  |
| FIG. 1.4. Triangle Zone evolution according to Charlesworth et al. (1985, 1987) .....  | 8  |
| FIG. 1.5. Reflection and transmission at an interface .....  | 9  |
| FIG. 2.1. Fallen Timber Creek location map .....   | 13 |
| FIG. 2.2. A portion of a NE-SW cross-section from the Fallen Timber Creek region ....  | 19 |
| FIG. 2.3. Surface geology, wells and seismic location map .....  | 21 |
| FIG. 3.1. Processing flow for seismic lines 2A and 2B .....  | 25 |
| FIG. 3.2. Examples of shot gathers of line 2B .....  | 27 |
| FIG. 3.3. An amplitude-frequency spectrum plot of a seismic trace from line 2B .....   | 30 |
| FIG. 3.4. CMP reflections from flat and dipping reflectors .....   | 37 |
| FIG. 3.5. DMO processing flow .....  | 39 |
| FIG. 3.6. Stacked section of line 2B .....   | 40 |
| FIG. 3.7. DMO-corrected stacked section of line 2B .....   | 41 |
| FIG. 3.8. F-D migrated section of the DMO-corrected stack of line 2B .....   | 46 |
| FIG. 3.9. Phase-shift migrated section of the DMO-corrected stack of line 2B .....   | 47 |
| FIG. 3.10. Stolt ( $f-k$ ) migrated section of the DMO-corrected stack of line 2B .....  | 48 |
| FIG. 3.11. Final ( $f-k$ ) migrated stack of line 2A .....   | 49 |
| FIG. 3.12. Final ( $f-k$ ) migrated stack of line 3 .....  | 50 |
| FIG. 3.13. Stolt ( $f-k$ ) migrated section of the offset limited stack using traces<br>within an offset -1500 to 1500 m ..... | 52 |
| FIG. 3.14. Stolt ( $f-k$ ) migrated section of the offset limited stack using traces<br>within an offset -2000 to 2000 m ..... | 53 |
| FIG. 3.15. Stolt ( $f-k$ ) migrated section of the offset limited stack using traces   |    |

|  |    |
|--|----|
| within an offset -2500 to 2500 m .....   | 54 |
| FIG. 4.1. Correlation between synthetic seismogram, sonic log and a portion<br>of seismic line 2B at well 16-6-32-5W5 .....  | 56 |
| FIG. 4.2. Correlation between synthetic seismogram, sonic log and a portion<br>of seismic line 2B at well 10-25-31-6W5 ..... | 57 |
| FIG. 4.3. Correlation between synthetic seismogram, sonic log and a portion<br>of seismic line 2B at well 5-14-31-6W5 .....  | 58 |
| FIG. 4.4. Correlation between synthetic seismogram, sonic log and a portion<br>of seismic line 2B at well 11-30-30-5W5 ..... | 59 |
| FIG. 4.5. Correlation between synthetic seismogram, sonic log and a portion<br>of seismic line 2B at well 6-4-31-5W5 .....   | 60 |
| FIG. 4.6. Interpretation of seismic line 2B .....  | 62 |
| FIG. 4.7. Interpretation of seismic line 2A .....  | 63 |
| FIG. 4.8. Interpretation of seismic line 3 .....   | 64 |
| FIG. 4.9. Close-up view of the antiformal stack .....  | 67 |
| FIG. 4.10. Close-up view of the pop-up structure .....   | 68 |
| FIG. 4.11. Time-structural contour maps of the frontal ramp and the back thrust .....  | 70 |
| FIG.4.12. Schematic model of the pop-up evolution .....  | 72 |
| FIG. 4.13. An alternative model of the pop-up evolution .....  | 72 |
| FIG. 4.14. Schematic model of the evolution of the pop-up structure<br>in the study area .....                               | 73 |
| FIG. 4.15. Rock sequences above the upper detachment and below the<br>antiformal stack and pop-up structure .....            | 75 |
| FIG. 4.16. An alternative interpretation of seismic line 2B .....  | 77 |
| FIG. 4.17. A deformed section and palinspastic reconstruction of the Triangle Zone<br>and the pop-up structure .....         | 79 |
| FIG. 4.18. A deformed section and palinspastic reconstruction of the alternative   |    |

|  |     |
|--|-----|
| interpretation of the Triangle Zone and pop-up structure .....                                     | 80  |
| FIG. 5.1. A schematic numerical model of the Triangle Zone .....                                   | 87  |
| FIG. 5.2. Synthetic zero-offset section .....  | 91  |
| FIG. 5.3. Stolt ( $f-k$ ) migrated section of the synthetic zero-offset section .....              | 93  |
| FIG. 5.4. Phase-shift migrated section of the synthetic zero-offset section .....                  | 94  |
| FIG. 5.5. F-D migrated section of the synthetic zero-offset section .....                          | 95  |
| FIG. 5.6. Synthetic P-P shot gathers .....   | 98  |
| FIG. 5.7. Processing flow for the synthetic P-P data .....   | 99  |
| FIG. 5.8. Synthetic P-P stacked section .....  | 100 |
| FIG. 5.9. Stolt ( $f-k$ ) migrated section of the full-offset stacked section .....                | 102 |
| FIG. 5.10. Phase-shift migrated section of the full-offset stack .....                             | 103 |
| FIG. 5.11. DMO-corrected, phase-shift migrated section .....                                       | 105 |
| FIG. 5.12. Offset-limited, stacked section .....   | 107 |
| FIG. 5.13. Migrated section of the offset-limited stack .....                                      | 108 |
| FIG. 5.14. Synthetic P-SV shot gathers .....   | 112 |
| FIG. 5.15. Processing flowchart for synthetic P-SV data .....                                      | 113 |
| FIG. 5.16. P and SV particle-motion directions .....   | 113 |
| FIG. 5.17. P-SV raypath geometry .....   | 114 |
| FIG. 5.18. Synthetic P-SV stacked section .....  | 116 |
| FIG. 5.19. Phase-shift migrated section of the P-SV stack .....                                    | 117 |
| FIG. 5.20. A cross-section of a thrust fault model and material parameters .....                   | 120 |
| FIG. 5.21. A zero-offset physical-modelling record from the thrust-fault model .....               | 122 |
| FIG. 5.22. The same record as in Figure 5.21 after predictive deconvolution,<br>AGC and mute ..... | 123 |
| FIG. 5.23. A zero-offset numerical-modelling record from the thrust fault model .....              | 125 |
| FIG. 5.24. The same record as in Figure 5.23 after AGC .....                                       | 126 |

## Chapter 1 - INTRODUCTION

### 1.1 Triangle Zones

Along most of the leading edge of the southern Alberta Foothills thrust and fold belt, a sequence of east-dipping autochthonous rocks, which marks the western flank of the Alberta syncline, is juxtaposed against west-dipping strata contained in imbricate thrust structures. These sequences of opposing dip are underlain by relatively undeformed rocks of Mesozoic to Paleozoic age that dip very gently to the west. This structural geometry is illustrated in Figure 1.1 and has been named the "Triangle Zone" by Gordy et al. (1977) due to its triangular geometry seen in seismic data. Other names have also been applied to describe this structural style, such as "passive roof duplex" (Banks and Warburton, 1986) and "front fold" (Dahlstrom, 1970). The Triangle Zone of the Canadian Rocky Mountains has since been studied by Jones (1982), Teal (1983), McMechan (1985), Charlesworth and Gagnon (1985), Price (1986), Charlesworth et al. (1987), MacKay (1991), Skuce et al. (1992), Jones et al. (1992), Sanderson and Spratt (1992), Hiebert (1992) and Slotboom (1992). It has also been a stereotype of one of the structural styles observed at the leading edges of thrust and fold belts around the world (Jones, 1982; Banks and Warburton, 1986; Morley, 1986; Vann et al., 1986; Skuce et al., 1992).

In Alberta, the Triangle Zone developed at the eastern margin of the thrust and fold belt of the Canadian Rocky Mountain Foothills as a result of eastward advancement of an allochthonous wedge of rocks into the foreland basin (Charlesworth et al., 1987; Price, 1986). The wedge tapers eastward and is encased between roof and floor thrusts which Jones (1982) defined as the upper and lower detachments respectively. The hinterland-verging roof thrust (upper detachment) dips to the east, and is a structural boundary that separates the autochthonous rocks of Upper Cretaceous to Tertiary age on its hanging wall from allochthonous rocks in its footwall. The floor thrust or the lower

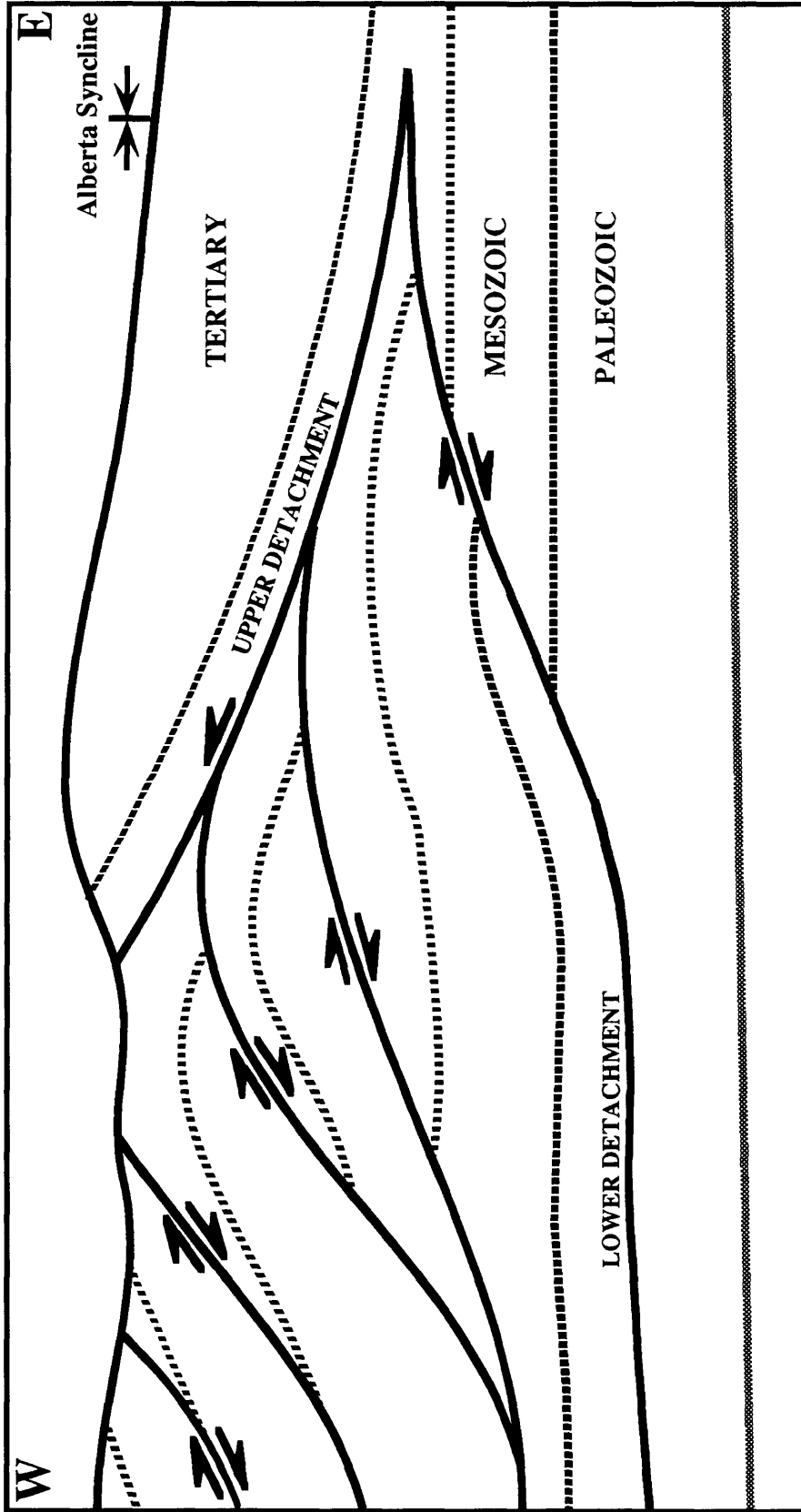


FIG. 1.1. Generalized structural geometry of the Triangle Zone, Canadian Rocky Mountain Foothills. The upper detachment marks the west flank of the Alberta syncline and merges with the lower detachment at the eastern tip of the most external wedge. The merging between the upper and lower detachments represents the limit of Foothills deformation (modified from Jones, 1982).

detachment is a surface common to the entire thrust and fold belt (MacKay, 1991). It separates allochthonous rocks in its hanging wall from autochthonous rocks in its footwall. The lower detachment exhibits a staircase geometry, with a ramp oblique to bedding, that cuts up-section towards the foreland. This ramp is connected with a flat, parallel to bedding, and merges with the upper detachment at depth. Generally the flats are in incompetent rocks (i.e., shales) whereas the ramps cut up-section through competent rocks (i.e., sandstones). The merging between the upper detachment and the upper flat of the lower detachment forms a frontal tip line of the thrust and fold belt in this region (Charlesworth and Gagnon, 1985; Morley, 1986). This buried frontal tip line marks the eastern extremity of the intercutaneous wedge, which migrates eastwards, along with tectonic delamination of the foreland succession, as the wedge is driven further into the foreland basin (Price, 1986; Lawton and Spratt, 1991).

Triangle Zones are believed to have formed at the deformation front throughout the Laramide orogeny (Jones, 1982; Charlesworth and Gagnon, 1985). The continuing progression of the intercutaneous wedge into the foreland basin causes stress upon the upper and lower detachments and the wedge will continue advancing and thickening until a critical point along the lower detachment is approached. At this critical point, a more external lower detachment surface is formed to accommodate the stress field. The deactivated part of the lower detachment and strata in its hanging wall are subsequently incorporated into the intercutaneous wedge and the process is repeated (Charlesworth and Gagnon, 1985). This continued deformation and incorporation of hanging wall strata into the wedge gives rise to the deformation of older strata within the intercutaneous wedge, lengthening of the upper flat of the lower detachment, and steepening of the upper detachment until a critical taper point is reached, beyond which wedging cannot continue. Then a new upper detachment develops towards the foreland, along with an abandonment of the old upper detachment which is passively folded and carried above the stacked

horses. Such a relict upper detachment was found and discussed by MacKay (1991).

Different interpretations regarding the relationship and interaction between the upper and lower detachments exist. Generally, the lower detachment is interpreted as being blind and merging with the upper detachment at the eastern edge of the most external wedge (Jones, 1982; Charlesworth and Gagnon, 1985; McMechan, 1985; Charlesworth et al., 1987). However, Slotboom (1992) shows that the upper and lower detachments do not necessarily merge at the frontal tip line of the thrust and fold belt, but instead shows that they may run parallel along bedding planes of Upper Cretaceous rocks, and that strain dissipates between them. The work of Skuce et al. (1992) substantiates this interpretation in that duplexes of Upper Cretaceous rocks in the Edson region were found to develop in the interval between the upper and lower detachments further to the east of the Triangle Zone in this area (Figure 1.2). This evidence suggests the continued interaction between these two fault surfaces beyond the main culmination of the Triangle Zone. However, in many cases, seismic data show that the lower detachment may in fact merge with the upper detachment (MacKay, 1991; Jones et al., 1992; see also section 4.3 in this thesis).

In addition to differing interpretations of the geometry of the Triangle Zone, the initial geometrical relationship between the upper and lower detachments has as well been contentious. Jones (1982) proposed that the upper and lower detachments were initially parallel or sub-parallel, forming along incompetent units, and that the wedge is developed by slices underthrusting beneath the upper detachment (Figure 1.3). As a result of the wedging, the upper detachment is passively uplifted, but still remains structurally in contact with undeformed strata in the foreland. Based on this model, the upper and lower detachments are in fact the roof and floor thrusts of the duplex structure (Vann et al., 1986). Charlesworth et al. (1987) argue that the subparallel, synchronous thrusting, as indicated by Jones, is dynamically unsound on the basis that since the upper and lower

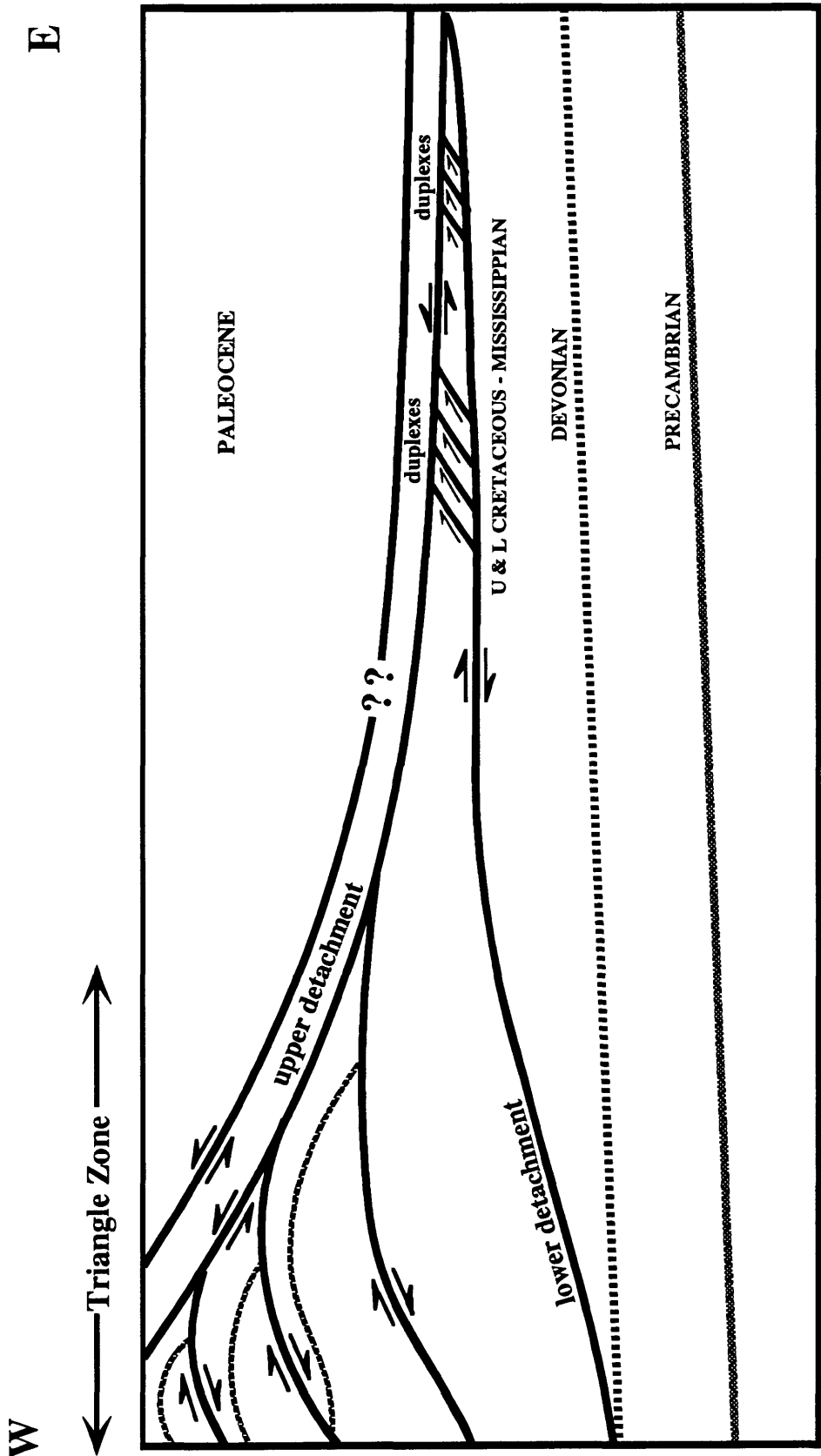


FIG. 1.2. Schematic cross-section of the Triangle Zone near Edson, west of Edmonton, Alberta showing that the merging between the upper and lower detachment does not take place at the deformation front but extends further to the east (i.e., 40 km. or more in this case). Note duplexes form between the upper and lower detachments (Modified from Skuce et al., 1992).

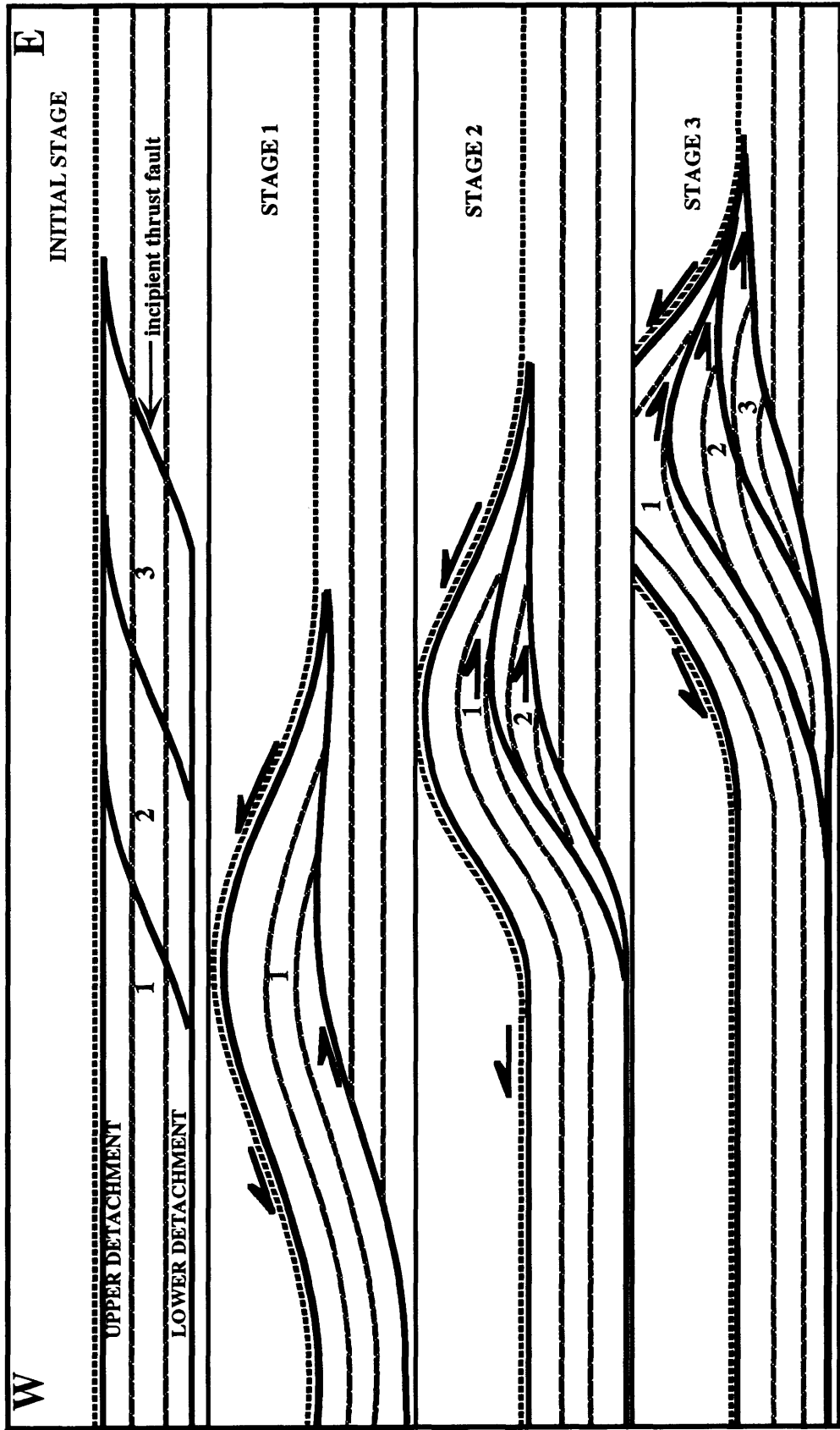


FIG. 1.3. Triangle Zone evolution according to Jones (1982). The upper detachment initially forms as a flat, and is later uplifted as a result of underthrusting beneath it.

detachments possess opposite vergence, or sense of displacement, they cannot have parallel orientations. They assert that the upper and lower detachments must initially form as conjugate faults, with a dip angle of greater than 30 degrees between the upper detachment and the highest flat of the lower detachment (Figure 1.4). According to their hypothetical model, the Triangle Zone has formed in cycles, along with the abandonment and development of new upper and lower detachments. Some field evidence supports this model since the upper detachment was found to initiate as a ramp in the Turner Valley region, southwest of Calgary (MacKay, 1991). In spite of this argument, the Jones model has been supported by considerable evidence that suggests a model of low-taper geometry for the eastern flank of Triangle Zones (Skuce et al., 1992; Teal, 1983; McMechan, 1985). In addition, interpretation of seismic data in this thesis (discussed in Chapter 4) firmly supports the presence of low-taper Triangle Zone geometry since the upper detachment in this area has a very low dip angle.

In Alberta a large number of seismic surveys have been conducted across the Triangle Zones since many gas, oil and coal accumulations have been discovered to lie concealed beneath this structural feature (Skuce et al., 1992; Jones, 1982; Charlesworth et al., 1987; Jones et al., 1992). However, the shallow geometry of Triangle Zones is often poorly imaged because most of the acquisition and processing parameters have been targeted to deeper Mississippian and Devonian carbonate reservoirs. Furthermore, it has been observed that the quality of seismic data deteriorates considerably in the zones below the cores of Triangle Zones. This is considered to be a result of chaotic geometry and complex velocity fields within the Triangle Zone, which lead to severe distortions of seismic raypaths. As well, the surface topography across the central part of the Triangle Zones is usually rugged, and is associated with exposed thrusts and near-surface velocity inversions which further degrade the quality of seismic data.

It is expected that detailed seismic modelling analysis, based on the interpretation

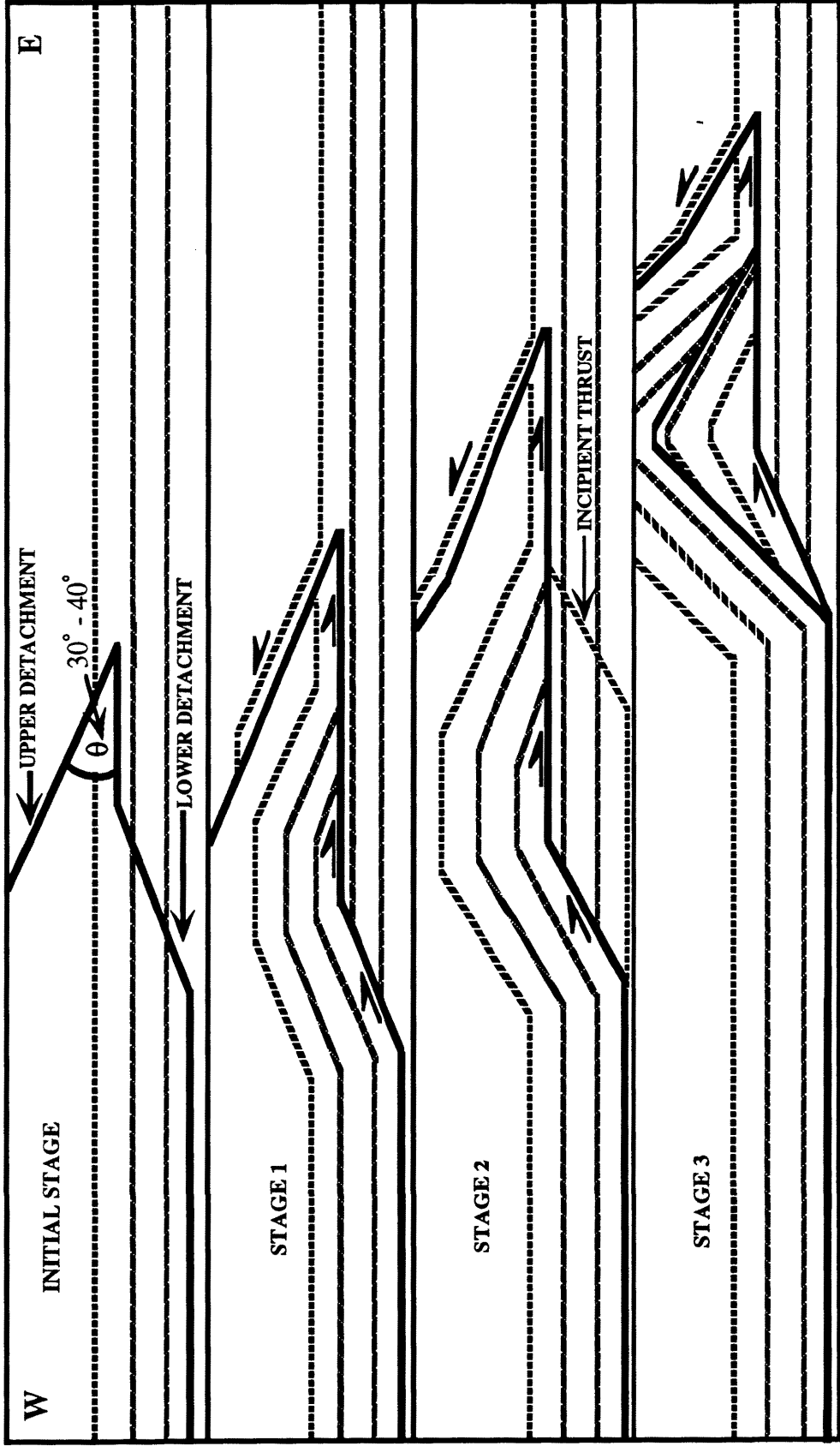


FIG. 1.4. Triangle Zone evolution according to Charlesworth et al. (1985, 1987). Compare this model with Jones' model in Figure 1.3 and note that the upper detachment in this case initially forms as an east-dipping ramp with an angle of 30-40 degrees between the highest flat of the lower detachment.

of high-resolution reflection seismic data, integrated with detailed surface geology, will provide an insight into the acquisition and processing problems associated with the Triangle zone and will help constrain the interpretations of the Triangle Zone geometry in nearby regions.

## **1.2 Converted Waves (P-SV)**

All previous seismic work in the Foothills has been based on compressional (P) wave data. However, there is now increased emphasis on the generation, detection and interpretation of shear-wave seismic data to provide additional information about subsurface lithology and structure. Shear waves are characterized by polarized particle motion perpendicular to wave propagation direction and can be generated either by the source or by mode-conversion (McQuillin et al., 1984). In the latter case, shear waves are generated when a P-wave impinges upon an acoustic impedance boundary at non-normal incidence (Figure 1.5). This type of shear wave is generally referred to as P-SV and can be recorded using radial-component geophones (Dobrin and Savit, 1988). Generally, P-SV data are recorded in conjunction with P-P data. The major application of this integrated technique is in lithologic and stratigraphic determination via the analysis of  $V_p/V_s$  ratio (e.g., Tatham and Stoffa, 1976; Tatham, 1982). In addition, P-SV data are also used in structural imaging (Lawton and Harrison, 1991).

In this study, P-SV seismic data in a complex structural environment were evaluated and compared with P-P data by means of seismic modelling analyses. Some important geometrical aspects and processing procedures of the P-SV data are also discussed.

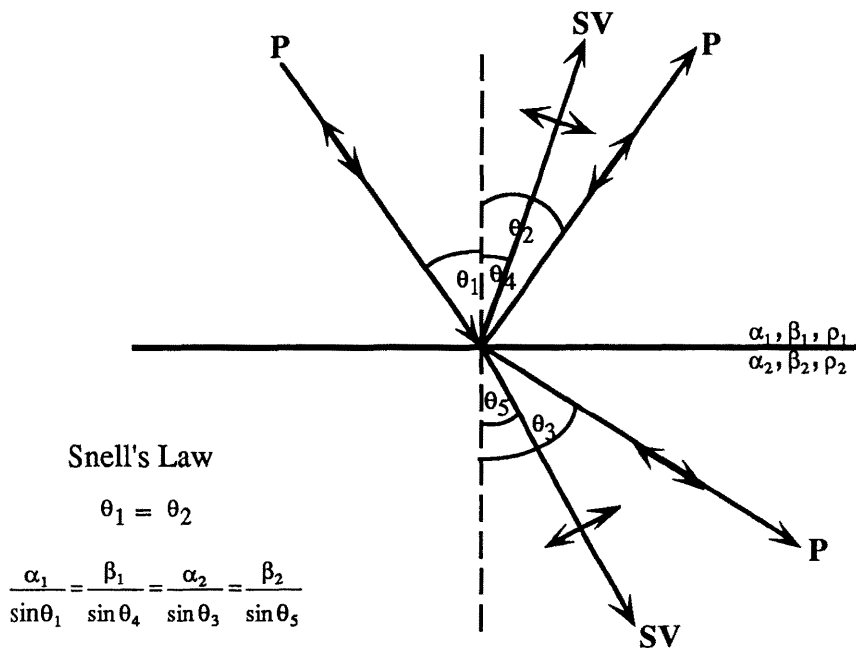


FIG. 1.5. Reflection and transmission at an interface:  $\alpha$  and  $\beta$  are P-wave and S-wave velocities;  $\rho$  is density (modified from McQuillin et al., 1984).

### 1.3 Objectives and Structure of the Thesis

The major goal of this research project has been to undertake a seismic processing and interpretation study and a seismic modelling analysis of the Triangle Zone, northwest of Calgary in the Canadian Rocky Mountain Foothills. The particular objectives that are addressed in this thesis are:

- 1) to delineate the Triangle Zone geometry in this region, with a specific emphasis on the structural relationship between the upper and lower detachments;
- 2) to elucidate the detailed three-dimensional (3-D) geometry of structures present beneath the east-dipping upper detachment in this region;
- 3) to investigate seismic artifacts or velocity anomalies caused by the Triangle Zone

- with respect to the interpretation of deeper horizons, e.g., Mississippian and Devonian formations which are of exploration interest in western Canada;
- 4) to determine problems in acquiring and processing seismic data across this structural feature and provide possible methods to overcome these problems;
  - 5) to evaluate the feasibility and values of using converted shear-wave data (P-SV) in conjunction with the conventional seismic data (P-P) in this complex structural environment.

Chapter 2 provides a description of the study area, geological background and stratigraphy of the key geologic markers utilized in this study. In Chapter 3, general information about the seismic data and processing methods applied to the data are described. Conventional processing procedures, migration and offset-limited stack tests, including the theoretical background of each process, are discussed in this chapter. Chapter 4 presents interpretation of the field seismic data including balanced cross-sections. Investigation of velocity anomalies below the Triangle Zone and an evaluation of P-SV analysis in a complex structural environment are discussed in Chapter 5. Chapter 6 contains the conclusions and recommendations drawn from the results of this research.

## **1.4 Geophysical and Geological Data used in this Thesis**

This research project was carried out using various geophysical and geological data as follows :

### **1.4.1 Conventional Seismic Data**

Three conventional seismic lines (FTC-2A, 2B and 3), collected by Petrel Robertson Ltd. Calgary, were donated to the project. The data were reprocessed, as described in Chapter 3, to enhance the shallow parts of the sections.

### **1.4.2 Synthetic Seismic Data**

Both physical and numerical seismic data were generated for this study. The numerical-modelling data were recorded from a model of the Triangle Zone, based on the interpretation of the conventional seismic data. Three data modes were collected, i.e., zero-offset, offset P-P and offset P-SV. These data were used to investigate velocity anomalies below the Triangle Zone core, and to evaluate processing algorithms such as offset-limited stack, DMO and migration.

The physical-modelling data were acquired from a generic model of a thrust fault containing high-velocity rocks in its hanging wall overlying lower-velocity rocks in its footwall. The goal was to characterize seismic expressions of this structural feature and to assess our ability to image subtle structures beneath this high-velocity layer.

### **1.4.3 Well-Log Data**

Sonic and density logs of wells in the study area were utilized to generate synthetic seismograms which were then used to tie geological information to seismic data. Interval velocities of the key geologic formations were also derived from the sonic logs of these wells.

### **1.4.4 Surface Geology**

Surface geology as incorporated into the seismic interpretation was obtained from the work of Soule (1993) who mapped the Grease Creek area and the Triangle Zone in this region at a scale of 1:20,000.

## **1.5 Software used in this Research**

The processing of the seismic data was undertaken on a UNIX-based Sun SPARC Station network. All of the seismic data were processed using the Inverse Theory and

Applications (ITA) software, except for the P-SV common-conversion point binning and polarity reversal that were performed using software developed by the CREWES Project (The University of Calgary).

Well-log digitizing and generation of synthetic seismograms were undertaken using Digirat and GMA (LOGM) modelling software, respectively. Seismic interpretation was performed both manually and using a Landmark Seismic Interpretation workstation.

Numerical-modelling seismic data were generated using a UNISEIS ray-tracing modelling package. Physical-modelling data were collected from the physical seismic modelling facility at the Department of Geology and Geophysics, The University of Calgary. The thesis was written on a Macintosh computer using Microsoft Word and Canvas software packages.

## Chapter 2 - GEOLOGY

### 2.1 Study Area

The study area is located in the region of Fallen Timber Creek, approximately 75 km northwest of the city of Calgary, and about 10 km southwest of Sundre (Figure 2.1). The area is encompassed by Townships 30-32, Ranges 4-6 west of the fifth meridian (see Figure 2.3 for seismic line locations).



Fig. 2.1. Fallen Timber Creek location map.

## **2.2 Stratigraphy**

Table 2.1 provides a lithologic description of rock formations in the Foothills and Front Ranges, west of Calgary, including average interval velocities between key geologic markers. These velocities were derived from sonic logs and from velocity analyses during the processing of seismic data which is discussed in Chapter 3.

The following summary of lithology and stratigraphy is intended as a general account used for the structural interpretation in this thesis. Detailed lithologic and stratigraphic descriptions can be found in the references cited. All rock formations in this region are of sedimentary origin and are described in ascending order.

### **2.2.1 Cambrian**

The Cambrian sections do not crop out in the study area and were not encountered by the wells used in the interpretation. They are predominantly fined-grained limestones interbedded with oolitic limestone with minor amounts of dark grey and grey-green shale and argillite (Beach, 1943). Seismic reflections from the Cambrian interval are interpreted to be strong, continuous-amplitude events which dip gently to the southwest.

### **2.2.2 Devonian**

Rocks of Devonian age are divided into two major marine units, namely the Fairholme and the overlying Palliser Groups. The Wabamun and Leduc Formations, which are in the Palliser and Fairholme Groups respectively, were encountered in the wells 5-14-31-6W5, 10-25-31-6W5 and 6-4-31-5W5 (shown in Figure 2.3), and therefore are used as key seismic horizons in the interpretations in this thesis.

The Wabamun Formation is characterized by tight micritic limestone in part with dolomite which has traces of infilled animal burrows. The basal part is gradational with silty and argillaceous dolomite, shale and siltstone which mark the regressive phase

| Age           | Formation or Group | Lithology   | Average Seismic Velocity (m/s) |
|---------------|--------------------|-------------|--------------------------------|
| TERTIARY      | PASKAPOO           |             | 3350 - 3650                    |
| CRETACEOUS    | UPPER              | EDMONTON    |                                |
|               |                    | BEARPAW     |                                |
|               |                    | BELLY RIVER |                                |
|               | LOWER              | WAPIABI     |                                |
|               |                    | CARDIUM     |                                |
|               |                    | BLACKSTONE  |                                |
|               |                    | BLAIRMORE   |                                |
| JURASSIC      | KOOTENAY           |             |                                |
| TRIASSIC      | FERNIE             |             |                                |
| PERMO-PENN    | SPRAY RIVER        |             |                                |
|               | ROCKY MTN.         |             |                                |
| MISSISSIPPIAN | MOUNT HEAD         |             |                                |
|               | TURNER VALLEY      |             |                                |
|               | SHUNDA             |             |                                |
|               | PEKISKO            |             |                                |
|               | BANFF              |             |                                |
|               | RUNDELE            |             |                                |
| DEVONIAN      | PALLISER           |             |                                |
| UPPER         | FAIRHOLME          |             |                                |
| CAMBRIAN      | ? U ?              | ARCTOMYS    |                                |
|               | MIDDLE             | PIKA        |                                |
|               |                    | ELDON       |                                |
|               |                    | STEPHEN     |                                |
|               |                    | CATHEDRAL   |                                |
| PRE CAMBRIAN  | HUDSONIAN          |             |                                |

Table 2.1. Table of Formations in the Foothills and Front ranges, west of Calgary. Major detachment horizons are indicated by arrows. Solid arrows indicate the detachment horizons in the study area (modified from Gallup, 1975).

culminating in an unconformity which interrupted the marine environment of the Upper Devonian (Jones and Workum, 1978).

The Leduc Formation is a shelf-carbonate complex with reefal buildups. It is predominantly light brown-grey, medium crystalline dolomite (Jones and Workum, 1978).

### **2.2.3 Mississippian**

The Turner Valley Formation used in this interpretation is in the Rundle Group which conformably overlies the Banff Formation. It consists of massive beds of marine limestone with black cherty limestone in the basal part, and crinoidal limestones and dolomites with calcareous quartzites in the middle and upper units respectively (Beach, 1943). It is not exposed in the study area but was encountered in the wells mentioned earlier.

### **2.2.4 Jurassic**

The Jurassic Fernie Formation is a deep-shelf marine unit. It is composed mainly of non-resistant, black marine shales with high carbonaceous content (Jones and Workum, 1978). The Fernie Formation does not crop out in the study area but is an important detachment horizon.

### **2.2.5 Cretaceous**

#### **2.2.5.1 Blairmore Group**

The Blairmore Group is Lower Cretaceous in age. It comprises non-marine sandstone, siltstone, shale, coal and cobble conglomerates. The sandstone and conglomerate units are resistant to erosion and commonly form prominent ridges in the

Alberta Foothills belt. The Blairmore Group can be grossly subdivided into a lower and an upper part. The lower part is characterized by a massive pebble conglomerate bed and coarse-grained sandstones. The conglomerates exhibit considerable uniformity in size and lithology of the component pebbles. The upper part of the Blairmore Group is composed largely of light to dark green shales and siltstones interbedded with light greenish grey crossbedded sandstones (Beach, 1943).

#### 2.2.5.2 Blackstone Formation

The Blackstone Formation is a black marine shale sequence. It abruptly overlies the Blairmore Group and is gradationally overlain by the Cardium sandstone. The Blackstone Formation comprises black, generally fissile shale that is less silty and less concretionary than the Wapiabi shale. This unit is extremely incompetent and commonly contorted and repeated by thrusting (Jones and Workum, 1978). It is an important detachment horizon in the Alberta Foothills thrust and fold belt.

#### 2.2.5.3 Cardium Formation

The Cardium Formation is characterized by resistant sandstones with intervening shale beds and local conglomerates. The sandstones are mainly fine-grained, siliceous, very finely laminated and well cemented (Jones and Workum, 1978).

The upper contact of the Cardium Formation with the basal part of the Wapiabi Formation is sharp and marked at the upper most fine-grained sandstone unit below the pebble and grit beds of the Wapiabi Formation. The lower contact of the Cardium Formation is defined at the base of the thickly bedded sandstone which grades to thinly bedded sandstone, shale and interbedded shale of the Blackstone Formation (Stott, 1963).

#### 2.2.5.4 Wapiabi Formation

The Wapiabi Formation consists of marine black shales with thin sandstone, concretionary and silty interbeds. It overlies the Cardium Formation sharply and grades upwards into sandstones of the Belly River Formation. Structurally, the Wapiabi Formation is severely contorted and repeated by thrusting (Jones and Workum, 1978).

#### 2.2.5.5 Brazeau Formation

The Brazeau Formation consists of alternating units of sandstone, siltstone, shale and mudstone with minor amounts of coal and conglomerate. The sandstones are fine-to coarse-grained, grey and greenish grey, feldspathic, massive to bedded. The mudstones are greenish grey, green and grey with rubbly, blocky disintegration (Ollerenshaw, 1975).

Southwest of Calgary, where the Bearpaw shale is present, the Brazeau Formation can be divided into the Belly River Formation (Lower Brazeau), characterized by massive and cross-bedded sandstones interbedded with shale beds and coals, and the Edmonton Group (Upper Brazeau) which is a fining-upward sequence of intercalated continental channel sandstones and rubbly shales. Where the Bearpaw shale does not exist, the Belly River and the Edmonton Group are grouped into the Brazeau Formation.

### 2.2.6 Tertiary

The Paskapoo Formation is early Tertiary in age (Paleocene or Eocene). It consists mainly of sandstone, shale, minor coal and conglomerate. The Paskapoo Formation overlies Upper Cretaceous rocks unconformably in the east and conformably to the west (Jones and Workum, 1978). Following the model of Jones (1982), these strata are contained within the upper detachment and are interpreted to be passively uplifted by underthrusting of the Upper Cretaceous rocks.

## 2.3 Surface Geology

Surface geology in the study area was mapped by Mackay (1939), Hume and Hage (1941), Beach (1942), Hume and Beach (1944), and Ollerenshaw (1974). All of these previous maps were compiled on a 1:250,000 Calgary-map sheet by Ollerenshaw (1978). Figure 2.2 is a portion of a NE-SW cross-section (Ollerenshaw, 1978) which is oriented approximately in the same direction as line 2B (see line location in Figure 2.3). In this cross-section the Triangle Zone is shown as an antiformal stack of Upper Cretaceous rocks developed beneath an upper detachment at the eastern edge of the deformation belt. Also indicated in the eastern part of the Triangle Zone is a west-dipping thrust that cuts up-section through Mesozoic rocks towards the foreland. No back thrust associated with this young thrust is defined in the cross-section. It is also interesting to note that the upper detachment in this cross-section is shown as a blind thrust. This implies that, from west to east, there is no distinction in structural geometry of exposed rocks across the main culmination of the Triangle Zone. However, the seismic data, used in this structural interpretation (discussed in Chapter 4), clearly show that the upper detachment crops out, and acts as a structural boundary that separates allochthonous rocks in its footwall from autochthonous rocks in its hanging wall.

The area was recently remapped by Soule (1993) at a scale of 1:20,000. Figure 2.3 shows a portion of his map including the locations of seismic lines and wells used in this structural interpretation. Only the Upper Brazeau Formation (Upper Cretaceous) and Tertiary rocks are exposed in the study area. The surface expression of the Triangle Zone in this region is a NW-SE trending en echelon anticline of the Upper Cretaceous rocks juxtaposed with Tertiary rocks in the foreland. The continuity of the east-dipping upper detachment, as shown in this map, was determined based solely on the interpretation of the seismic data because outcrops of this fault are poorly exposed in the study area (G.S. Soule, personal communication).

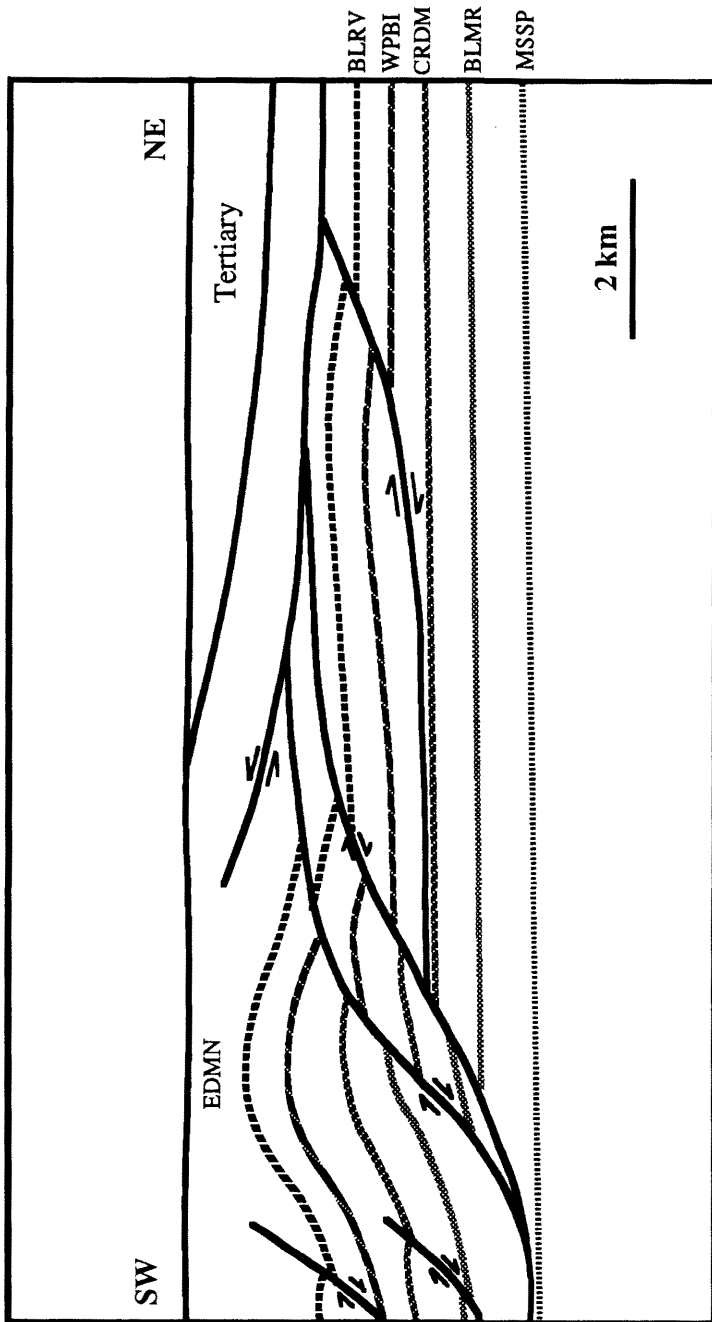


FIG. 2.2. A portion of a NE-SW cross-section from the Fallen Timber Creek region showing the Triangle Zone developed at the eastern edge of the deformed belt, EDMN=Edmonton Triangle Zone, BLRV=Blairmore Group, WPBI=Wapiabi Formation, CRDM=Cardium Formation, BLMR=Blairmore Group, MSSP=Mississippian Formation (from Ollerenshaw, 1978).

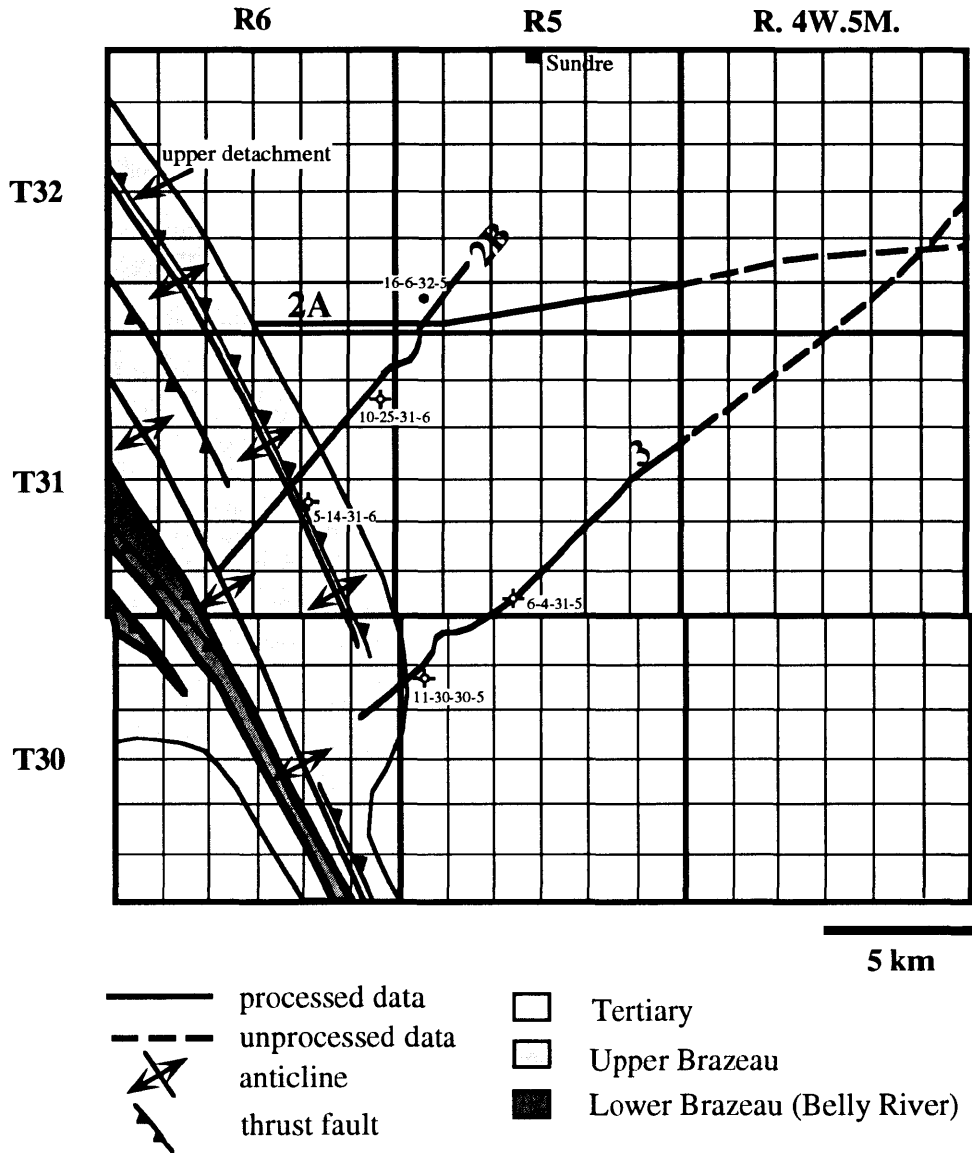


FIG. 2.3 Surface geology, wells and seismic location map.

## Chapter 3 - SEISMIC DATA PROCESSING

### 3.1 Introduction

This chapter describes the processing procedures applied to the conventionally recorded (P-P) seismic lines 2A, 2B and 3. The processing flow for line 2A and 2B is outlined in Figure 3.1. Line 3 was processed by Manmohanvir Sihota (The University of Calgary) using essentially the same flow and parameters.

All processing was performed on a Sun SPARC Station network using Inverse Theory and Applications (ITA) software. In section 3.2, the seismic data and acquisition parameters are discussed. Preprocessing procedures and prestack processing are described in sections 3.3 and 3.4 respectively. Poststack processing is summarized in section 3.5. The data from seismic line 2B will be used to illustrate the processing steps.

### 3.2 Seismic Reflection Data

The seismic data presented here were acquired by Petrel Robertson in January 1990, using P-wave vibroseis sources and vertical-component geophones. A location map showing the seismic lines is displayed in Figure 2.3. Line 2B is oriented approximately NE-SW across the Triangle Zone, northwest of Calgary. Its entire length of 13.5 km was processed. This seismic line intersects with the line 2A.

The western half of line 2A is oriented approximately E-W. Its orientation on the eastern end changes to NE-SW. It intersects with lines 2B and 3. The total length of this line is about 26.5 km but only the western 15 km was processed in this study, since only this portion crosses the Triangle Zone.

Line 3 is about 27.5 km in total length and intersects with line 2A at its northeastern end. It is oriented in the same direction as line 2B, but is about 10 km further to the southeast. Only the southwestern half of the line (approximately 17 km) was

processed in this project.

The data were recorded using vibroseis as a seismic source with a sweep length of 12 s, a sweep frequency from 12-96 Hz, and split-spread geometry. The recording instrument was a 240-channel Sercel system with 10-Hz geophones. Each geophone array consisted of 12 geophones spread over 33 m. The average group interval was 33 m with offset ranges from 66 m to 3993 m on both sides of the shot. The average shotpoint interval was 99 m, and the data were recorded to 3 s with a 2-ms sampling rate. The spread configuration and shotpoint interval gave a maximum subsurface coverage of 40-fold. However, the actual fold varied considerably because the lines were crooked and shot intervals were not constant in some areas. Table 3.1 gives a summary of the data-acquisition parameters used in this survey. Figure 3.1 shows the processing flow, with each processing step discussed in the following sections.

### **3.3 Preprocessing**

#### **3.3.1 Demultiplexing and Preliminary Editing**

The field data used for the study were recorded in multiplexed format, i.e., time-sequential mode. However, all the processing procedures required the data to be in a trace-sequential format. Demultiplexing, a matrix-transpose operation, provided this conversion.

After demultiplexing, the shot records were plotted and examined for dead traces and unusable records. Lines 2A and 2B contained some noise test and refraction records which were removed from the processing sequence. Dead traces within usable records were muted or zeroed after the geometry step.

|                          |   |
|--------------------------|---|
| <b>Spread Geometry</b>   | <b>120x120, 3993-66-*-66-3993</b>       |
| <b>Source Interval</b>   | <b>99 m</b>                             |
| <b>Receiver Interval</b> | <b>33 m</b>                             |
| <b>Acquisition Fold</b>  | <b>40</b>                               |
| <b>Seismic Source</b>    | <b>Vibroseis</b>                        |
| <b>Sweep</b>             | <b>12 s, 12 sweeps, freq 12-96 Hz</b>   |
| <b>Geophone Type</b>     | <b>Geo, 10 Hz, 12 inline over 33 m.</b> |
| <b>Instruments</b>       | <b>SERCEL / FPCS</b>                    |
| <b>Channels</b>          | <b>240</b>                              |
| <b>Tape Format</b>       | <b>SEG D</b>                            |
| <b>Field Filter</b>      | <b>out / 178 Hz, Notch : out</b>        |
| <b>Sample Rate</b>       | <b>2 ms</b>                             |

Table 3.1. Field Acquisition Parameters.

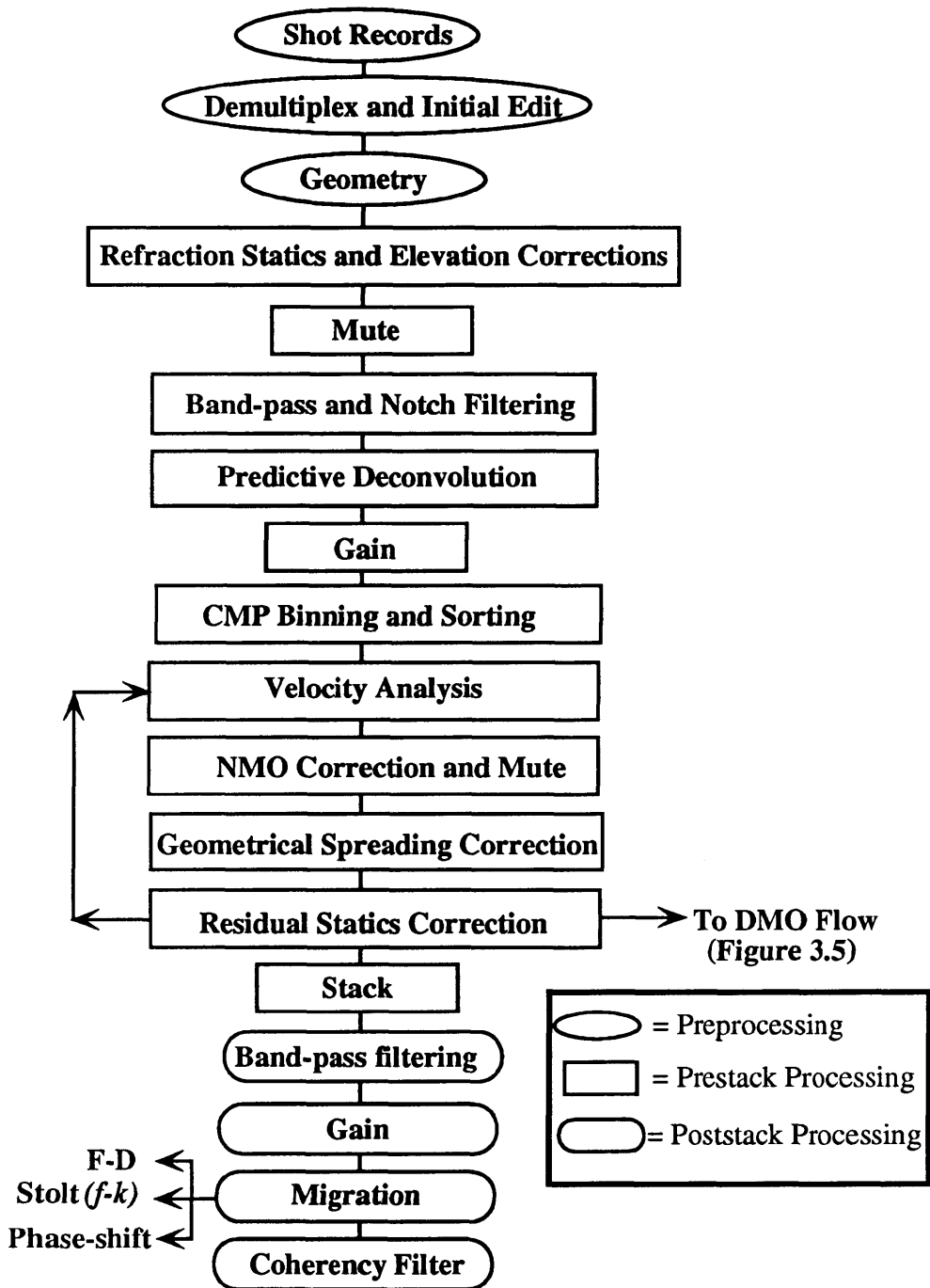


FIG. 3.1. Processing Flow for seismic lines 2A and 2B.

### **3.3.2 Geometry**

Geometry establishes a tie between recorded seismic data and field positional survey information. This was accomplished in two consecutive steps. The first was to create observer and survey files from the field information and the second was to write these data to the seismic trace and file headers. At this step, survey information, i.e., shotpoint and receiver station coordinates, including the spread geometry of the survey lines, were incorporated into the seismic data.

The final data sets, after preliminary editing and geometry, were composed of 125 records for line 2B and 136 records for line 2A. Examples of the shot records of line 2B, collected over the Triangle Zone core (the western half of the line) and its eastern limb, are shown in Figure 3.2 A and B respectively. The shot records are generally characterized by reasonably good signal-to-noise ratio, especially those acquired over the eastern limb of the Triangle Zone. However, the quality of these records degrades over the culmination of the Triangle Zone, due to severe statics and scattering. Some of the shot records are contaminated with constant-frequency noise which severely masks some parts of the data. This noise is caused from power lines and has a constant frequency of 60 Hz. It was suppressed by notch filtering, discussed later in this chapter.

## **3.4 Prestack Processing**

### **3.4.1 Refraction Statics and Datum Elevation Corrections**

A comparison between the shot records in Figure 3.2 shows that statics are more pronounced over the Triangle Zone core than over its eastern limb. These statics are time shifts due to rugged topography, exposed thrusts and near-surface velocity complexity. To overcome these static problems, two correction methods were applied during data processing, i.e., refraction statics and residual statics corrections. The refraction statics

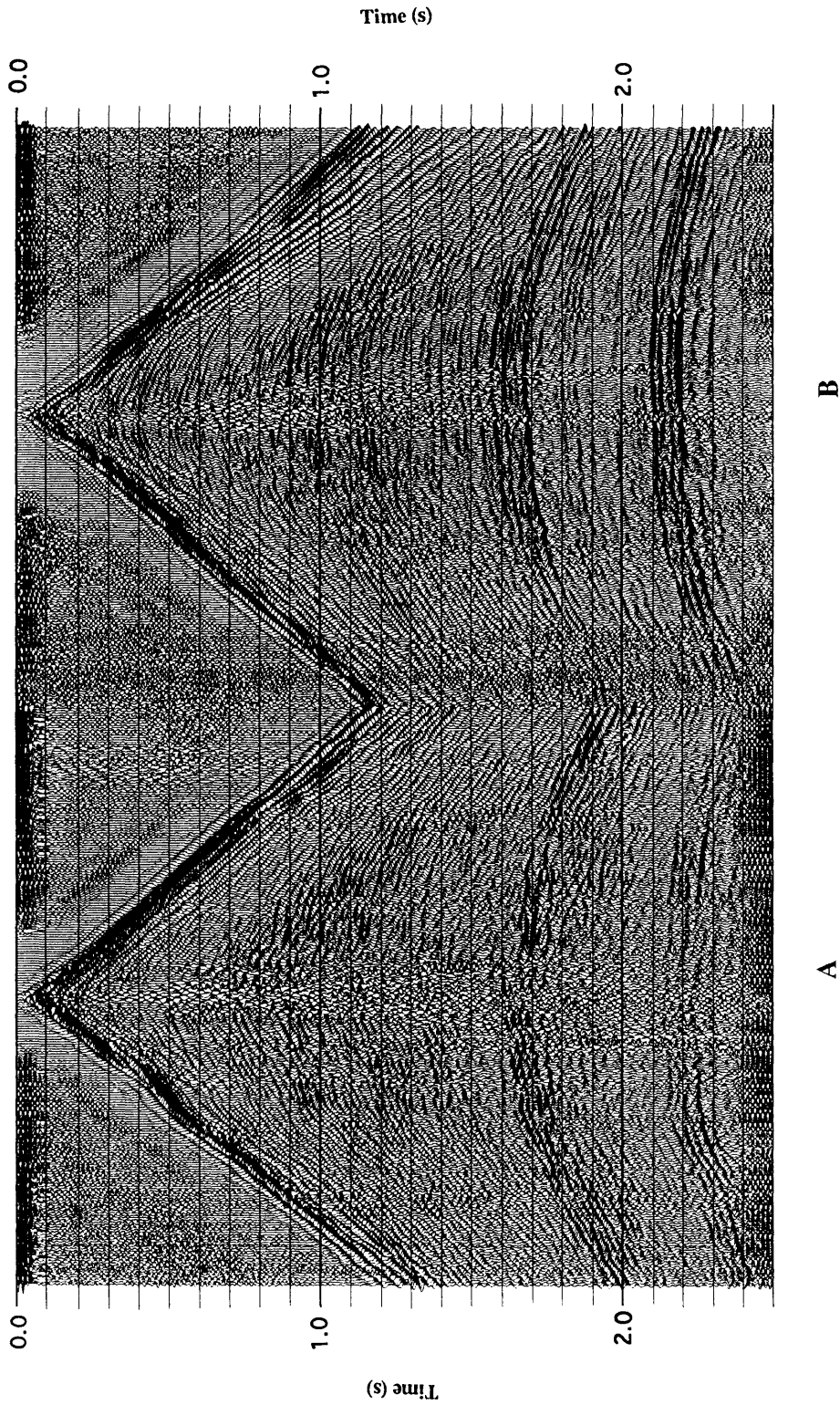


FIG. 3.2. Examples of shot gathers of line 2B from the Triangle Zone core (A), and the eastern limb (B). An AGC with a window of 0.75 s was applied. Note that statics are more severe in record (A).

method used first-arrival information obtained directly from the shot records. Residual statics were applied after normal-moveout (NMO) correction, as described later in this chapter.

Refraction statics and elevation corrections were applied to correct for seismic time delays due to the weathering layer and variable surface topography. Time corrections were computed by hand-picking the first breaks of each shot record. These picks were used to determine the thicknesses and velocities of the weathering, sub-weathering and bedrock layers which were subsequently used to derive a total static correction for each trace, and to correct them to a constant datum. Typically, the datum level is chosen to be close to, or slightly higher than the base of the weathering layer, in order to preserve shallow information (Dobrin and Savit, 1988). Here, the datum level was 1350 m, which is the average elevation of line 2B. A replacement velocity of 3750 m/s, based upon analysis of the first-break picks, was used to calculate the time corrections.

### **3.4.2 First-Break Muting**

Although the first-break signals convey useful static correction information, they must be excluded from the reflection data set. These signals generally have large amplitudes, and could be a serious source of noise if not removed. Not only do they mask usable reflection signals or cancel out useful information during the stacking process (discussed later in this chapter), but they can also cause misinterpretation in the shallow part of the section. For instance, bands of noise or dipping spurious events could be interpreted as the flanks of a near-surface anticline, syncline or front thrust.

Muting, or zeroing, of the first breaks was carried out manually for each record. The patterns were designed to minimize mutes of the near-offset traces as they contained useful information about shallow Triangle Zone reflections, particularly for those records

acquired over the Triangle Zone core.

### **3.4.3 Band-Pass and Notch Filtering**

Field-recorded seismic data possesses a wide frequency bandwidth which contains both noise and signal. However, the usable signal in conventional seismic data is generally confined to a specific bandwidth, e.g., approximately 10-70 Hz (Yilmaz, 1987). Above and below this frequency range is mainly noise which should be attenuated as much as possible.

The goal of frequency filtering in seismic data processing is to pass desirable signals while rejecting others, e.g., ground roll, random noise and power-line noise. Filtering has many forms, such as band-pass filtering, notch filtering, low-pass and high-pass filtering. Filter parameters are usually designed in the frequency domain, assuming a zero-phase operator. The corresponding time-domain filter operator is then derived by the Fourier transform technique and applied to the seismic data to reject or pass signals as desired.

In the processing of lines 2A and 2B, both band-pass and notch filtering were used. The band-pass filter was applied prestack, before deconvolution, with a broad four-point filter having corner frequencies of 10/15-75/80 Hz. This filter suppressed ground roll energy as well as high-and low-frequency random noise. These parameters were chosen based on a plot of the amplitude spectrum (Figure 3.3) which indicated that the bandwidth of most of the recorded energy was confined to this range. The parameters for the notch filter were 57/59-61/63 Hz. This attenuated the 60 Hz power-line noise.

### **3.4.4 Predictive (Gapped) Deconvolution**

Ideally, it is most desirable to obtain seismic traces which resemble spike sequences of reflection coefficients at times corresponding to reflections from boundaries

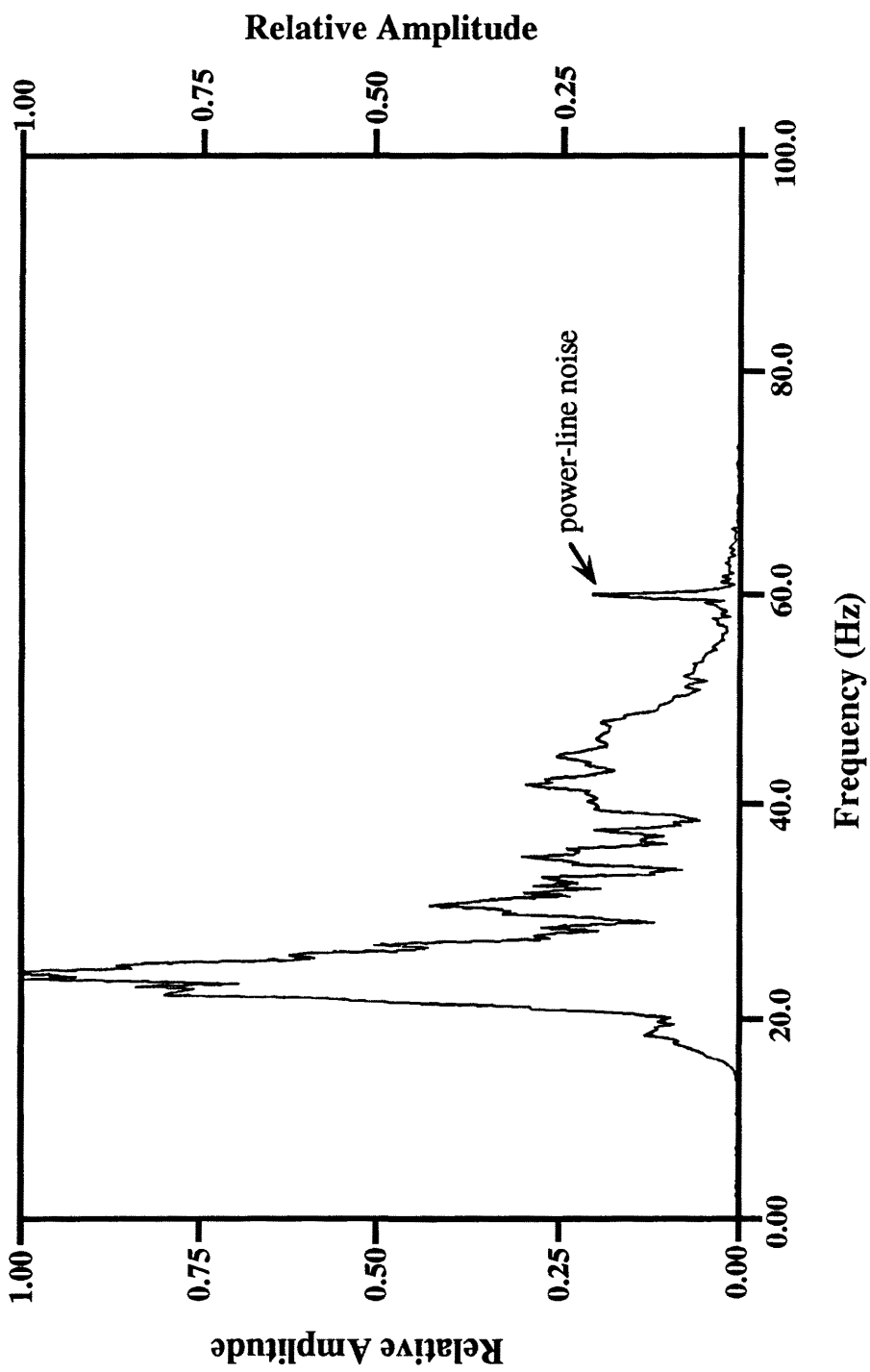


FIG. 3.3. An amplitude-frequency spectrum plot of a seismic trace from line 2B.

in the subsurface. Real seismic data departs considerably from this ideal as it is a complex waveform resulting from the convolution of the seismic wavelet with the Earth's impulse response (reflection-coefficient series). Furthermore, noise is also present in the field data, further complicating the recorded waveforms (McQuillin et al., 1984).

Deconvolution is an inverse filtering method which reverses the process of convolution of the seismic wavelet and the reflection-coefficient series. Its purpose is to obtain the reflection-coefficient series by compressing the source wavelet contained in the recorded seismic trace. Deconvolution can be applied either prestack or poststack but is usually applied prestack, before velocity analysis and NMO correction (Krebes, 1989).

In this study, predictive deconvolution was applied prestack to the shot records using a gap length of 2 ms, an operator length of 0.09 s, along with 1% prewhitening. Note that the gap length was made equal to the field sample rate (i.e., 2 ms) so as to obtain a spiking deconvolution operator (Yilmaz, 1987). The operator length was determined based on rigorous testing and evaluation using the same prewhitening value. It was found that a range of operator lengths between 0.08 and 0.10 s yielded comparatively reasonable results in terms of signal-to-noise ratio and reflection enhancement. Therefore an average value of 0.09 s was chosen.

### **3.4.5 Gain**

The amplitude of a seismic wave decays while travelling from the source, which is attributable to geometrical spreading of the wavefronts, reflection and transmission losses and anelastic absorption (Krebes, 1989). Geometrical-spreading (spherical-divergence) effects exert a major influence on the decay of seismic amplitudes and must be compensated (Newman, 1973).

The gain function applied to correct for geometrical spreading in this processing is defined by Newman (1973) as :

$$D_0 = \frac{tV_{\text{rms}}^2}{V_1} \quad (3.1)$$

where  $D_0$  is the gain function,  $V_1$  is velocity in the first layer and  $V_{\text{rms}}$  is the rms velocity to an horizon corresponding to the two-way travel time  $t$ . The gain function in this case was applied after NMO correction although it could have also been applied before NMO correction.

Following the geometrical-spreading correction, trace balancing was applied to correct for trace-to-trace amplitude inconsistencies. The trace-balancing gain function used here was time-invariant and is expressed as :

$$G(t) = \frac{1}{\sum_{t_2}^{t_1} A^2(t)} \quad (3.2)$$

where  $G(t)$  is the gain function and  $A(t)$  is the trace amplitude at time  $t$ . A time window of 1.5 to 2.3 s, which contained some lateral amplitude inconsistencies, was used to trace-balance the data.

Another type of data gaining used in this study was automatic gain control (AGC). This gaining works by applying a time-variant scale factor, which is computed by the ratio of the desired output level of the signal to the mean amplitude within a specified time window, and is applied to the sample at the center in that window. The window then slides down one sample and the new scale factor is derived and applied in the same manner (Krebes, 1989). As indicated in the processing flow in Figure 3.1, AGC was applied prestack, after deconvolution, with a broad window length of 1.0 s, and it was reapplied poststack with a window length of 0.75 s. A smaller AGC window was used poststack in order to enhance subtle reflections below the Triangle Zone core.

### 3.4.6 Data Sorting

The next step was to sort the traces into the common-midpoint (CMP) domain. Because both seismic lines were slightly crooked, it was necessary to rebin the data in order to optimize the CMP fold along each line. Crooked-line binning and sorting consisted of 3 steps :

- 1) creating a slalom line, which is an imaginary survey line along which the CMP binning and sorting will be performed;
- 2) selecting CMP bin dimensions to form a binning window, and positioning this binning window along the specified slalom line;
- 3) sorting seismic traces to CMP domain.

A series of coordinates which form a slalom line were selected based on examination of the plots of reflection points along the crooked line. CMP bin dimensions, i.e., bin width and bin height, were then defined and positioned along this slalom line. During the positioning processes, seismic traces that fell within the same CMP-binning window were grouped as the same CMP gather, whereas those that did not fall within any binning windows were flagged as dead and excluded from the data set.

In practice, the bin width is usually set equal to the stacked trace spacing (i.e., half the average station interval) and the bin height is set to four times the bin width (ITA Insight/1- Prestack Reference Guide, 1992). However, it was found during processing that a large number of seismic traces fell outside this usual bin dimension. Therefore, it was decided to use larger bin heights in order to retain the high fold characteristics of both lines. This larger bin height was justifiable because the structure does not vary rapidly along strike. A series of bin heights were tested based on a constant bin width of 16.5 m which is equivalent to the average trace spacing of these data sets. A bin height of six times the trace spacing was found to yield optimum result for line 2B and a bin height of eight times the trace spacing provided optimum fold for line 2A.

### 3.4.7 Velocity Analysis

Velocity analysis, based on a velocity spectrum analysis technique, was carried out on common-offset stacks. The velocity spectrum analysis technique was composed of two steps (Yilmaz, 1987) :

- 1) computing the velocity spectrum by measuring signal coherency on the input gathers in small windows that follow a hyperbolic trajectory;
- 2) choosing velocity functions from the derived velocity spectrum that produce the highest coherency at times with significant event amplitudes.

Initial velocity spectra were computed from common-offset stacks using the interval velocity bounds of 2000 and 6500 m/s which were considered to cover the range of average interval velocities of most sedimentary rocks in the study area (Dobrin and Savit, 1988). The velocities were assessed in steps of 50 m/s. These preliminary velocity spectra were then picked manually to generate rms velocity functions. Based on these initial velocities, NMO-corrected gathers and a brute stack section were generated and examined. The NMO-corrected gathers were subsequently passed to a residual static correction step. Following this, the velocity analysis was again undertaken on a more detailed, iterative basis, i.e., using small station intervals (e.g., 350 m) for velocity-spectrum computations, particularly over the Triangle Zone core.

### 3.4.8 Normal-Moveout (NMO) Correction

Before seismic traces in each CMP gather can be stacked, they have to be corrected for time delays due to NMO which is the increase in reflection time with increasing source-receiver offset. The required time correction for NMO is :

$$t_{\text{NMO}} = t_x - t_0 \quad (3.3)$$

where, 
$$t_x^2 = t_0^2 + \frac{X^2}{V_{\text{rms}}^2},$$

$t_{\text{NMO}}$  is the normal moveout (NMO) time correction,  $t_x$  is the traveltime for a source-receiver offset of  $x$ ,  $t_0$  is the two-way traveltime along the vertical path at the midpoint location and  $V_{\text{rms}}$  is the rms velocity which can be obtained from the velocity analysis discussed earlier.

### 3.4.9 Surface-Consistent Residual Statics Corrections

The seismic traveltime delays due to the effects of topographic irregularities were partly corrected by the refraction static solutions described in section 3.4.1. Nevertheless, the technique was not able to handle short-wavelength effects caused by local or rapid changes in surface elevation, variations in the velocity of the weathering layers or other anomalous near-surface conditions (Dobrin and Savit, 1988). To overcome these residual time shifts, surface-consistent residual static corrections were applied.

The most important assumption of the technique is that reflection traveltime delays depend only on source and receiver locations at the surface, not on their raypaths in the subsurface (Yilmaz, 1987). This assumption is generally valid since the weathering layers usually have much lower velocity than the underlying bedrock. This causes the upgoing raypaths to bend to near-vertical according to Snell's Law.

Yilmaz (1987) shows that the residual statics for each individual trace can be approximately determined by :

$$T_{ijh} = S_i + R_j + G_{kh} + M_{kh} X_{ij}^2 \quad (3.4)$$

where

$T_{ijh}$  = the total traveltime from shot point  $i$  to receiver position  $j$  from the  $h$ th horizon

$S_i$  = residual time shift associated with source at the  $i$ th location

$R_j$  = residual time shift associated with receiver at the  $j$ th location

$G_{kh}$  = the difference in two-way time at a reference CMP location and the traveltime at the  $k$ th CMP along the  $h$ th horizon, and  $M_{kh}X_{ij}^2$  is the residual moveout time for a source-receiver separation of  $X$ .

Application of residual static corrections comprises 3 steps :

- 1) Picking observed times  $T'_{ij}$  via a pilot trace scheme. The process involves crosscorrelating a stacked trace with individual traces in that gather to determine individual time shifts  $T'_{ij}$  for each trace. Based on the time-shifted traces in this gather, a new stacked trace, namely an updated pilot trace is constructed and the crosscorrelation process is repeated to generate the final pilot trace. This trace is subsequently crosscorrelated with traces of the next gather to produce a preliminary pilot trace for that gather. The process is continued for every gather in the entire CMP-NMO-corrected data set;
- 2) Decomposition of all the  $T'_{ij}$ s to their constituents on the right side of equation 3.4 using a least-squares method. The mathematical details of this step can be found in Yilmaz (1987), Hatton et al. (1988) and Krebs (1989);
- 3) Applying the results from step 2 to traveltimes of the CMP gathers prior to NMO corrections.

During the crosscorrelation step, the crosscorrelation window and the maximum allowable time shift have to be specified to prevent an unrealistically large time shift being applied. The window of 0.4 to 2.4 s, in which all the coherent events were confined, along with a maximum time shift of 35 ms were chosen. This maximum time shift was determined based on an observation from the shot records, followed by iterative tests of residual statics computations which showed that the maximum time shifts of this data set were approximately 30 to 40 ms.

After the application of residual statics corrections, the velocity analysis, NMO correction and stack were repeated and new residual static values were calculated. These iterative processes were performed until the optimum stacked sections were obtained.

### 3.4.10 Dip-Moveout (DMO) Correction

Dip moveout (DMO) was undertaken on seismic line 2B with the aim of correcting for the detrimental effects of reflections from dipping layers. Figure 3.4 shows schematic diagrams of CMP reflections from a flat layer and a dipping layer, respectively. In the dipping-layer case, reflections deviate from the true common midpoint (CMP) and will be detrimental in generating a stacked section. Therefore, DMO has to be applied to correct for these shifts in spatial positions. The main benefits of including DMO in the processing sequence are to correct for reflection-point smear by laterally shifting the reflection points to their true zero-offset positions, and obtaining

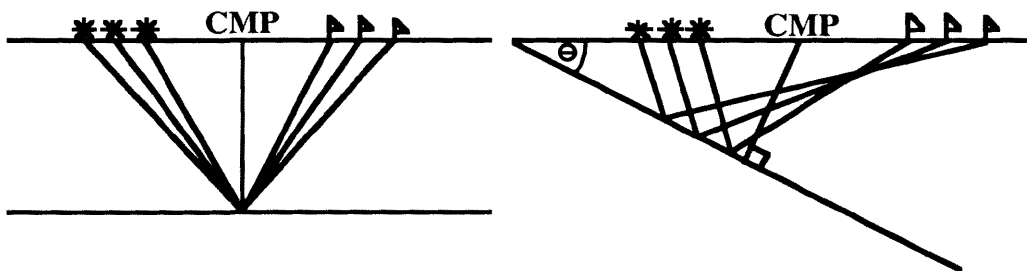


FIG. 3.4. CMP reflections from flat and dipping reflectors. Note that in the case of a dipping reflector, subsurface reflection points depart from CMP position, which results in reflection smear in the stacked output.

stacking velocities, after correction for DMO, that are dip-independent (Notfors and Godfrey, 1987).

The relationship between the NMO velocity and the medium velocity above a dipping reflector is

$$V_{\text{NMO}} = \frac{V}{\cos\theta} \quad (3.5)$$

where  $V_{\text{NMO}}$  is the NMO velocity,  $\theta$  is the reflector dip and  $V$  is the medium velocity above that dipping reflector (Dobrin and Savit, 1988). This relationship implies that NMO velocity for a dipping event is higher than the true medium velocity  $V$ . It also indicates that, in the presence of dipping events adjacent to flat events, a problem arises because two or more NMO velocities are required to preserve both flat and dipping events in the stacked section. Unfortunately, conventional NMO and stacking permits only one choice of an NMO velocity for a particular CMP and traveltime. Thus, choosing an NMO velocity is equivalent to choosing an optimally stacked dip angle for that CMP and travel time (Hale, 1984).

The DMO technique (also known as prestack partial migration) addresses this problem. It converts non-zero-offset raypaths to their approximate zero-offset positions using a wave-theoretical process based on the assumption of a constant-velocity medium. Another positive feature of this technique is that it yields a dip-independent characteristic of the stacking velocity, since the zero-offset raypath does not depend on the dip angle.

There are many algorithms to accomplish DMO correction. The detailed mathematical derivations and limitations of some commonly used techniques can be found in Hale (1984), Notfors and Godfrey (1987), and Deregowski (1986).

The processing flow summarized in Figure 3.5 was used to perform DMO correction on line 2B. Line 2A and line 3 were not DMO corrected since they do not possess steeply dipping events or conflicting dips as does line 2B, and also because it was found during the DMO application for the line 2B that the process was very time-consuming and did not provide obvious improvements to the stacked output (discussed in section 3.4.11).

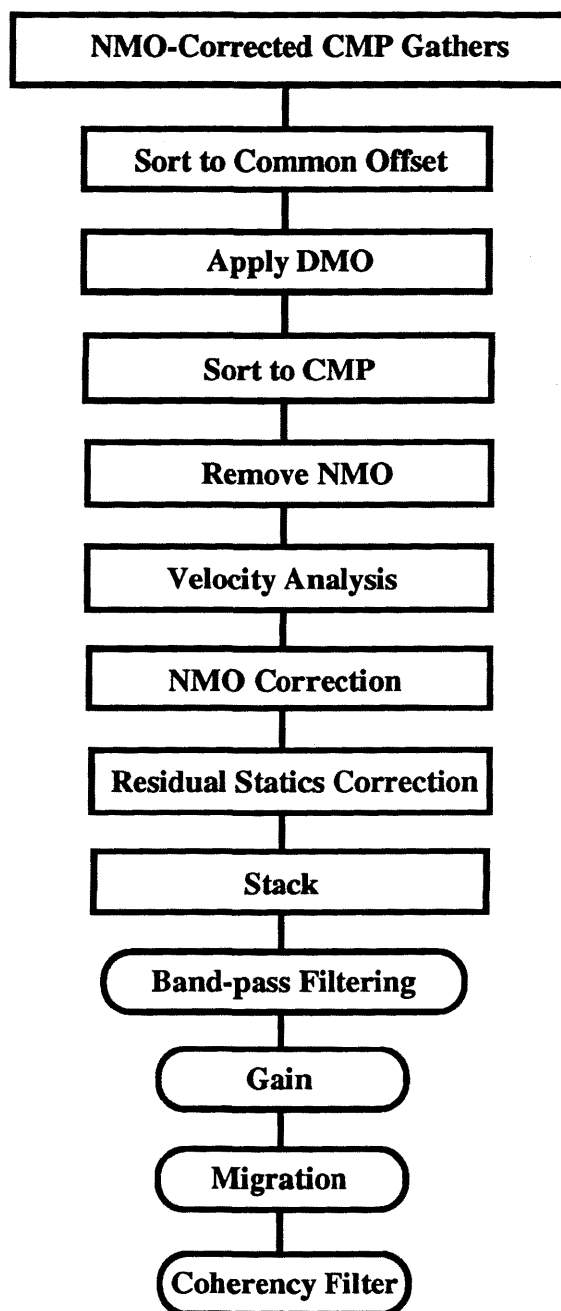


FIG. 3.5. DMO Processing Flow as applied to line 2B.

The DMO algorithm employed in this task was based on a Fourier transform technique which performs DMO correction in the frequency-wavenumber domain based upon a constant-medium velocity assumption (Hale, 1984). It requires the data to be NMO-corrected and sorted into a common-offset domain. As indicated in Figure 3.5, after the application of DMO, further velocity analysis and residual statics corrections were repeated because the DMO-corrected velocity functions are theoretically different from the non-DMO-corrected velocity functions.

#### **3.4.11 Stacking**

Seismic traces within each NMO-corrected CMP gather were summed or stacked to produce one trace at that CMP. Stacking enhances coherent reflections and suppresses multiples and random noise. Theoretically, the signal-to-noise ratio after stack is increased by an order of  $\sqrt{N}$ , where  $N$  is the fold or number of traces in the CMP gather (Dobrin and Savit, 1988).

The non-DMO and DMO-corrected stacks for line 2B are plotted in Figures 3.6 and 3.7 respectively. Comparison between these sections shows that DMO did not provide improved imaging of dipping events in the core of the Triangle Zone, which was the major target for DMO application in this processing. This is likely the result of velocity variations across the western limb of the Triangle Zone which violated the constant-velocity assumption required for this technique to perform well. However, it is observed that reflection continuity of later events in the eastern end of the DMO-corrected stack (e.g., in the time interval between 1.6 and 2.2 s of the section in Figure 3.7) is better than that of the non-DMO corrected stacked section (Figure 3.6). This is believed to be due mainly to better velocity functions and statics solutions following DMO.

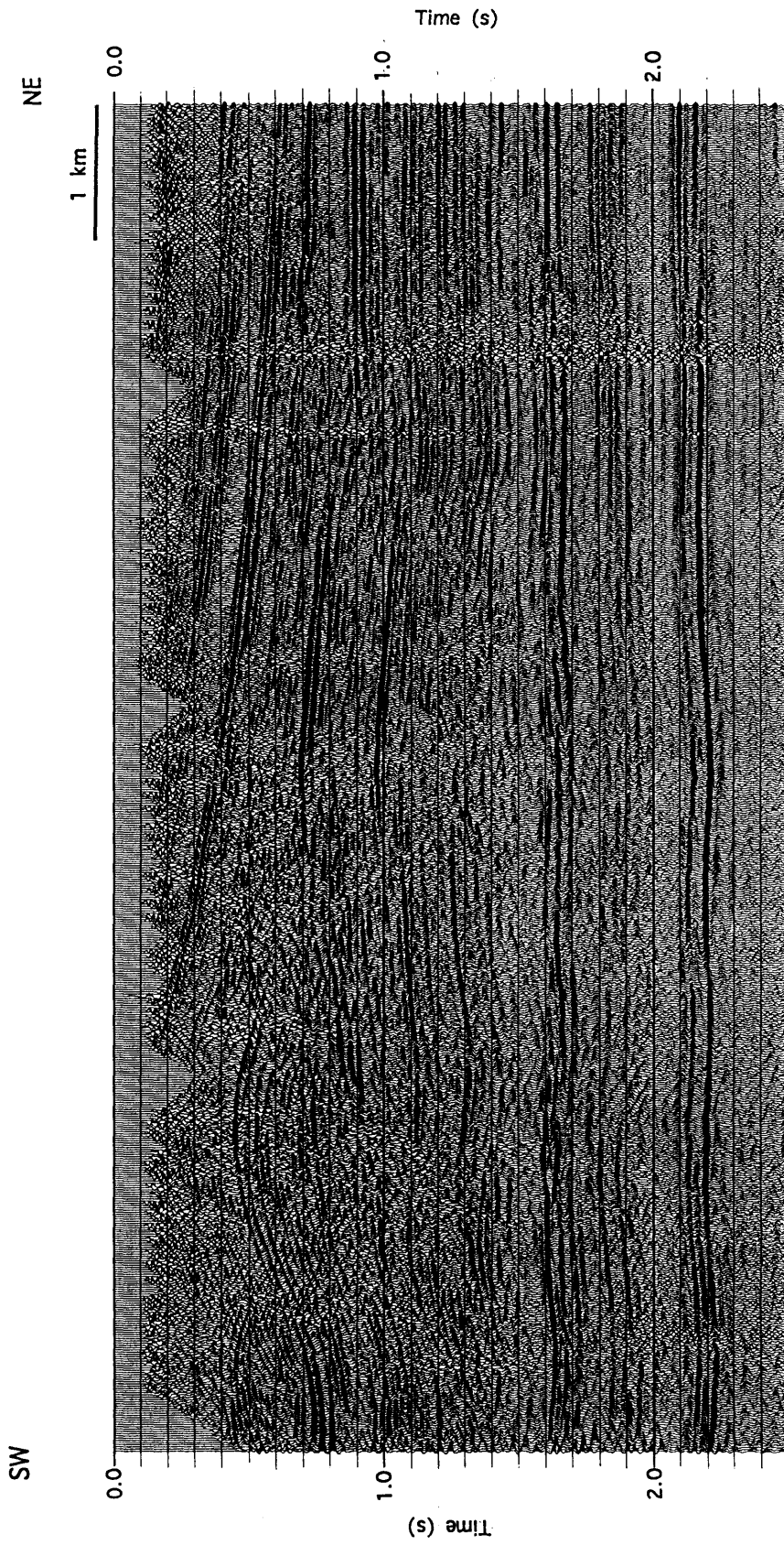


FIG. 3.6. Stacked section of line 2B generated from the flow in Figure 3.1. DMO was not applied to this section.

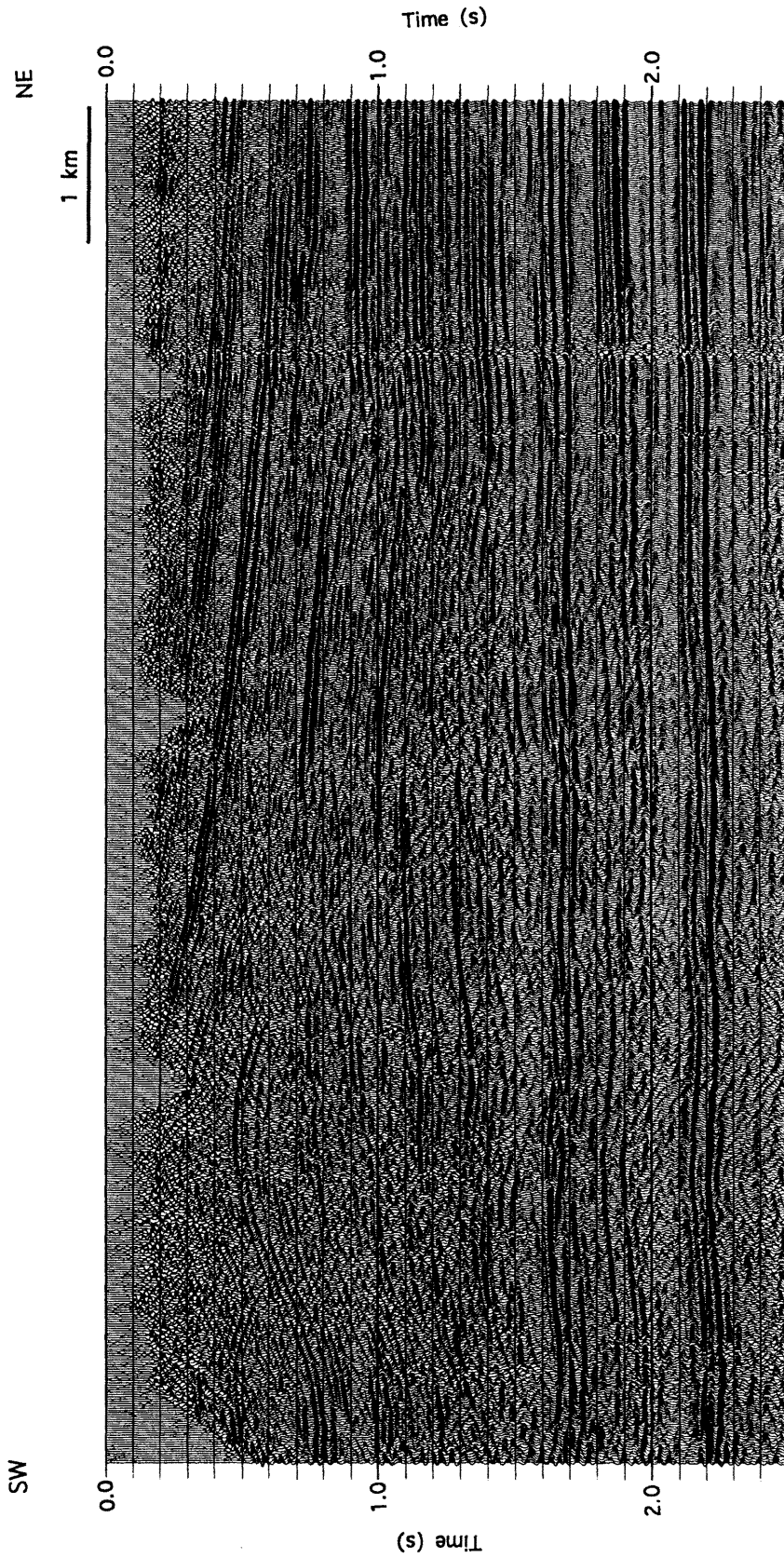


FIG. 3.7. DMO-corrected stacked section of line 2B. Compare this Figure with Figure 3.6 and note that no obvious improved continuity in the Triangle Zone core is obtained.

## 3.5 Poststack Processing

Poststack processing was intended to improve the signal-to-noise ratio of the stacked section and reposition the dipping reflections to their true spatial locations. The poststack processing steps included band-pass filtering, gain, migration and multichannel coherency filtering. Band-pass filtering and gain were discussed previously in prestack processing.

### 3.5.1 Migration

In a stacked seismic section, reflections are plotted directly below their common midpoint locations regardless of their true spatial positions. These reflections represent true subsurface spatial locations only if they were generated from flat reflectors. In the presence of dips, stacked events appear downdip from and with less dip than their true positions (Dobrin and Savit, 1988). In order to obtain correct spatial images of the dipping reflectors, these reflections have to be migrated.

Three migration algorithms, i.e., Stolt ( $f-k$ ) migration (Stolt, 1978), phase-shift migration (Gazdag, 1978) and finite-difference (F-D) migration (Claerbout and Doherty, 1972) were tested on the DMO-corrected stacked section of line 2B. The phase-shift and F-D migrations performed in the depth domain, i.e., downward continuation of the migration operators was defined as a discrete depth step whereas the Stolt migration was applied in the time domain.

#### 3.5.1.1 Finite-Difference Migration

The finite difference (F-D) technique migrates seismic data by means of downward continuation of the one-way scalar wave equation followed by imaging. The imaging principle states that the wavefront shape satisfying  $t = 0$  in the wave equation directly corresponds to the reflector shape at that depth (Yilmaz, 1987). This technique

uses a stacked section as the initial wavefield and downward extrapolates the wavefield in depth with a specified discrete depth step. At each depth step, the wavefield is evaluated for  $t = 0$  to obtain migrated energy. The process is continued for the next depth step until the entire stacked section is migrated.

In practice, the F-D migration technique requires a velocity grid file. This is generated from well velocity information or directly from a stacking-velocity file. The depth-step interval and frequency bandwidth to be migrated also need to be specified. Frequency specifications can be time-variant.

In migrating line 2B, a velocity grid file was generated directly from the stacking-velocity file. A depth-step interval of 20 m, along with time-variant frequencies ranging from 10-80 Hz in the early part, to 7-70 Hz in the later part of the section, were used. These parameters were determined on the basis of iterative tests. However, it was noticed that velocity functions were the most crucial factor in the quality of the migrated outputs. The rms velocity functions that were applied to generate the stacked section were found to result in overmigration, and the optimum velocity functions in this migration were in the range of 70-80 % of the true rms velocity functions.

#### 3.5.1.2 Phase-Shift Migration

The phase-shift technique is based on the same principles as the F-D technique, i.e., downward continuation of the wavefield followed by imaging (Yilmaz, 1987). However, the numerical operations are defined in the frequency-wavenumber domain. Downward continuation of the wavefield is performed by means of a phase-shift or rotation of the phase angles of the Fourier coefficients (Gazdag, 1978).

Practically, the technique requires the same parameters as the F-D migration, i.e., depth-step, frequency and velocity functions. In order to compare the efficiency of these two techniques, the same parameters as applied to the F-D technique were used in this

processing, except for the velocity functions. In specifying the phase-shift migration velocities, the velocity grid file, which is mandatory for the F-D technique, was not required. The rms or interval velocity functions can be applied directly. Similar to the F-D technique, the actual (100%) rms velocity functions produced an overmigrated result, and values of 80% of the actual rms velocity functions were again used.

### 3.5.1.3 Stolt ( $f-k$ ) Migration

The Stolt migration technique is based upon a constant-velocity assumption. Theoretically, it can migrate dips up to 90 degrees but cannot handle strong lateral velocity variation (Dobrin and Savit, 1988). This technique migrates the stacked data by stretching the time section to a pseudo-depth domain to approximate a constant-velocity section, and then Fourier transforming the data into the frequency-wavenumber domain. The migration operation involves mapping the frequency to the vertical wavenumber axis, then inverse Fourier transforming and unstretching the data back into the normal time-space domain.

In practice, the Stolt migration technique requires only one velocity location, along with a desired frequency bandwidth to be migrated. Unlike the F-D and phase-shift techniques, the frequency specifications cannot be time-variant. Initially, a similar frequency range as applied for the F-D and phase-shift migration cases (e.g., between 7 and 80 Hz) were employed. However, it was observed that these parameters produced inferior results in the later part of the section, especially below the Triangle Zone core. Thus, a smaller frequency range of 7-65 Hz was applied which provided a reasonable result. As well, an initial velocity function was arbitrarily selected from the rms-velocity file at approximately the middle of the line. This velocity function was, however, modified iteratively based on comparison of the results from this technique with the F-D and phase-shift results.

### 3.5.2 Coherency Filter

Following migration, signal-to-noise ratio enhancement via the coherency filter was applied (KLSTAK in the ITA software package). The technique analyzes a sliding trace window, containing a specified number of traces, to yield an estimate of the coherent component of that window. The input data trace in the middle of the analyzed window is then replaced by the estimated component. The sliding window is then advanced by a single trace between successive analyses (ITA Insight/1 Poststack Reference Guide, 1992). Three traces within each selected window were found to yield optimum outputs in both lines 2A and 2B.

The final migrated stacks of line 2B based on the F-D, phase-shift and  $f-k$  techniques are displayed in Figures 3.8, 3.9 and 3.10 respectively. The final  $f-k$  migrated stacks of line 2A and line 3 are shown in Figures 3.11 and 3.12. Comparison among Figures 3.8 to 3.10 indicates that velocity variations across the Triangle Zone core in this region may not be too severe. This was inferred from the observation that all of these migration algorithms yielded similar results in terms of the repositioning of events and improvement in signal-to-noise ratio. However, careful inspection of these migrated sections shows that smeared events below the core of the Triangle Zone are still present. These may be the result of including incoherent full-offset traces in the stack. It was therefore decided to undertake offset-limited stack tests to determine if using only near-offset traces to stack can improve the image of reflectors below the Triangle Zone core.

### 3.5.3 Offset-Limited Stack

The initial stacks produced in this study used every trace within each CMP gather. The stacking process assumes that all traces are perfectly NMO-corrected before being stacked. However, in real data this assumption is often violated. In a complex structural environment, the seismic traveltimes depart from hyperbolic moveout at long offset due

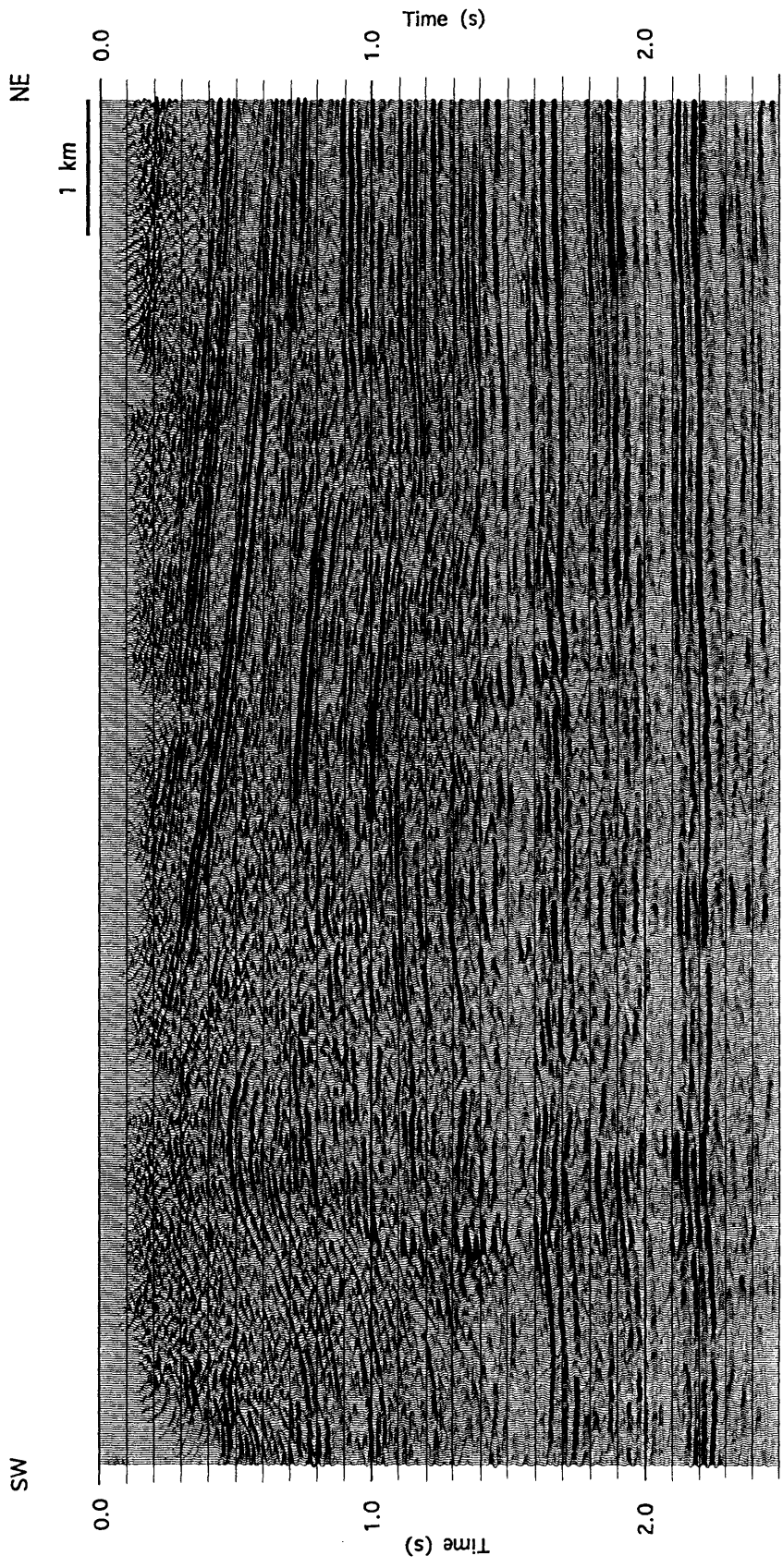


FIG. 3.8. F-D migrated section of the DMO corrected stack of line 2B using 80% of true rms velocities. The maximum dips to migrate were 85 degrees, along with frequency bandwidth between 7-80 Hz.

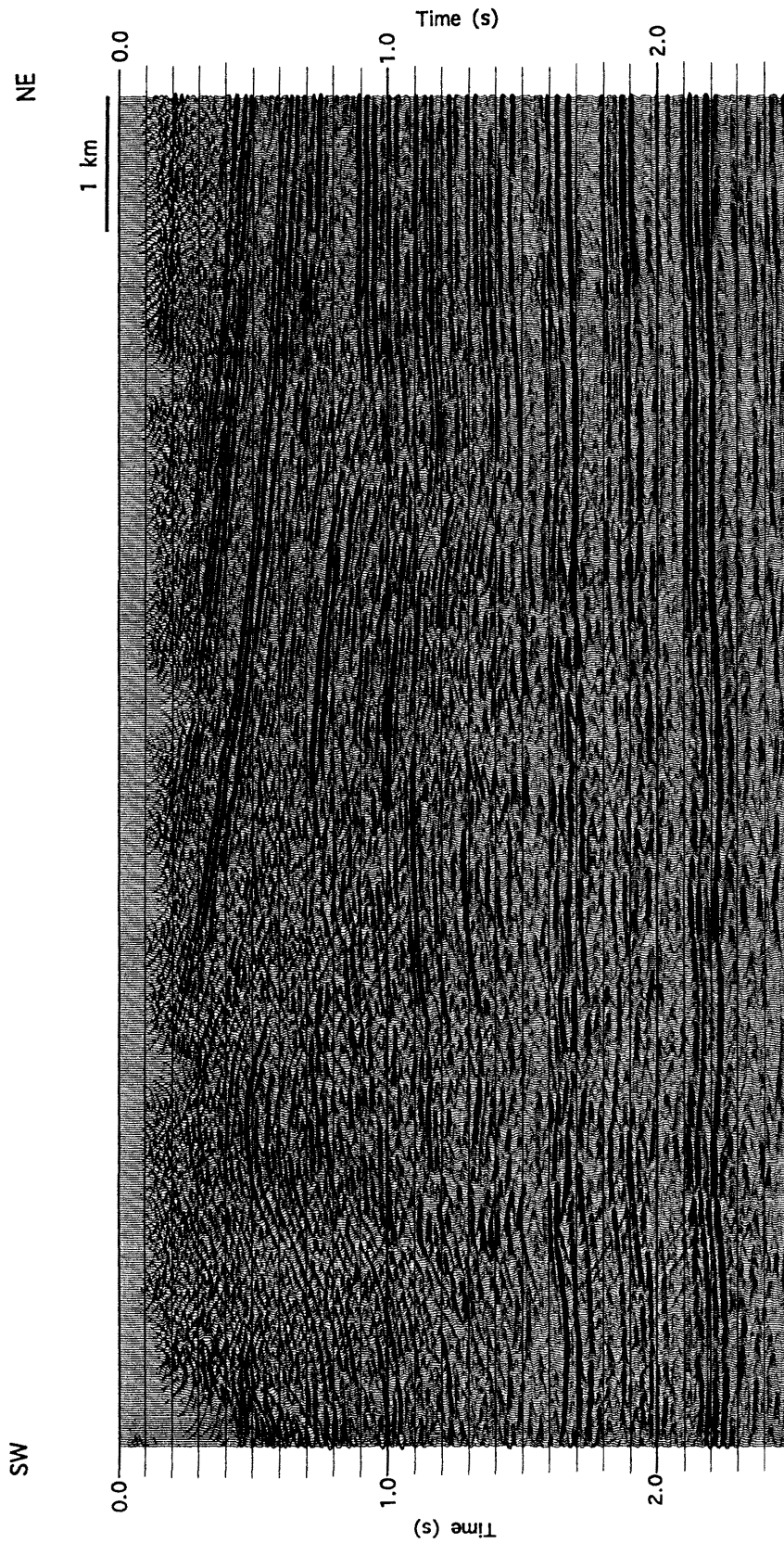


FIG. 3.9. Phase-shift migrated section of the DMO corrected stack of line 2B using 80% of true rms velocities. The maximum dips to migrate were 85 degrees, along with frequency bandwidth between 7-80 Hz.

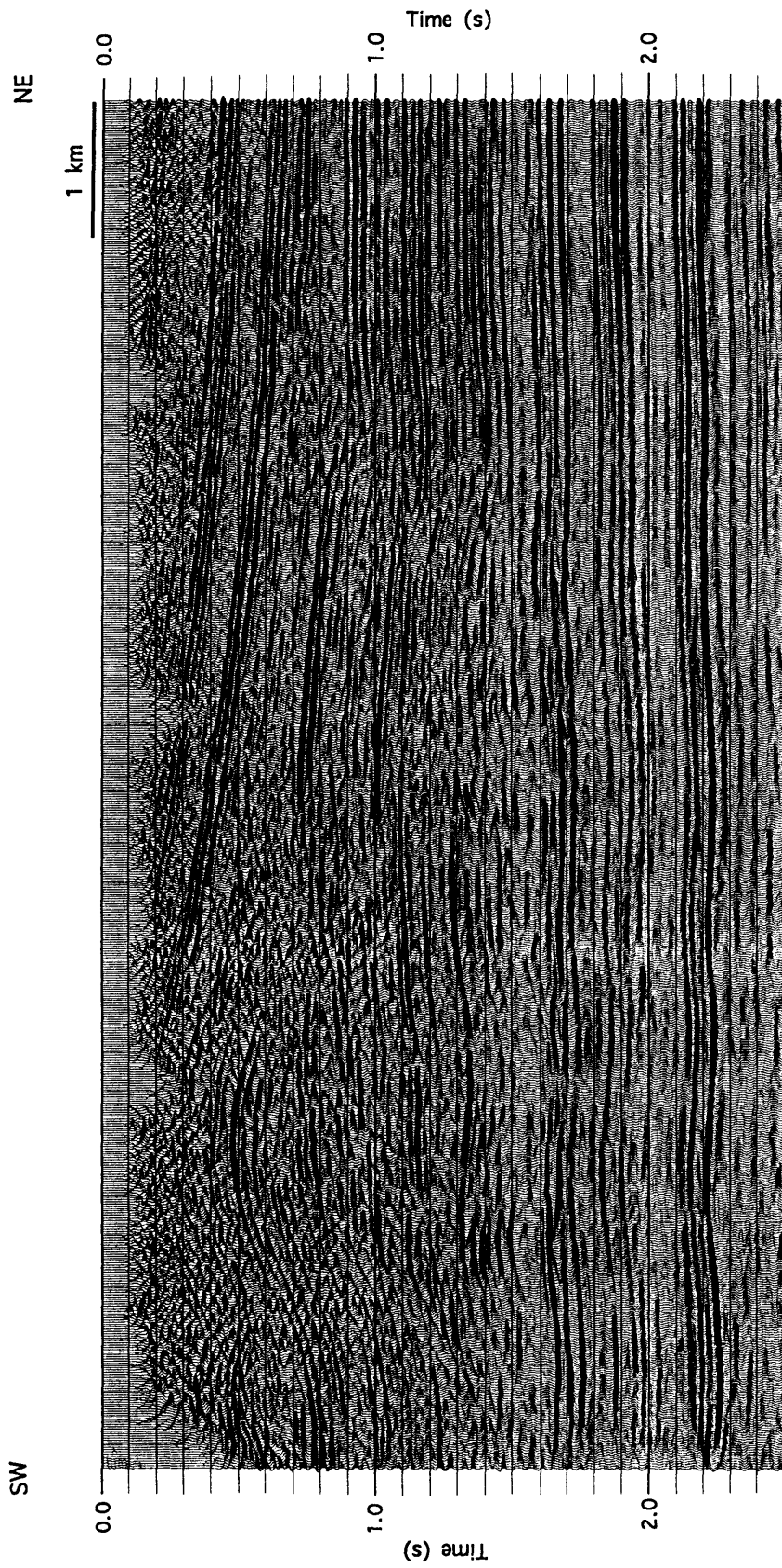


FIG. 3.10. Stolt ( $f-k$ ) migrated section of the DMO corrected stack of line 2B using frequency bandwidth between 7-65 Hz.

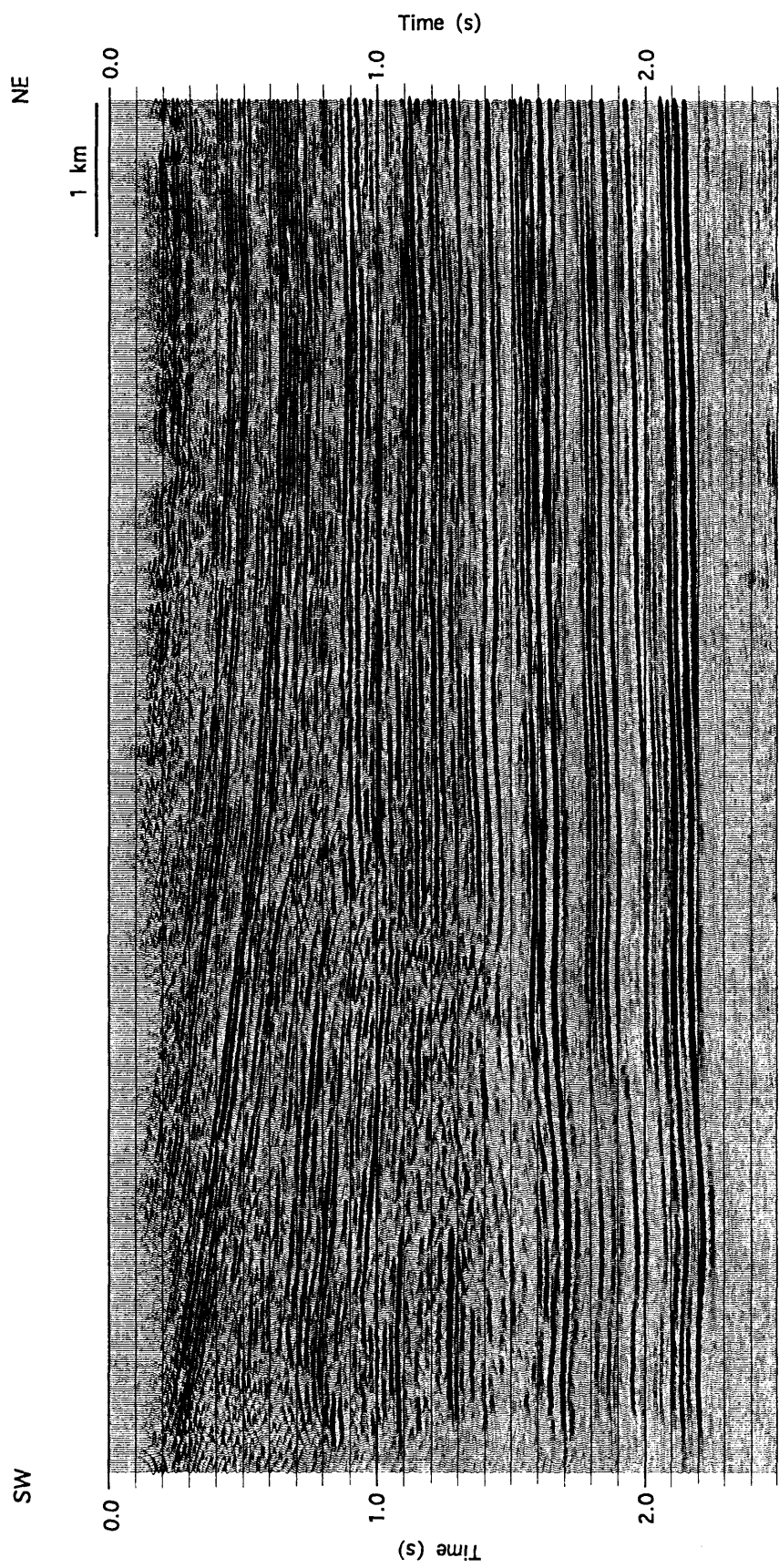


FIG. 3.11. Final ( $f-k$ ) migrated stack of line 2A.

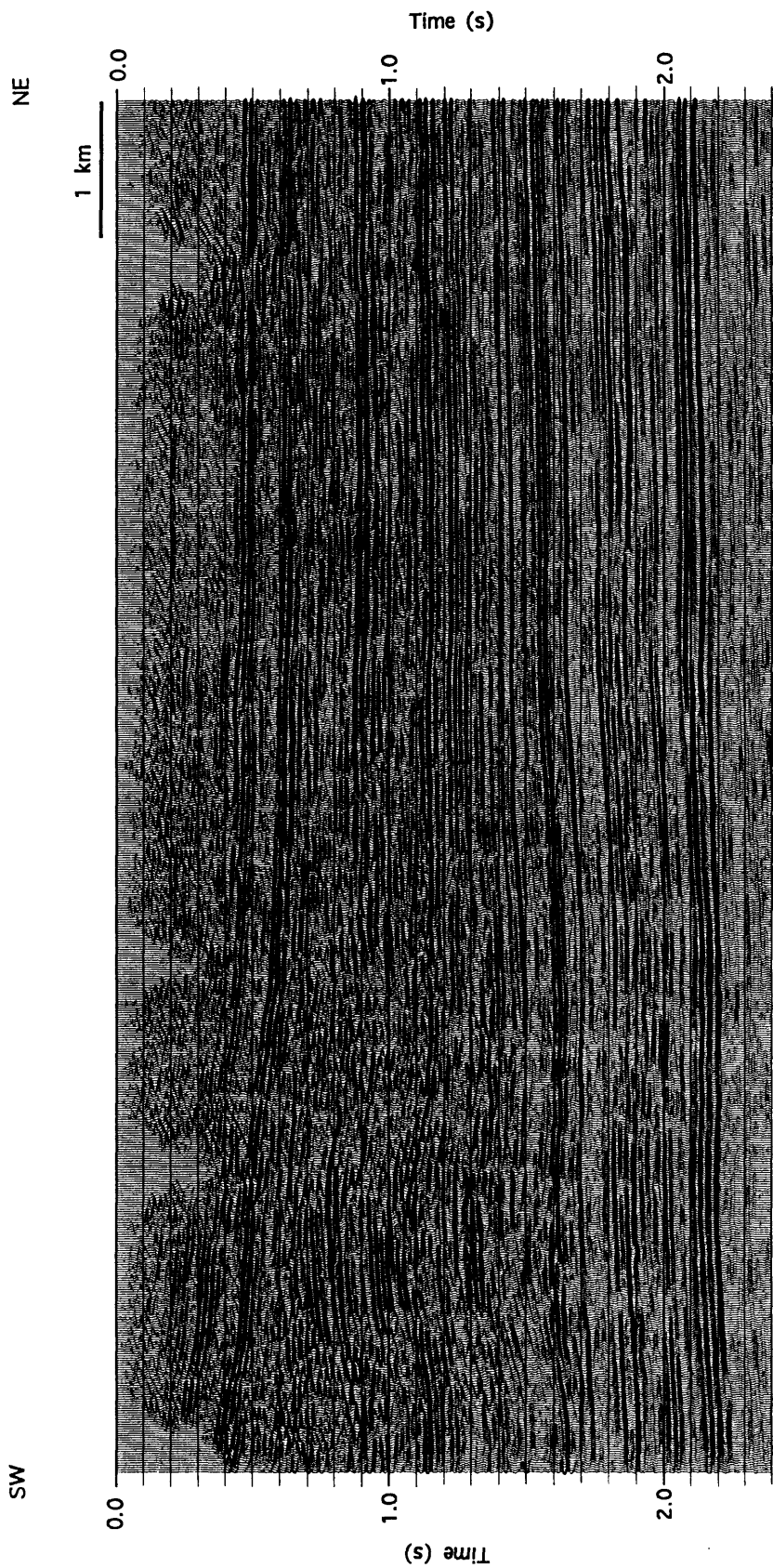


FIG. 3.12. Final ( $f-k$ ) migrated stack of line 3.

to the overlying velocity structure. Also, phase distortion from NMO stretch and directivity effects (Hatton et al., 1988), including possible interference from converted-shear waves are more pronounced at far offsets.

These problems imply that using only near-offset traces in the stack should produce a better result in terms of reflection continuity. However, a significant drawback of this technique is the correspondingly lower signal-to-noise ratio of the output, as the multiplicity or fold is reduced proportionally.

Using source-receiver offset ranges from -1500 to 1500 m, -2000 to 2000 m and -2500 to 2500 m, with respect to the full offset range of -3993 to 3993 m, offset-limited stack sections were generated based on the same processing procedures that were applied to the full-offset processing. The  $f$ - $k$  migrated stacks of line 2B, based on these offset ranges, are plotted in Figures 3.13 to 3.15 respectively. Improved reflection continuity, particularly for events below the antiformal stack (indicated by arrows in Figures 3.14) can be seen. However, it is observed that the achievements from this method were limited to certain offset ranges, e.g., from -2500 to 2500 m or -2000 to 2000 m. Further reduction in offset to 1500 m or less did not improve the quality of the output. Instead, events below the antiformal stack are contaminated with noise due to the reduced signal-to-noise ratio.

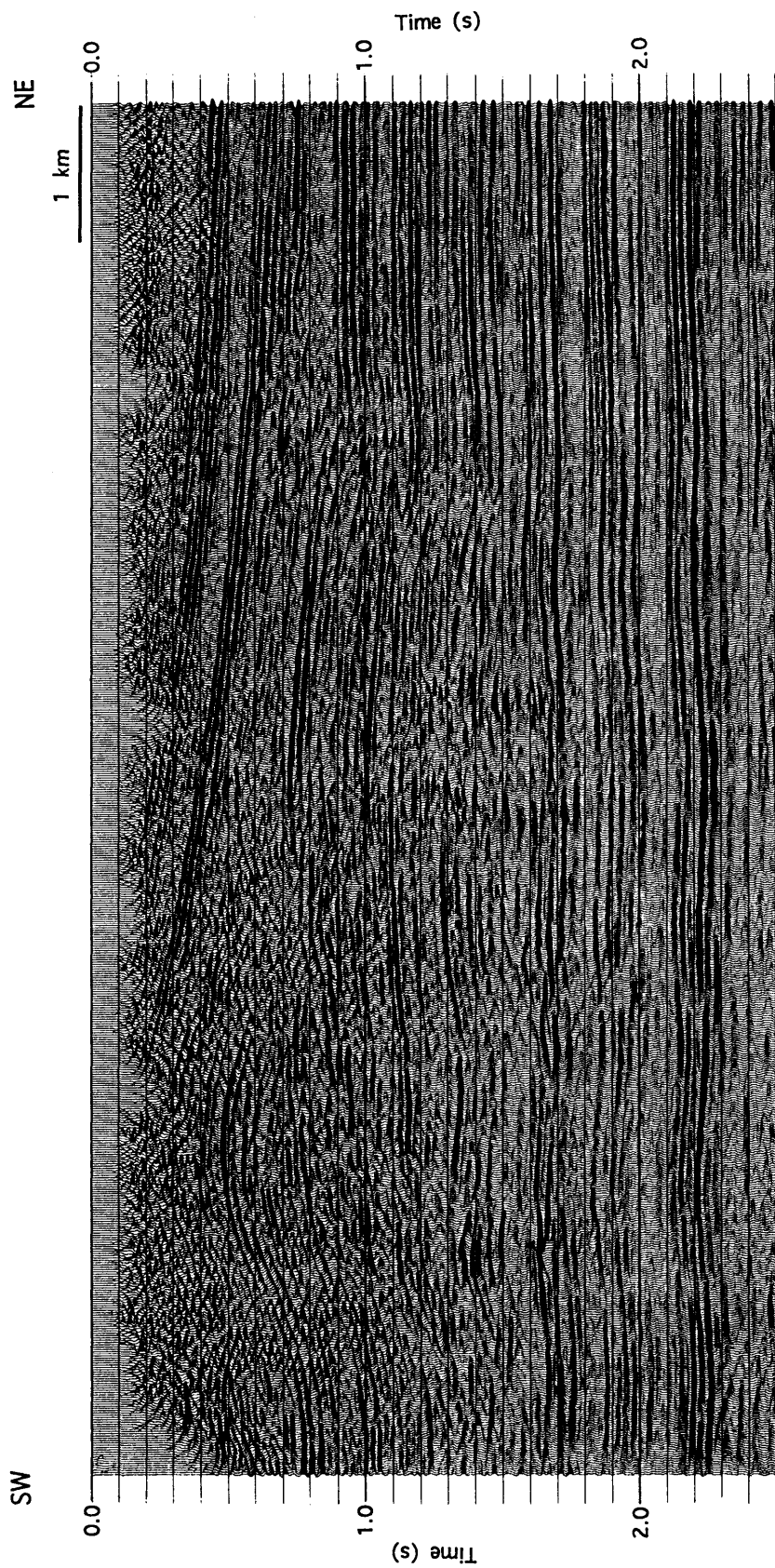


FIG. 3.13. Stolt ( $f-k$ ) migrated section of the offset limited stack using traces within an offset -1500 to 1500 m with respect to the full offset range of -3993 to 3993 m.

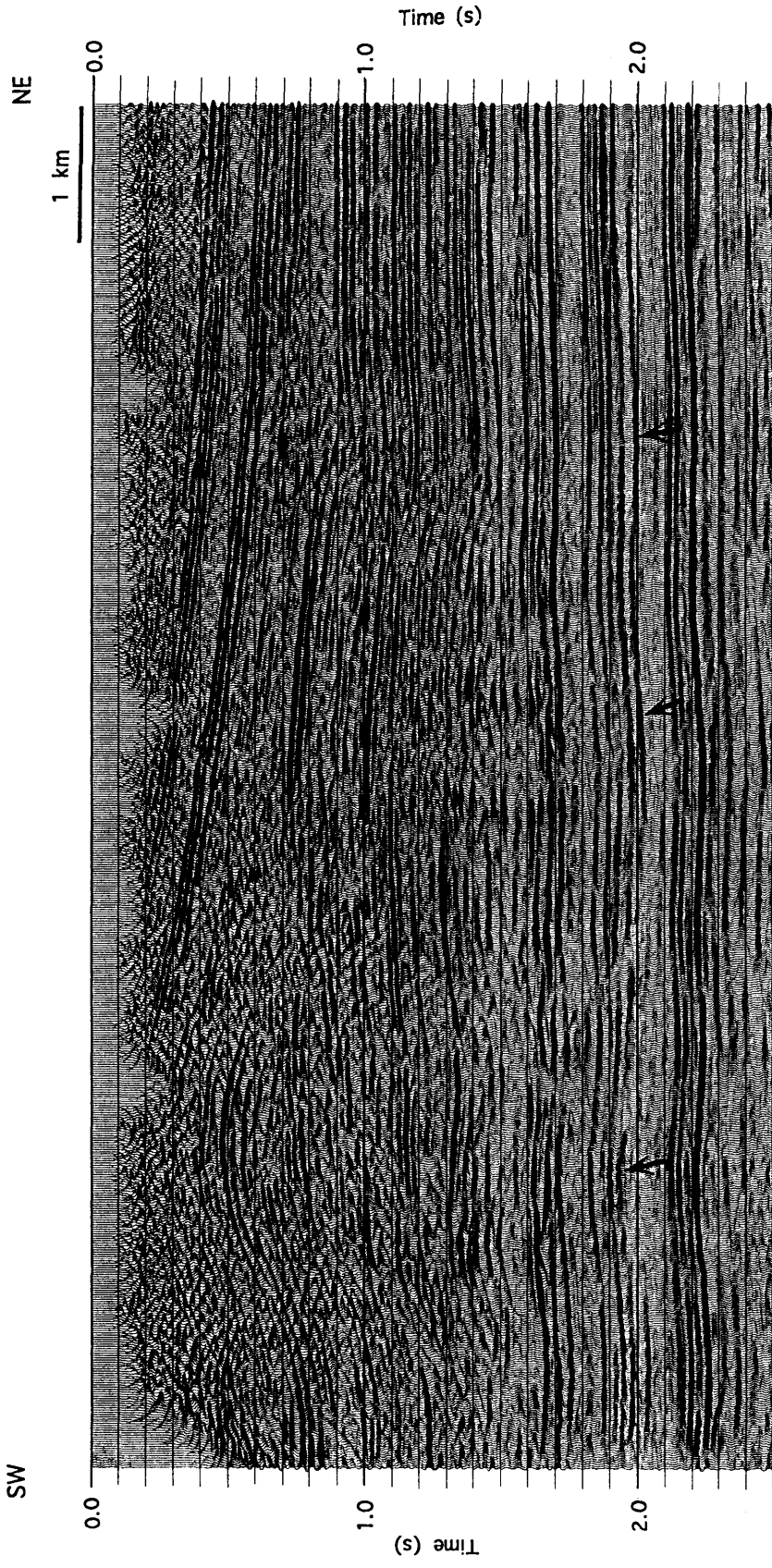


FIG. 3.14. Stolt ( $f-k$ ) migrated section of the offset limited stack using traces within an offset -2000 to 2000 m with respect to the full offset range of -3993 to 3993 m. Compare this Figure with the full-offset migrated section in Figure 3.10 and note improved continuity of reflections indicated by arrows.

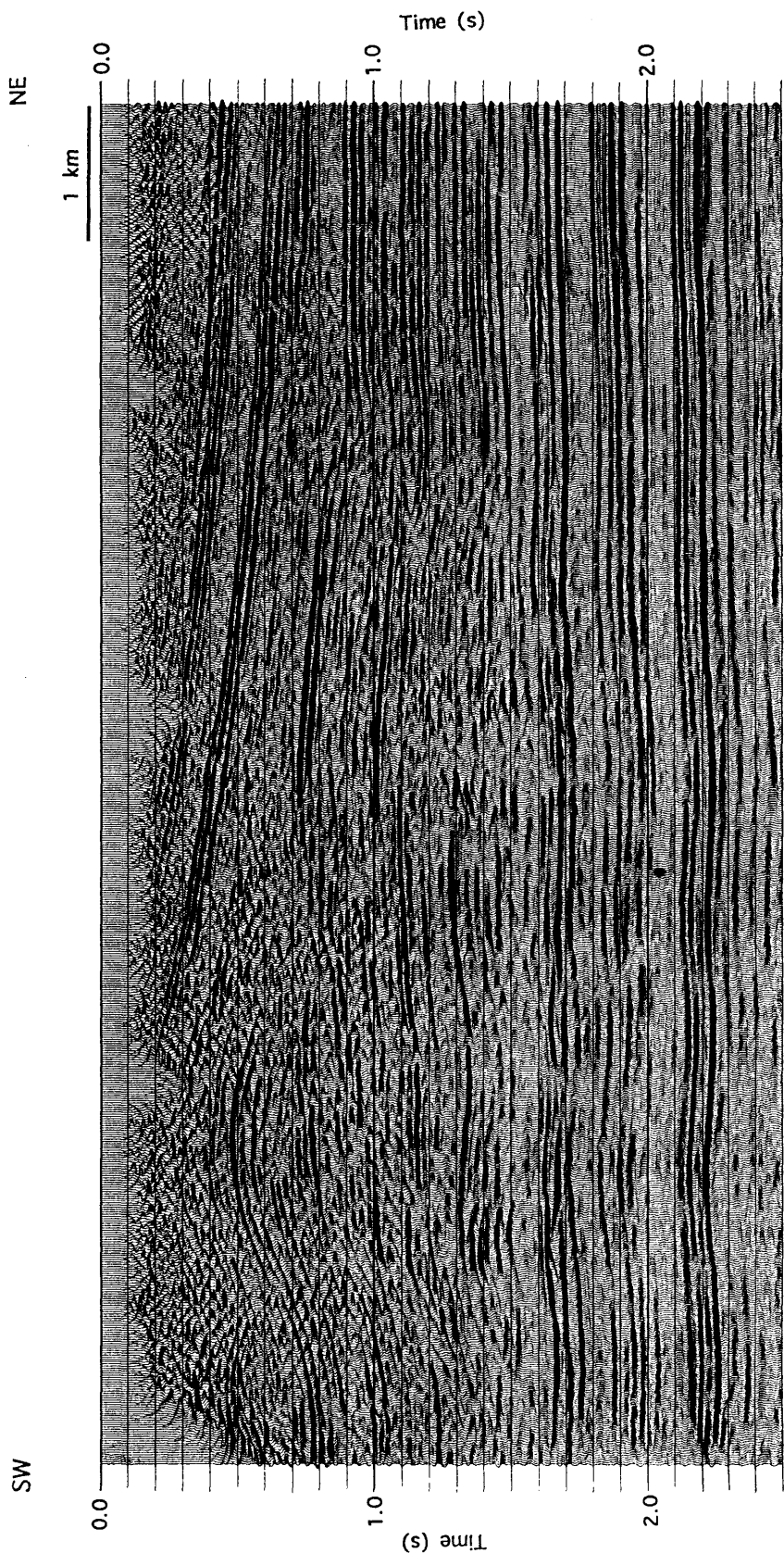


FIG. 3.15. Stolt ( $f-k$ ) migrated section of the offset limited stack using traces within an offset -2500 to 2500 m. Compare this Figure with Figures 3.10 and 3.14, and note the same improvements of reflection continuity as indicated by arrows in Figure 3.14.

## **Chapter 4 - SEISMIC INTERPRETATION**

### **4.1 Introduction**

This chapter discusses the interpretation of the processed seismic data, including techniques used and assumptions made to constrain the interpretation of the structural geometry in the study area. The seismic line locations, surface geology and stratigraphy of the key geologic markers used have been presented in Chapter 2.

Major discussions in this chapter are directed towards the Triangle Zone geometry and other frontal thrust structures in this region. Specific topics addressed are the geometries of the upper and lower detachments, antiformal stack and pop-up structure, rock sequences overlying and underlying the Triangle Zone, and techniques for constructing balanced cross-sections.

Initial interpretation of these structural features was undertaken based mainly on seismic character and well information in the study area. The concepts of the Triangle Zone and thrust-front structural styles, as discussed by Jones (1982), Butler (1982), Charlesworth et al. (1987), Vann et al. (1986) and Morley (1986) were also incorporated to constrain the interpretation. However, the final interpreted geometry was obtained from cross-section balancing which was performed in collaboration with Gregory S. Soule (The University of Calgary).

### **4.2 Seismic Correlation and Interpretation**

Synthetic seismograms, generated from sonic and density logs in wells located along the line 2B and line 3, were used to correlate the seismic data to the geology. Correlations between seismic data and these synthetic seismograms are displayed in Figures 4.1 to 4.5. The markers indicated in the correlations were obtained from the Correlation Chart of the ERCB (Energy Resources Conservation Board). Generally, ties

### WELL 16-6-32-5W5

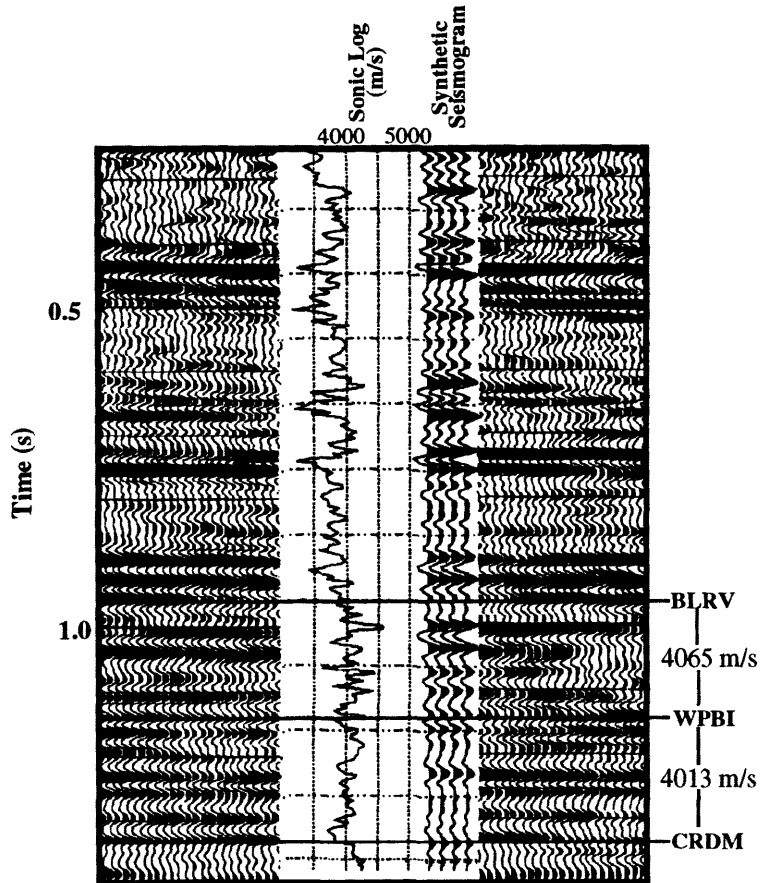


FIG. 4.1. Correlation between synthetic seismogram, sonic log and a portion of seismic line 2B at well 16-6-32-5W5. Velocities indicated are average interval velocities. A Ricker wavelet with a central frequency of 30 Hz is used to construct the seismogram. Locations of the well and seismic line are shown in Figure 2.3, (BLRV=Belly River, WPBI=Wapiabi, CRDM=Cardium).

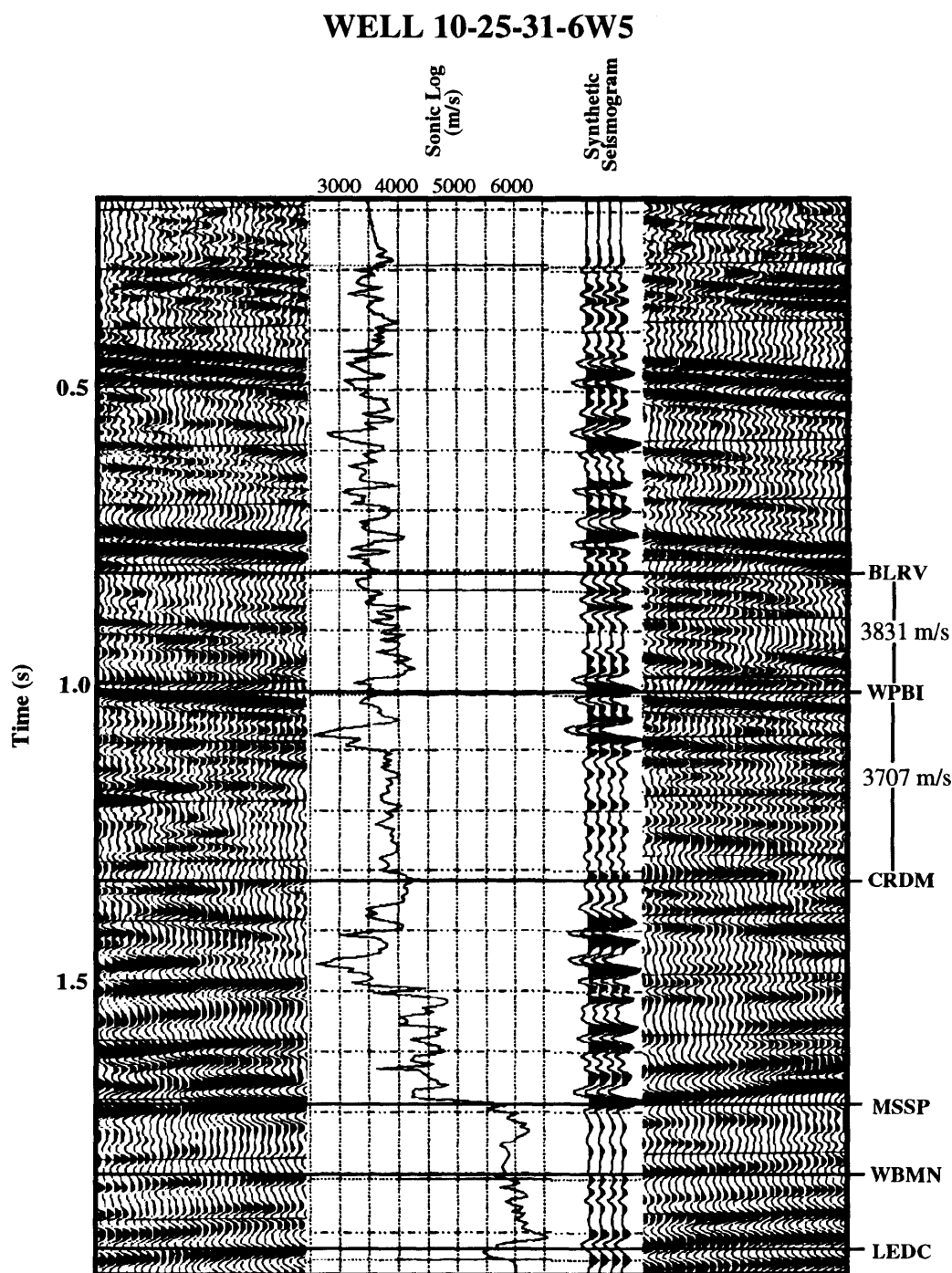


FIG. 4.2 Correlation between synthetic seismogram, sonic log and a portion of seismic line 2B at well 10-25-31-6W5. Velocities indicated are average interval velocities. A Ricker wavelet with a central frequency of 30 Hz is used to construct the seismogram. Locations of the well and seismic line are shown in Figure 2.3, (BLRV=Belly River, WPBI=Wapiabi, CRDM=Cardium, MSSP=Mississippian, WBMN=Wabamun, LEDC=Leduc).

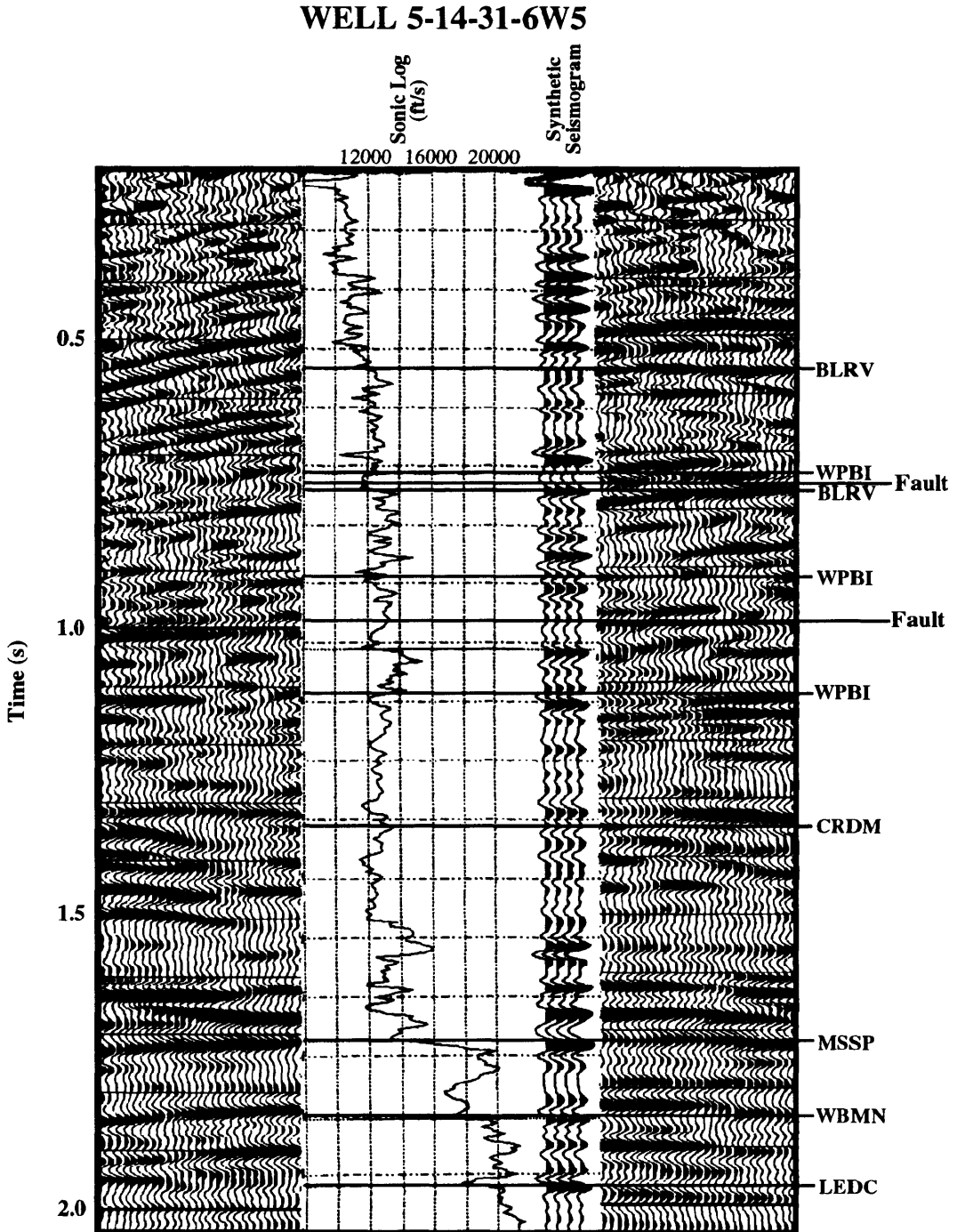


FIG. 4.3. Correlation between synthetic seismogram, sonic log and a portion of seismic line 2B at well 5-14-31-6W5. A Ricker wavelet with a central frequency of 30 Hz is used to construct the seismogram. Locations of the well and seismic line are shown in Figure 2.3.

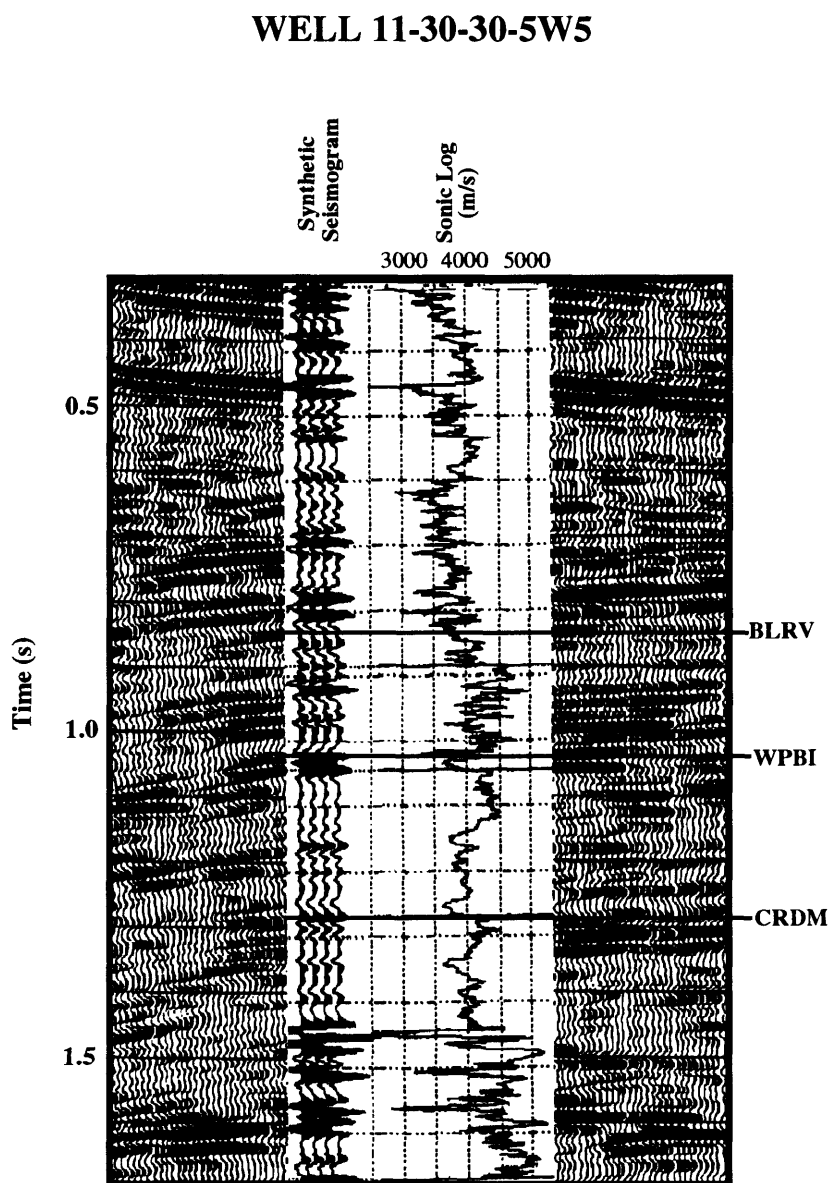


FIG. 4.4. Correlation between synthetic seismogram, sonic log and a portion of seismic line 3 at well 11-30-30-5W5. A Ricker wavelet with a central frequency of 33 Hz is used to construct the seismogram. Locations of the well and seismic line are shown in Figure 2.3.

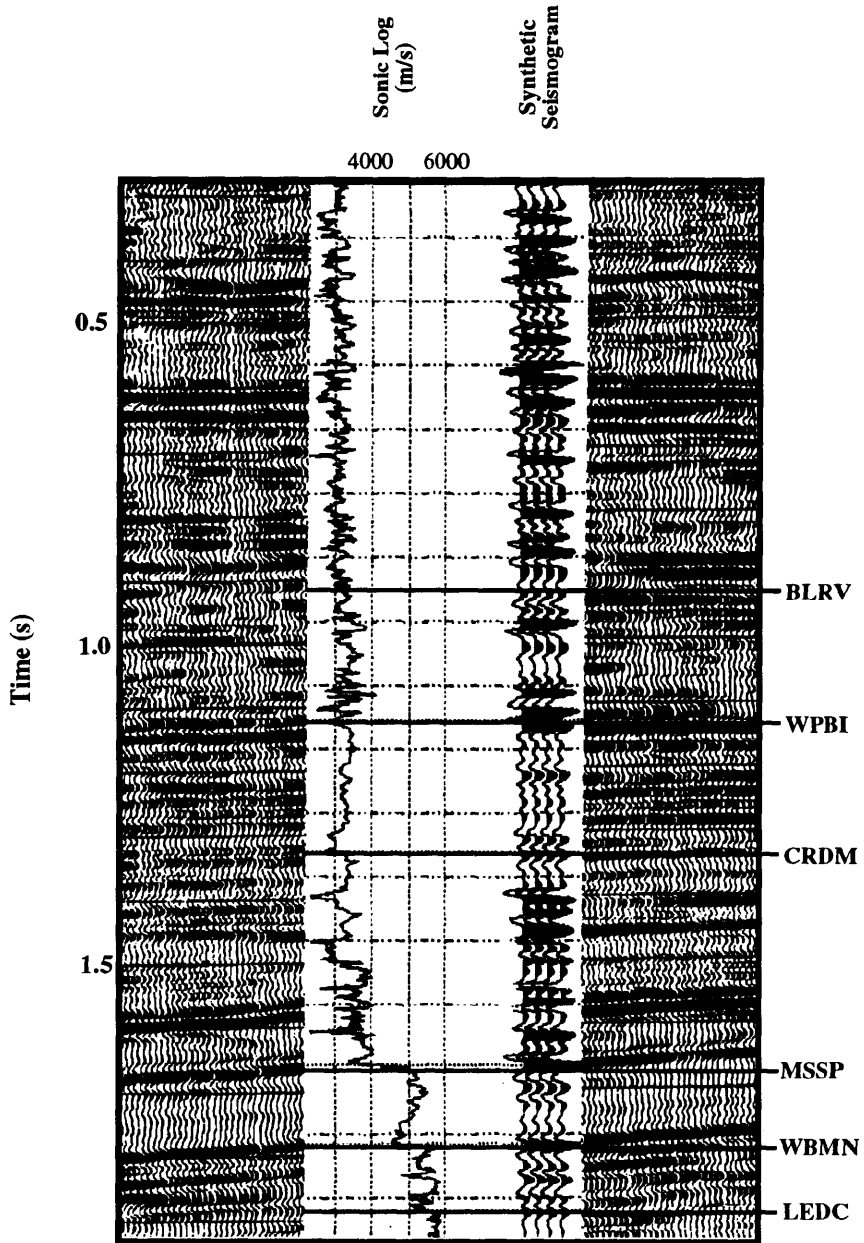


FIG. 4.5. Correlation between synthetic seismogram, sonic log and a portion of seismic line 3 at well 6-4-31-5W5. A Ricker wavelet with a central frequency of 35 Hz is used to construct the seismogram. Locations of the well and seismic line are shown in Figure 2.3.

and correlations at these well locations are reasonable in terms of seismic character and time intervals between key geologic markers, particularly for the easternmost wells of the study area (i.e., 16-6-32-5W5 and 6-4-31-5W5). For the wells in the western, structurally complex parts of the lines (i.e., 11-30-30-5W5, 10-25-31-6W5 and 5-14-31-6W5), ties and correlations were slightly difficult due to the presence of dipping reflectors and also because the seismic data quality deteriorates slightly in this area. Initial ties between synthetic seismograms and seismic data were made on later events, e.g., Mississippian and Devonian horizons which are relatively flat and can be identified across the seismic sections. Subsequently, geological markers in the early parts of synthetic seismograms were transferred to the seismic data with reference to these deep correlations. Interpretations of the seismic data are displayed in Figures 4.6 to 4.8 for lines 2B, 2A and 3 respectively. The seismic data image frontal structures in the Triangle Zone. An antiformal stack is imaged at the western end of line 2B, and is bounded by roof and floor thrusts. A pop-up feature, enclosed by relatively young thrust faults, is interpreted to exist to the east of the main structural high on all three seismic sections.

The upper detachment of the Triangle Zone in this region exhibits a listric trajectory and dips towards the foreland at an angle of approximately 10 degrees in the west, decreasing to zero degrees in the east where it parallels bedding planes in Upper Cretaceous rocks. The lower detachment is interpreted as being blind and exhibits a staircase geometry with a ramp dipping to the southwest. The ramp cuts up-section through the Cretaceous sequences towards the foreland, connected to a long flat which is parallel to the upper detachment.

Beneath the Triangle Zone core, an undulating geometry of Paleozoic rocks is interpreted. They are considered to be velocity pull-up effects caused by lateral velocity variations in the shallow parts of the sections, associated with subtle compressional structures in the foreland.

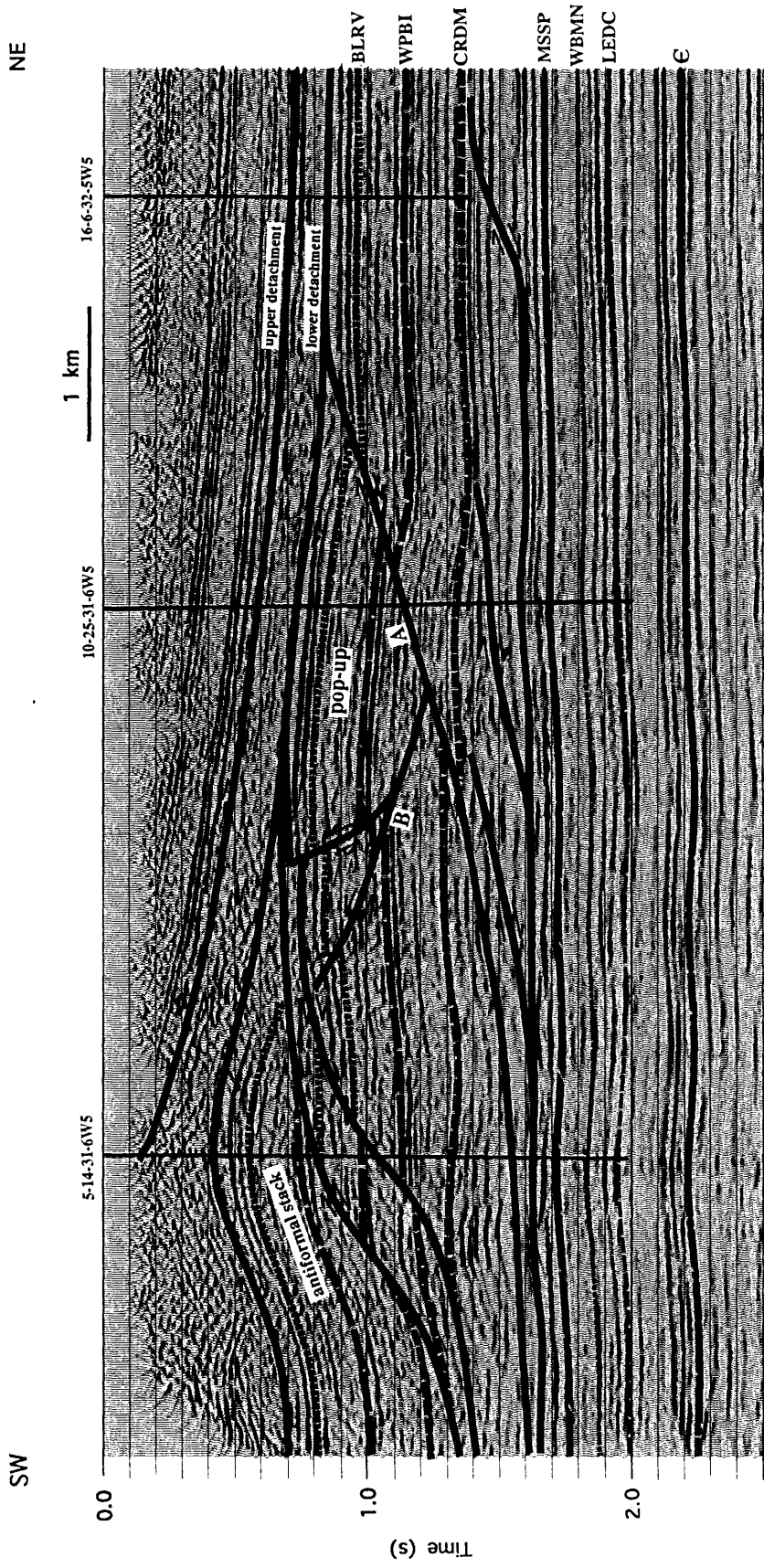


FIG. 4.6. Interpretation of seismic line 2B. The uninterpreted section is shown in Figure 3.14. The frontal ramp and back thrust are indicated by A and B respectively. Time structural contour maps of these faults are shown in Figure 4.11.

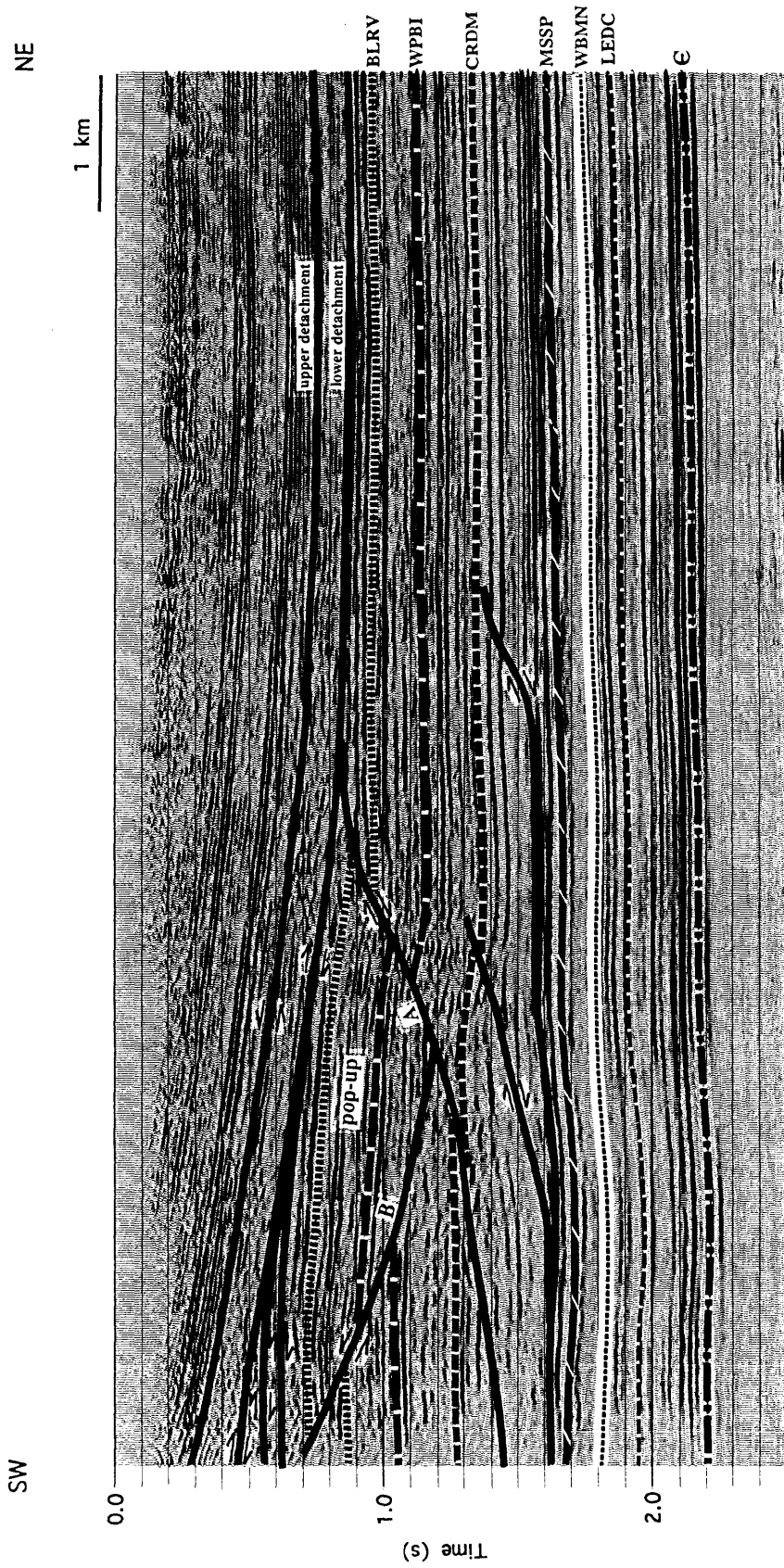


FIG. 4.7. Interpretation of seismic line 2A. The uninterpreted section is shown in Figure 3.11. The frontal ramp and back thrust are indicated by A and B respectively.

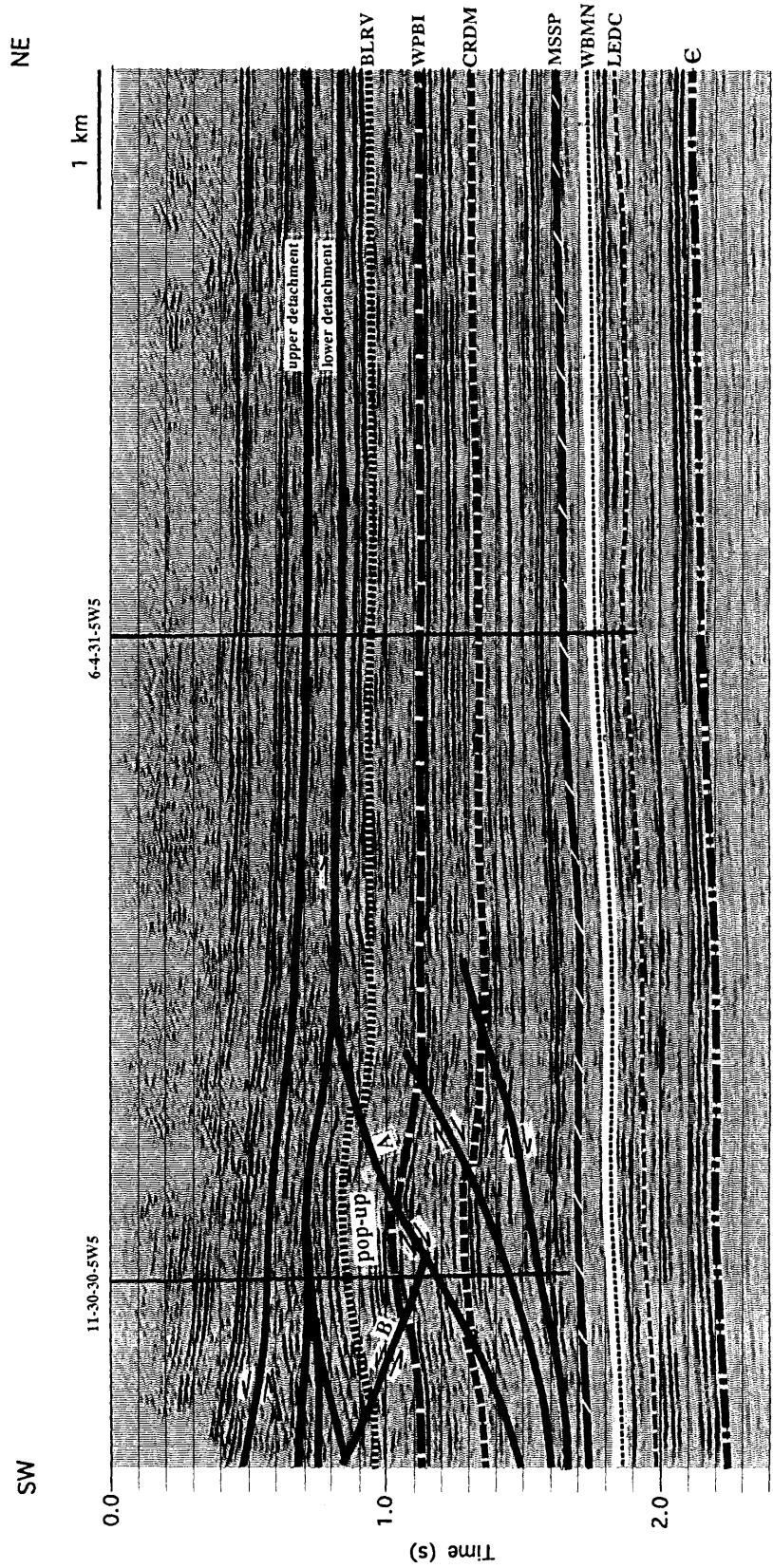


FIG. 4.8. Interpretation of seismic line 3. The uninterpreted section is shown in Figure 3.12. The frontal ramp and back thrust are indicated by A and B respectively.

The following are detailed structural interpretations and descriptions of the structural features in the study area:

#### **4.2.1 The Upper and Lower Detachments**

The upper detachment is a structural boundary that separates the allochthonous wedge of Upper Cretaceous rocks in its footwall from relatively undeformed Upper Cretaceous and Tertiary strata in its hanging wall. Its stratigraphic position was interpreted from the seismic sections in that reflections below this horizon are chaotic and discontinuous, whereas those above it are relatively layered and conformable, indicating an unconformity or abrupt change in seismic character. With respect to structural style of the Triangle Zone in Alberta (Jones, 1982; Charlesworth et al., 1987), the upper detachment is a back thrust possessing a southwesterly vergence. Time-to-depth conversion based on available velocity information indicates that the upper detachment in the study area has a very low dip of approximately 10 degrees in the west. Its dip gradually decreases to the northeast of the section and it becomes flat, running along bedding planes of Upper Cretaceous rocks. Differential folding of the upper detachment, due to underthrusting below it, can also be seen locally (Figure 4.8).

The ramp of the lower detachment or floor thrust can be defined rather clearly on seismic line 2B. It is interpreted on the basis of the abrupt termination and displacements of the key seismic horizons, i.e., the Belly River, Wapiabi and Cardium events (Figure 4.6). The lower detachment is northeasterly verging and exhibits a staircase geometry with a southwest-dipping ramp that cuts up-section through the Cretaceous sequences towards the foreland. The ramp angle, measured from the interpreted seismic data, is approximately 30 degrees. The ramp is connected to a long upper flat, which is here interpreted to be parallel to the upper detachment, so that strain of rocks dissipates between these two horizons (see section 4.3 for an alternative interpretation). The lower

flat of the lower detachment cannot be identified easily in the seismic data. However, it is expected to be located slightly above the Mississippian rocks. This was inferred from the geometry of the forethrust of the pop-up structure and other minor thrusts seen in the eastern part of the seismic sections, which all detach along a horizon above the Mississippian event (discussed in section 4.2.3).

It should be noted that the fault that bounds the eastern side of the pop-up structure (Figures 4.10) can be regarded as the most recent lower detachment in this region. However, for convenience in discussion and explanation, it is termed the forethrust in this thesis and will be discussed separately in section 4.2.3.

#### **4.2.2 Antiformal Stack**

An antiformal stack of horses of Cretaceous rocks is found beneath the surface expression of the Triangle Zone. Figure 4.9 shows a close-up view of this structural feature taken from seismic line 2B. It is bounded on its top and bottom by roof and floor thrusts which converge towards the east. The horses enclosed in the antiformal stack dip to the southwest and are folded by the emplacement of younger horses below them. The uppermost horse is more folded and its ramp is separated laterally from the lowermost horse. Faults within the antiformal stack also exhibit a staircase geometry with relatively steeply southwest-dipping ramps. These faults are in fact relict lower detachments which were abandoned and incorporated into the hanging wall of the more frontal thrust during the foreland-directed advancement of the intercutaneous wedge (Charlesworth et al., 1987).

#### **4.2.3 Pop-Up Structure**

The pop-up structure is formed beneath the west flank of the Alberta syncline, approximately 2 km to the east of the antiformal stack (Figures 4.6-4.8 and Figure 4.10).

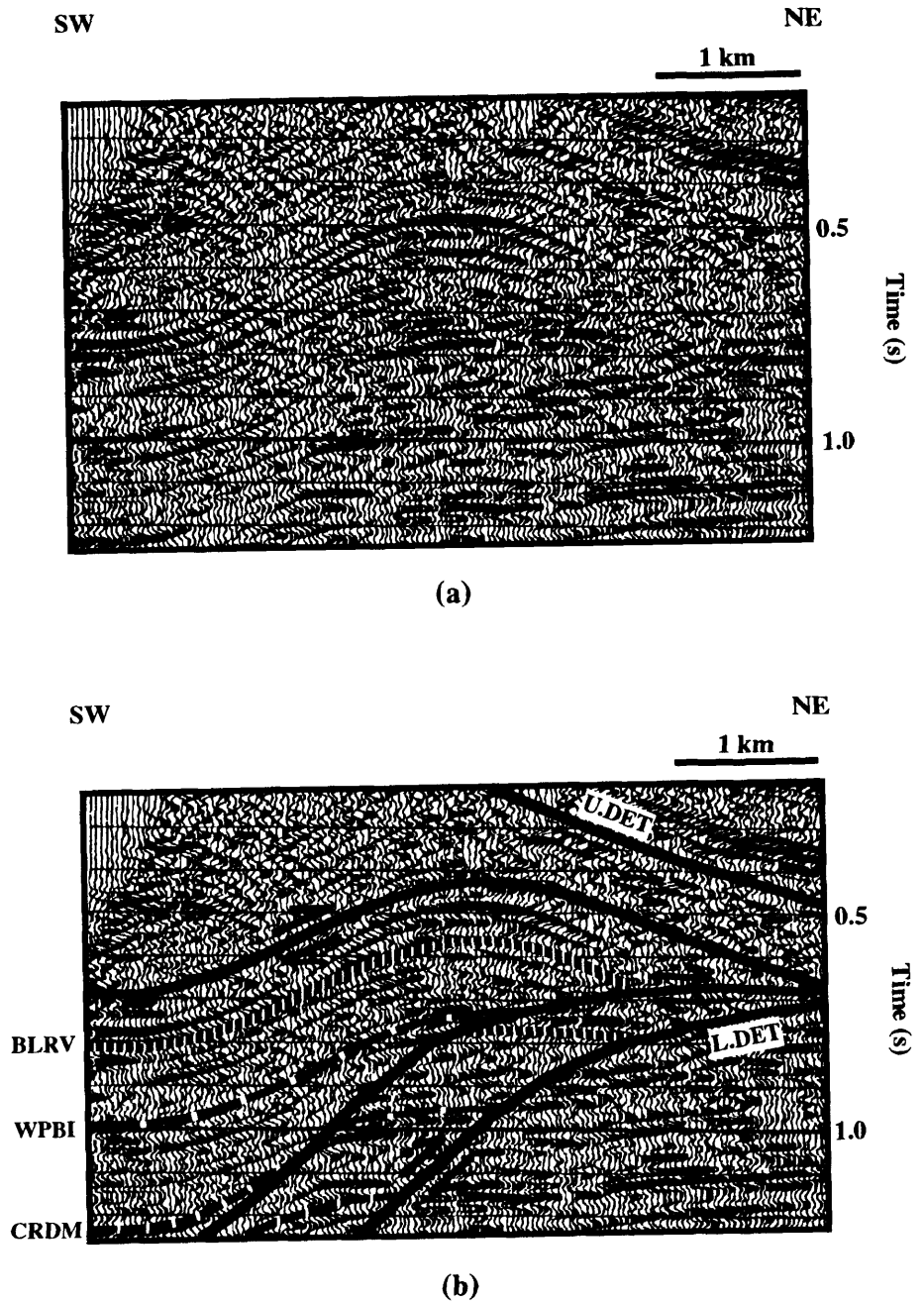


FIG. 4.9. Close-up view of the antiformal stack, without interpretation (a) and with interpretation (b). The section was taken from seismic line 2B (Figure 4.6).

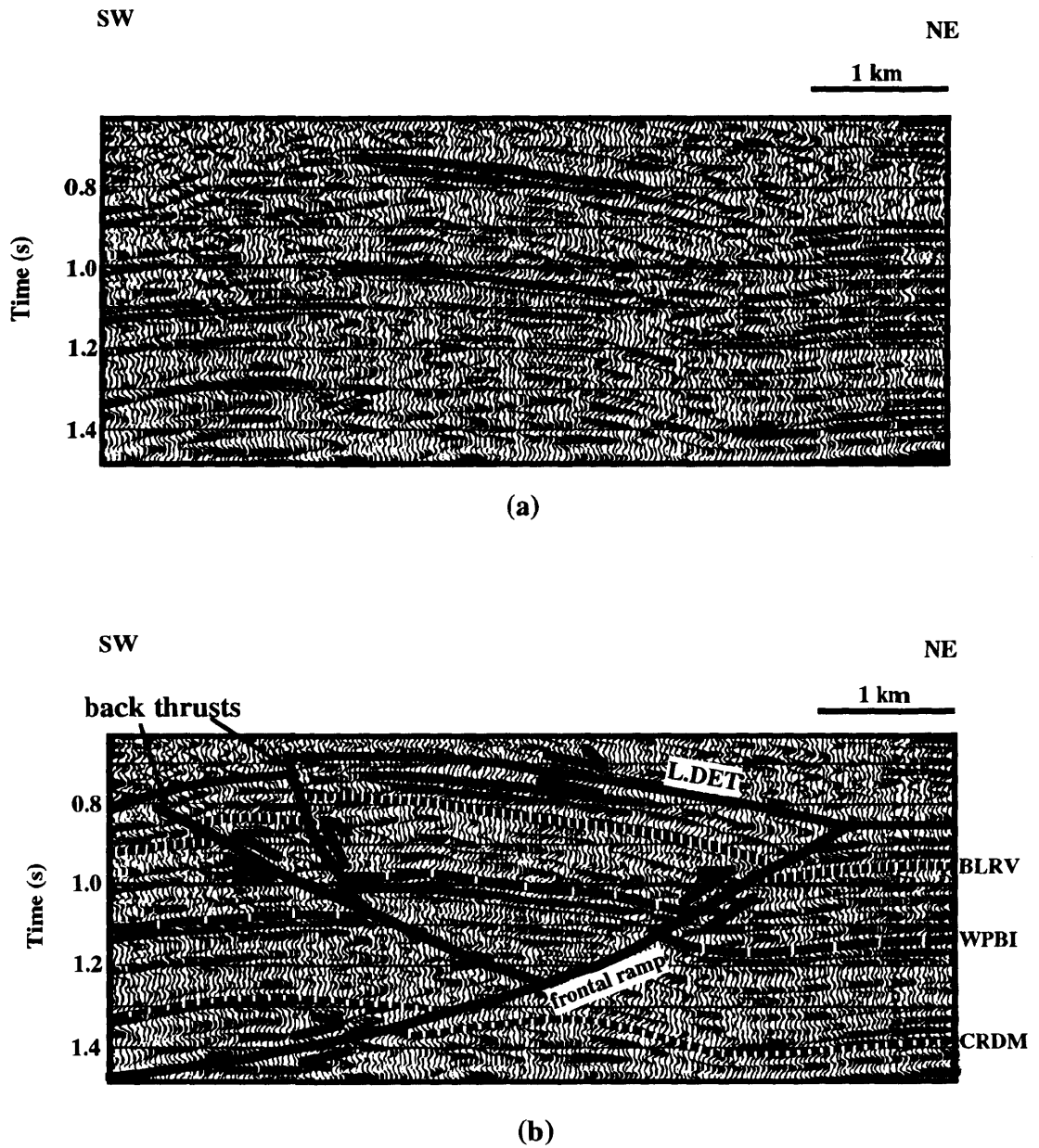


FIG. 4.10. Close-up view of the pop-up structure, without interpretation (a) and with interpretation (b). The section was taken from seismic line 2B (Figure 4.6).

It is enclosed between three faults; namely, an abandoned lower detachment along its top, and on its eastern and western sides by a northeast-verging forethrust and a southwest-verging back thrust respectively. The pop-up forethrust is listric in style and is interpreted to detach above Mississippian rocks, presumably within the Jurassic Fernie Group. The pop-up back thrust displays a smooth listric trajectory that steepens upwards. This listric trajectory causes the rotation of the pop-up block and another back thrust is developed to the west of it (see section 4.2.4 for more discussion).

Figures 4.11 A and B show time-structural contour maps of the forethrust and a back thrust of the pop-up structure, respectively. These contour maps indicate that the pop-up is NW-SE trending and exhibits a 3-D curvature style conformable to surface geology in this area (discussed in Chapter 2). In the southeastern part of the study area, as seen in line 3 (Figure 4.8), strata within the pop-up dip southwest and only small fault displacements are present. The geometry of the pop-up in this part is interpreted to be the initial stage of a new development of an antiformal stack, as described in the previous section. It is noticed that, in the northwest of the study area, the strata within the pop-up have been rotated by back thrusting so that they appear to dip to the northeast (Figures 4.6 and 4.7).

The dimensions of the pop-up structure measured from seismic lines 2A and 2B are approximately 3.5 to 4.0 km wide and about 1 km thick. Its thickness was roughly measured from the flat surface that bounds its top to the point where the back thrust intersects the forethrust.

#### **4.2.4 Evolution of the Pop-Up Structure**

Several models exist to explain the evolution of pop-up structures. Morley (1986) follows Butler's (1982) model and states that a pop-up structure is a common thrust-front geometry which forms in association with a broad zone of low-strain and slow-stress

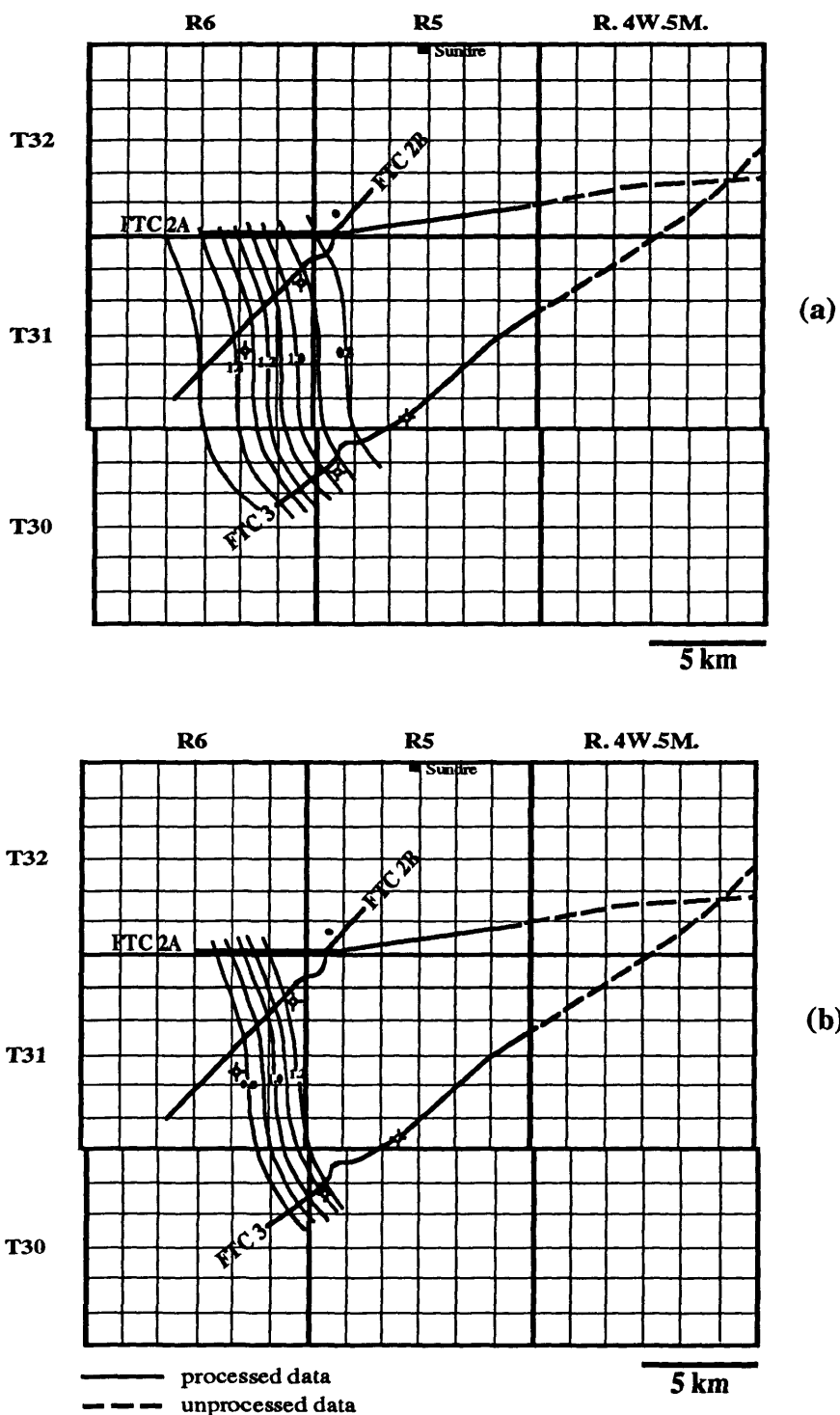


FIG. 4.11 Time structural contour maps of the frontal ramp (a) and the back thrust (b) of the pop-up structure showing a NW-SE trending en-echelon style of the pop-up. Times shown are in seconds and were measured from the seismic datum.

relaxation. It is developed in response to layer-parallel shortening brought about by stick-slip movement on the sole thrust. As the sole thrust sticks, weak stresses build up and give rise to local layer-parallel shortening. The sole thrust then unsticks, propagates and sticks again. These processes may be repeated before the absolute slip can be transferred to another horizon, resulting in the initiation of isolated anticlines followed by the formation of a back thrust (Figure 4.12). Restraint of a sole thrust propagating to a higher flat can result from various factors such as lithologic variations, reductions in pore-fluid pressure, vertical variations in competence within a thrust sheet, thrust-propagation rates etc., (Morley, 1986).

Butler (1982) discusses an alternative model for the development of a pop-up back thrust. He suggests that antithetic back thrusts can as well be a result of the rotation of the hanging-wall sheet above the footwall ramp of the forethrust. The rotation of the hanging-wall thrust sheet deters movement of the thrust sheet onto a higher flat. As a result, stresses are built up around this zone and eventually a back thrust develops to accommodate these stresses (Figure 4.13).

The pop-up structure in the study area appears to include characteristics of both models mentioned above. Its geometry seen in seismic line 3 (Figure 4.8) reflects the initial stage of pop-up evolution in which an anticline is formed in response to layer-parallel shortening, as illustrated in Figure 4.14A. As the sole thrust sticks, stress continues to build up from the attempted movement of the thrust sheet, and the first southwest-verging back thrust is initiated to accommodate these induced stresses (Figure 4.14B). Provided that the critical stick point of the sole thrust is not reached, the movement along the sole thrust beneath the back thrust will cause clockwise rotation of the pop-up block along this back-thrust trajectory (Figure 4.14C). Similarly, the clockwise rotation of the pop-up block along the listric trajectory of the first-initiated back thrust inhibits the southwest propagation onto the higher flat of the hanging wall

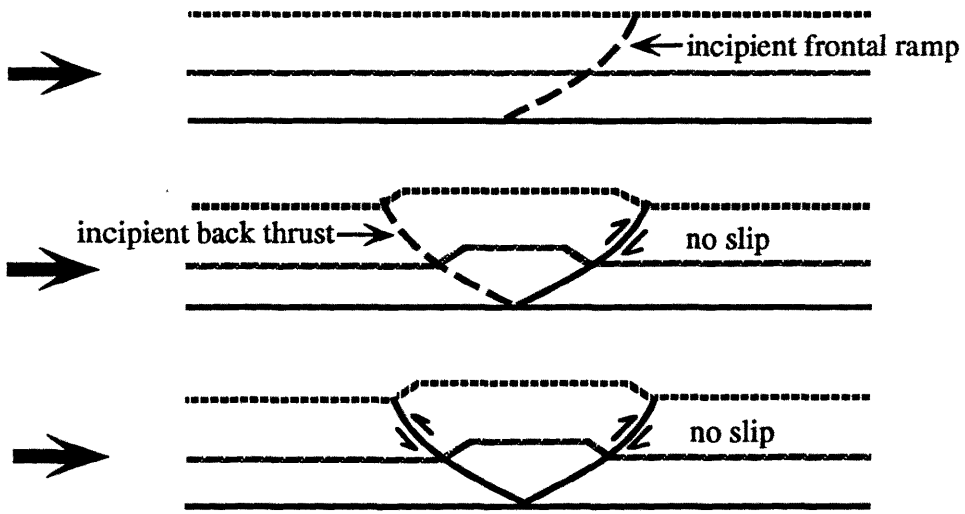


FIG. 4.12. Schematic model of the pop-up evolution according to Butler (1982) and Morley (1986). Solid arrows indicate thrust-propagation direction.

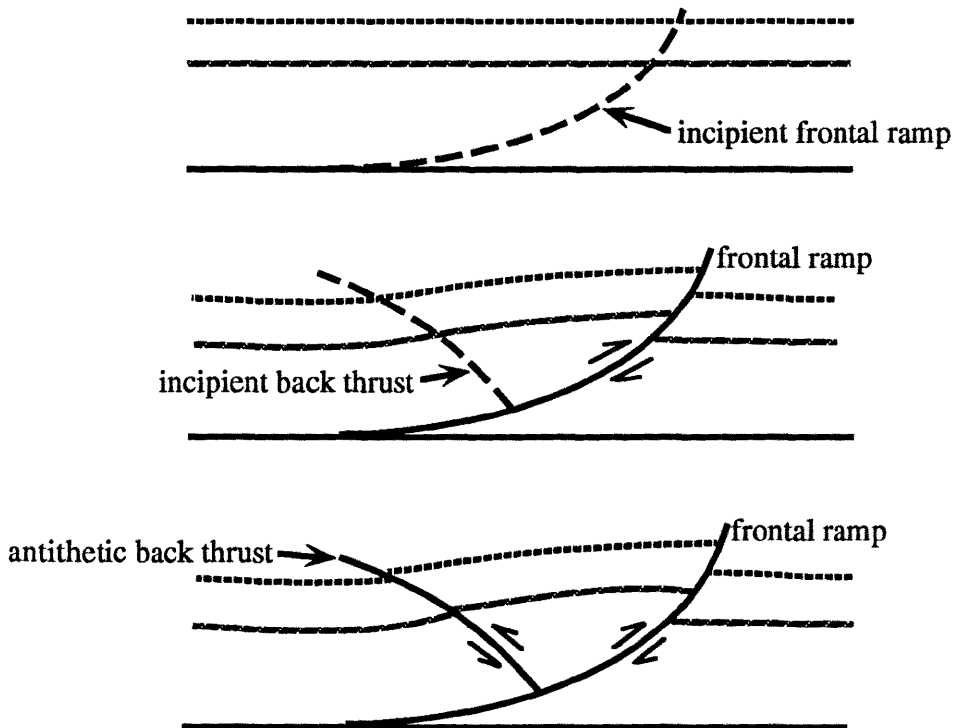


FIG. 4.13. An alternative model of the pop-up evolution. The listric geometry of the frontal ramp inhibits the propagation of the hangingwall sheet resulting in formation of an antithetic back thrust (modified from Butler, 1982).

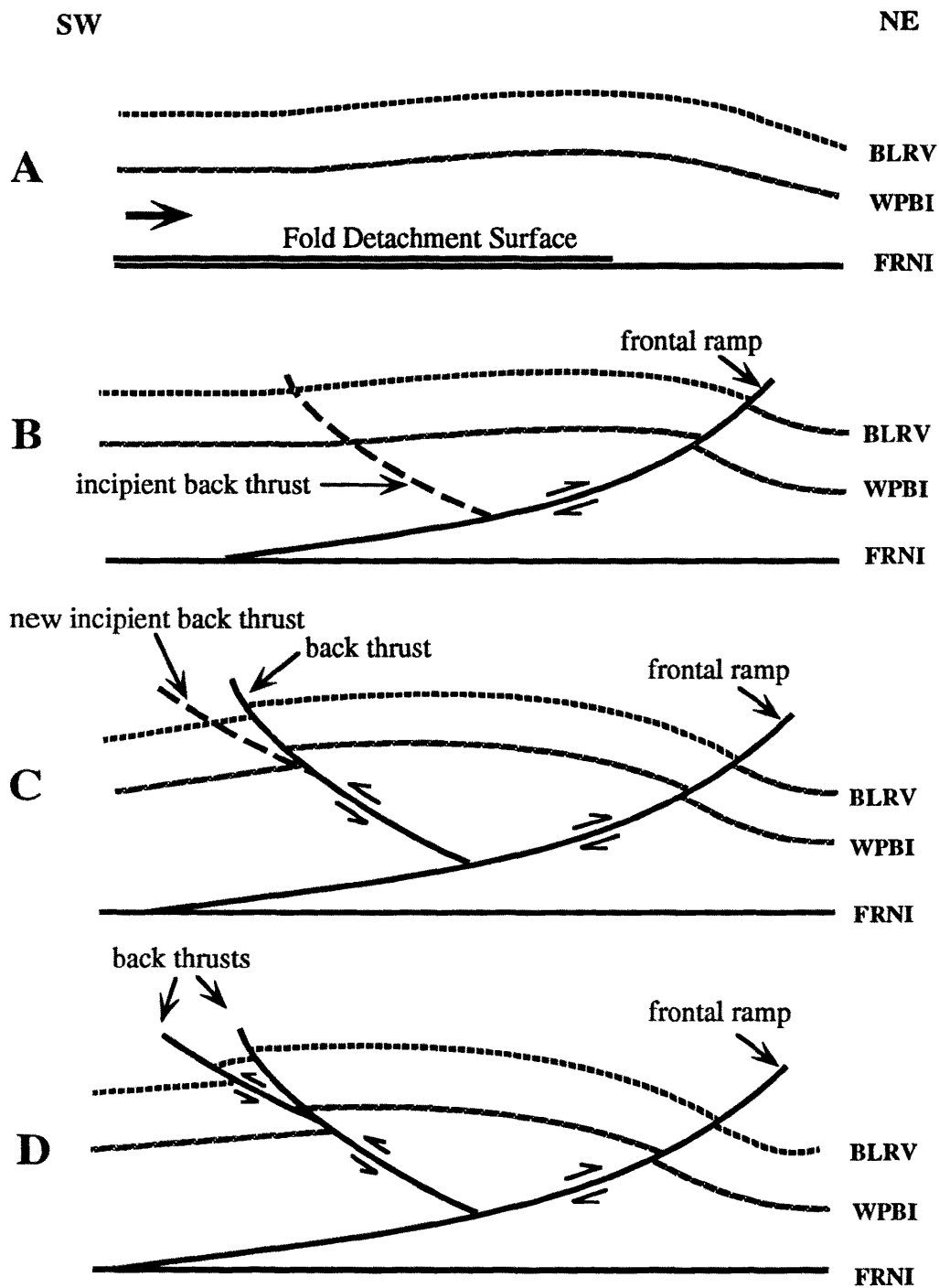


FIG. 4.14. Schematic model of the pop-up structure evolution in the study area. The restraint of the sole thrust propagation causes the formation of back thrusts.

sheet of this back thrust. Thus, either an antithetic northeast-verging thrust or a new back thrust which provides an easier gliding zone has to form to accommodate stresses. In the case sketched here, a new back thrust is formed, along which slip can be transferred to the footwall of the original back thrust (Figure 4.14D).

The reason for restraint of movement along the sole thrust or the stick-slip mechanism in this case is not thoroughly understood. However, examination of the sonic logs in this area shows that the average interval velocities of the Belly River and Wapiabi Formations in the well 16-6-32-5W5 (Figure 4.1) located on the eastern side of the pop-up structure are about 200 m/s higher than those in the well 10-25-31-6W5 (Figure 4.2) which penetrates the pop-up structure. This indicates that lateral density variations due to lithology or diagenesis do exist across this zone and may contribute to the stick-slip movement of the sole thrust.

#### **4.2.5 Rock Sequences Overlying and Underlying the Triangle Zone**

The sections overlying the upper detachment are relatively undeformed rock sequences of the Upper Cretaceous-Edmonton Group and the Tertiary-Paskapoo Formations (Figure 4.15a). These sedimentary sequences represent the west flank of the Alberta syncline (Jones, 1982) and have been passively uplifted by underthrusting slices beneath them. The dip of these rock sequences is analogous to the upper detachment geometry, i.e., gentle, listric with an angle of about 10 degrees near the core of the Triangle Zone and becoming flat toward the eastern part of the sections. The maximum thicknesses of these rock sequences, measured directly from seismic line 2B and converted to depth, are found to be about 1.2 km.

The rock sequences underlying the lower detachment are mainly carbonates of Paleozoic age. These strata exhibit an undulating geometry and dip slightly to the southwest (Figure 4.15b). Due to the presence of complex velocity fields across the

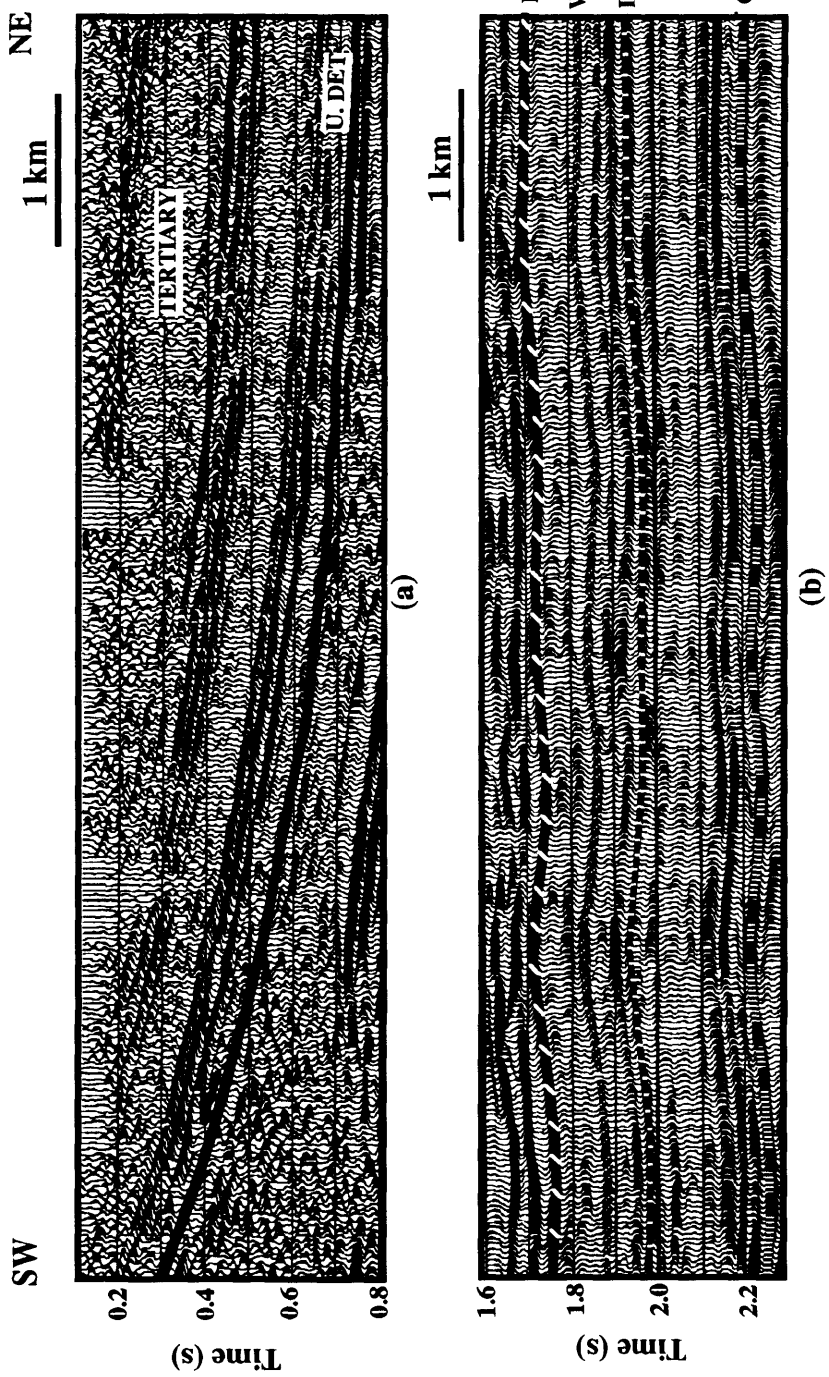


FIG. 4.15. Rock sequences above the upper detachment (a) and below the antiformal stack and pop-up structure (b). Note the undulating geometry of rock sequences in (b). The sections were taken from seismic line 2B (Figure 4.6).

Triangle Zone core, these time undulations are expected to be partially attributed to lateral velocity variations. Seismic modelling results substantiate this interpretation (discussed in section 5.2.5.2 of Chapter 5).

### **4.3 An Alternative Interpretation of the Triangle Zone Geometry**

The interpretations shown in Figures 4.6 to 4.8 are similar to that presented by Slotboom (1992), for the Wildcat Hills area. These interpretations show that the lower detachment of the Triangle Zone does not merge with the upper detachment at the usually expected location, i.e., the eastern tip of the most external intercutaneous wedge (Jones, 1982; Charlesworth et al., 1987). This structural style was adopted to explain thickening of rocks bounded by these two detachments. However, careful measurement of time intervals between the upper and lower detachments indicates that, from west to east, thickening of rocks gradually decreases to zero over the pop-up, and increases again around the eastern edge of the pop-up, then completely ceases (Figure 4.6). In addition, some reflections from Upper Cretaceous events over the western edge of the pop-up appear to be truncated against the upper detachment (Figure 4.8). This observation suggests the possibility of an alternative interpretation that the lower detachment may actually merge with the upper detachment at the location where the thickening first disappears over the pop-up, and that slight thickening around the eastern edge of the pop-up is local and was caused by the forethrust of the pop-up. This interpretation is presented in Figure 4.16, and a discussion of both possible models is presented in section 4.5.

### **4.4 Cross-Section Balancing**

Deformed-state and restored-state cross-sections of the Triangle Zone and pop-up structure were constructed based on well data and the interpretations of seismic line 2B (Figures 4.6 and 4.16). This seismic line covers all the major structures described

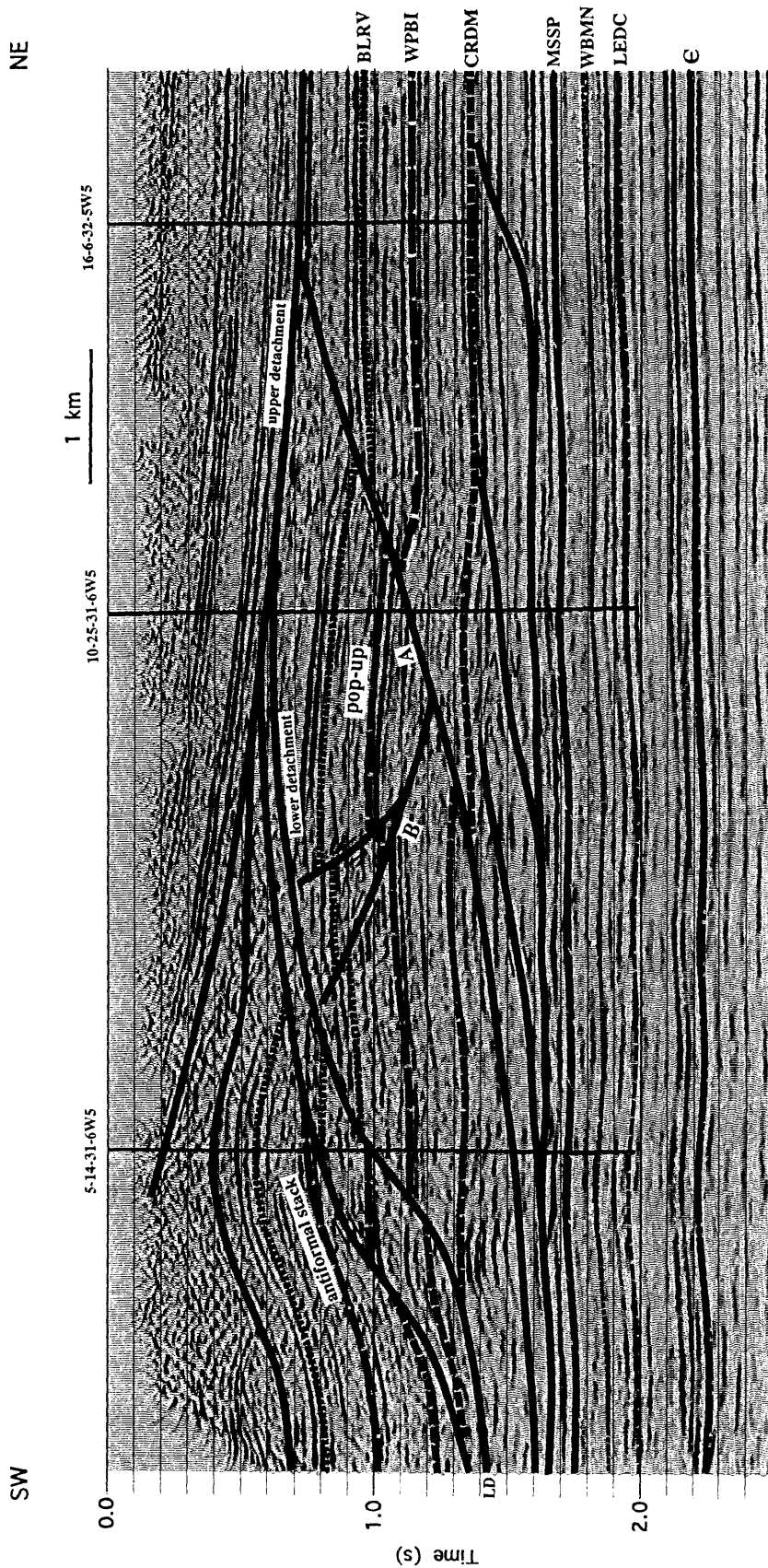


FIG. 4.16. An alternative interpretation of seismic line 2B showing that the lower detachment merges with the upper detachment over the pop-up structure (see text for more details).

previously and is oriented approximately perpendicular to strike, thus providing a representative geometry of the structures in the study area.

Four key seismic markers were employed to construct the deformed-state section, namely the Belly River, Wapiabi, Cardium and Mississippian Formations. Initial conversion of the seismic data from time to depth was undertaken using velocities and depth information from the sonic logs of wells located along the seismic line. The depth structure between wells was based on the interpretation of the seismic data and interpolation between wells.

The section was balanced using a constant-bed-length method (Dahlstrom, 1969). This method assumes no rock-volume loss or gain in the third dimension by deformation. It is also postulated that structures in the Rocky Mountain Foothills were formed long after the rocks were deposited. This single, post-depositional assumption eliminates the consideration of pronounced angular unconformities, structures growing during deposition and substantial amounts of compaction during deformation (Dahlstrom, 1969).

By geometrically removing the displacements on the faults along the key marker horizons, the deformed-state section is retrogressively restored from the youngest fault in the east to the oldest fault in the west. This method was performed along with unfolding of faults until the undeformed-state section was obtained. The fault-plane geometry derived during the intermediate restoring steps was constrained by the seismic images and the postulated ramp geometry, that is, except for the upper detachment and the pop-up back thrusts, all the ramps in this region dip southwest and cut up-section towards the northeast.

The deformed sections and palinspastic reconstructions of the two possible interpretations are displayed in Figures 4.17 and 4.18 in which deformational progressions of the structures from west to east are portrayed. The sections serve as a test

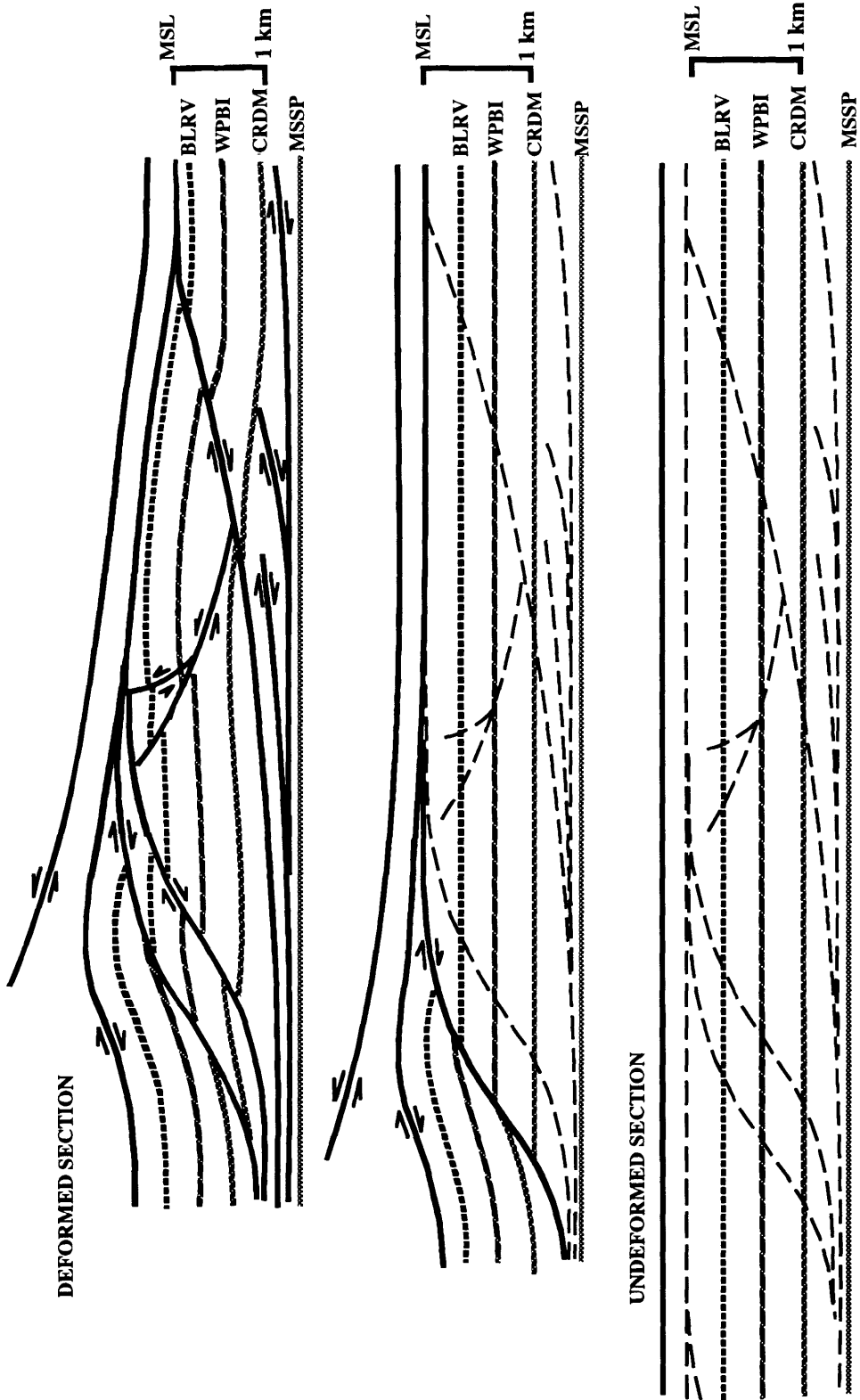


FIG. 4.17. A deformed section and palinspastic reconstruction of the Triangle Zone and the pop-up structure. Details of thrust sequences in the pop-up structure are illustrated in Figure 4.14.

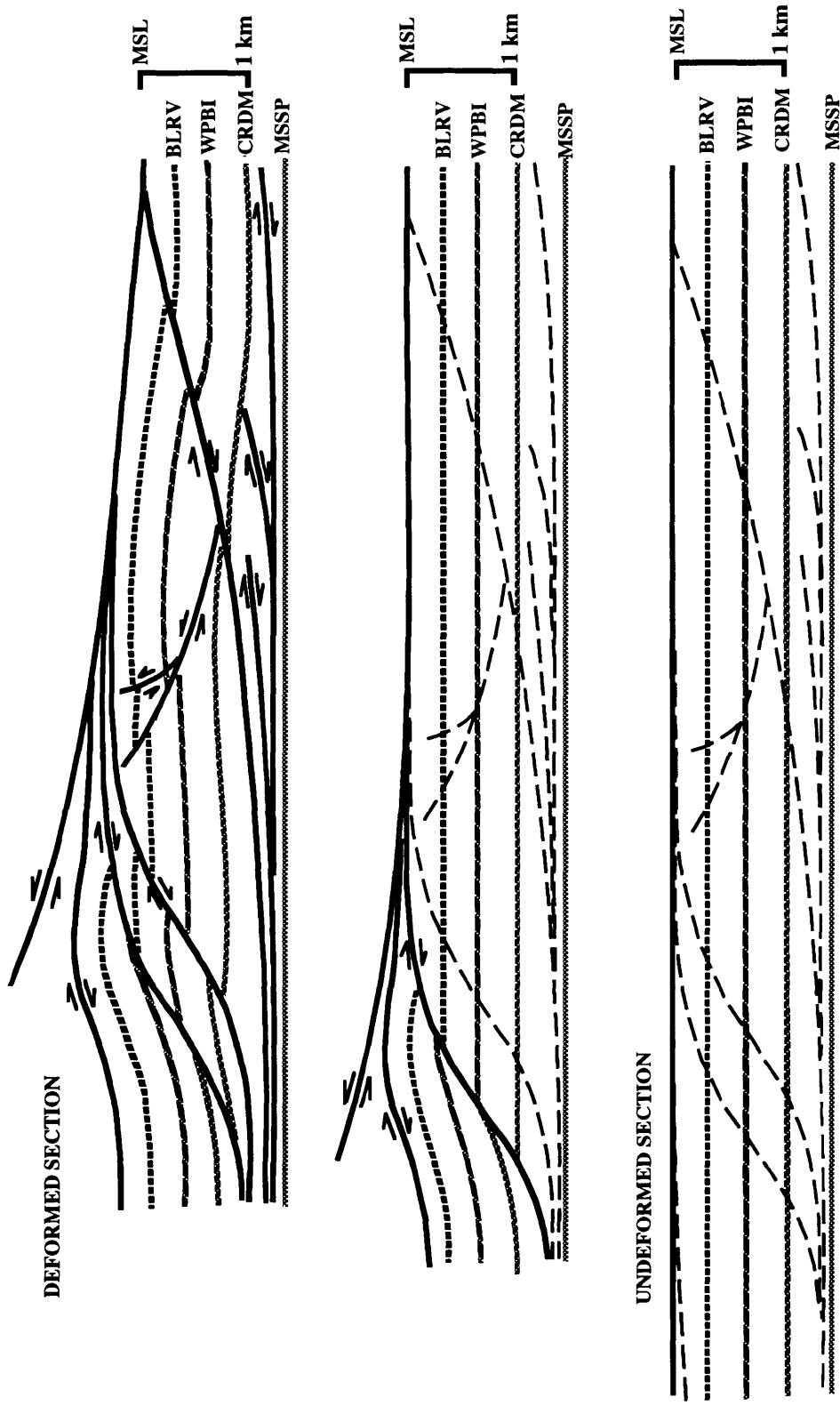


FIG. 4.18. A deformed section and palinspastic reconstruction of the alternative interpretation of the Triangle Zone and pop-up structure showing that the lower detachment merges with the upper detachment.

for geometric consistency of the fault trajectories and validity of the seismic interpretations in this study.

## 4.5 Discussion

Gentle folding of the upper detachment, as seen in all of the seismic lines (Figures 4.6 to 4.8), is of a particular interest in this structural interpretation as it suggests a passive-roof nature of this fault during the wedge advancement. This evidence, along with the very low dip of the upper detachment at its eastern limit, appears to be contradictory to the Triangle Zone model of Charlesworth et al. (1987) in which the initial stage of formation of the upper detachment is shown as a much higher dipping ramp (Figure 1.4). It is more likely that the upper detachment in this region initiated as a flat and was later passively uplifted by underthrusting below it. This concept is supported by the geometry of the pop-up structure, presently seen to be external to the antiformal stack. This incipient stage of formation of a new antiformal stack, with the upper detachment forming as a relatively flat horizon connected with a ramp of the lower detachment, is clearly evident. This geometry also suggests that the current lower detachment that bounds the easternmost antiformal stack was about to be abandoned with displacement occurring on the minor thrusts to the east. It is anticipated that with the continued eastward progression of the intercutaneous wedge, rocks in the hanging wall of the forethrust of the pop-up would eventually be incorporated into the wedge, along with steepening of the upper detachment and eastward shifting of the locus of the Triangle Zone.

The geometrical relationship between the upper detachment and the upper flat of the lower detachment remains ambiguous in this structural interpretation. The first model (Figure 4.6) shows the upper flat of the lower detachment as being parallel to the upper detachment, indicating an eastward extent of strain into the foreland, whereas an

alternative model (Figure 4.16) shows a merging of these two fault planes over the pop-up suggesting a relatively rapid cessation of strains toward the east within this interval. The former model is more flexible in that it allows for a long-distance shortening to occur in rocks of the Edmonton Group which was observed and documented by Slotboom (1992) and Skuce et al. (1992). However, since such evidence is not as clearly seen in the present study area, an alternative model was therefore proposed to accommodate the possibility of more abrupt cessation of strain toward the east. Evidence in support of this model is :

- 1) No obvious shortening of rocks bounded by the upper detachment and the upper flat of the lower detachment (e.g. Edmonton Group rocks) is seen beyond the eastern edge of the pop-up structure. This suggests that large-scale strain has probably ceased at this location which may indicate merging between these faults.
- 2) Differential folding of the upper detachment reflects layer-parallel shortening within the intercutaneous wedge. This, in turn, means the wedge could not move freely between the glide horizons. One possible explanation for retardation of the eastward advancement of the wedge is that a joined tip line formed or that they merged in the east (D. A. Spratt, personal communication).
- 3) The lithology of Edmonton Group rocks is mainly shale. Having an interval of only about 250 m of incompetent rocks between the upper and lower detachments means that, from a mechanical point of view, these two fault planes should merge.

In addition to these, it has been known that small passive-roof duplexes are present in the foreland, approximately 40 to 60 km east of the Triangle Zone (Skuce et al., 1992). The roof thrust of these duplexes was found to be a southwesterly verging

back thrust and is structurally connected with the upper detachment of the Triangle Zone . This evidence seems to substantiate the concept of long-distance strain propagation, as proposed in this structural interpretation and by Slotboom (1992). However, one major distinction between the interpretation of Skuce et al. (1992) and this interpretation is that foreland duplexes in their study area were found at the Cardium level, whereas this interpretation predicts that foreland duplexes, if present, should be found in the Edmonton Group, a much younger and shallower formation.

These ambiguities indicate a need for a number of NE-SW seismic profiles across the main culmination of the Triangle zone and extended further into the structured part of the foreland. These will establish a geometrical relationship between the foreland duplexes and the Triangle Zone, and verify if small scale shortening, as predicted by this interpretation, does in fact exist in rocks of the Edmonton Group, foreland of the main culmination of the Triangle Zone.

## Chapter 5 - SEISMIC MODELLING

### 5.1 Introduction

As mentioned in the previous chapter, deep reflections below the Triangle Zone have an undulating geometry. These time undulations were found to be quite consistent, both vertically and laterally, along the key geologic markers, and can best be observed in the seismic line 2B below 1.7 s (Figure 4.6). In the presence of complex velocity fields and velocity inversion in the Triangle Zone core, these features were expected to be partially attributed to seismic velocity anomalies.

Seismic modelling was undertaken to obtain a better understanding of the effects of shallow velocity anomalies on deep seismic imaging, as well as to confirm the interpreted Triangle Zone geometry discussed previously. Both numerical and physical seismic modelling analyses were performed and are discussed in this thesis. The numerical modelling case was aimed mainly at verifying the geologic interpretation of the seismic line 2B across the Triangle Zone regarding its structural components. The analyses were also extended to evaluate velocity-anomaly effects and processing problems such as migration, DMO and offset-limited stack.

In the physical seismic modelling experiments, a generic thrust-fault model, typical of the Canadian Rocky Mountain Foothills, was developed representing high-velocity carbonate rocks of Mississippian-to-Devonian age thrust over lower-velocity clastic rocks of Mesozoic age. The goal was to analyze the effects of this velocity inversion on our ability to characterize and image subtle structures below the thrust fault.

In addition to the major objectives outlined above, this study also evaluated the feasibility of using converted wave (P-SV) data in conjunction with conventional P-P data in areas with complex geological structure. Numerical P-SV data were acquired

and processed over a Triangle Zone model and the results were compared to those obtained for synthetic P-P data.

## **5.2 Numerical Seismic Modelling**

### **5.2.1 Background**

Numerical seismic modelling has been used in petroleum exploration and development for three main purposes:

- 1) to aid in seismic interpretation, particularly in complex structural regions such as thrust and fold belts or salt domes. Common applications, for example, are to evaluate velocity anomalies, out-of-plane events (side-swipe), raypath distortion and tuning effects, etc.;
- 2) to test processing parameters and assess new processing algorithms;
- 3) to design acquisition parameters which will ensure optimum fold, especially for 3-D surveys as well as for 2-D surveys with inconsistent spread geometry (i.e., crooked lines).

Moreover, numerical seismic modelling is also used for other minor purposes, such as time-to-depth conversion (McClellan et al., 1991).

At present, two numerical seismic modelling techniques are available, namely, ray tracing and wave-equation techniques. In ray tracing, the propagation of the seismic wavefront is represented indirectly by raypaths obeying Snell's Law, whereas the wave-equation technique models the wavefront propagation directly from the physical changes (i.e., pressure and particle displacement) in the subsurface that are associated with the seismic disturbance (Fagin, 1991).

Ray tracing has advantages over the wave-equation technique in terms of processing time and its capability to display ray diagrams, which are useful in correlating

synthetic seismic events with their corresponding reflection points. The wave-equation technique, on the other hand, cannot display such diagrams. Its sole output is the final seismic record (Fagin, 1991). This leads to possible interpretation difficulties in identifying the synthetic events, especially for the complex models.

This study has employed normal-incidence ray tracing to generate synthetic zero-offset P-P data, and multioffset ray tracing to generate synthetic P-P and P-SV shot gathers. These synthetic data sets were acquired using UNISEIS ray-tracing software. The Uniseis approximates diffractions by treating a diffractor as a buried point source. A range of shooting angles or aperture for rays that beam out from this point is chosen by the user and diffractions are then calculated for which initial amplitudes are a function of the depth of that point source. As well, attenuation and geometrical spreading effects can be corrected for by specifying an average velocity field of the entire model (Landmark Uniseis, 1988).

### **5.2.2 Model Construction and Physical Parameters**

The 2-D geologic model representing the Triangle Zone in the study area is displayed in Figure 5.1, with physical parameters summarized in Table 5.1. The model was constructed based mainly on the initial interpretation of the seismic line 2B and well information as discussed in Chapter 4. Fourteen geologic markers ranging from Cambrian to Tertiary in age were used to build the model on the basis that they are well identified and can be correlated across the seismic sections (Figures 4.6 to 4.8). The model comprises two east-dipping layers, which represent Tertiary rocks of the eastern limb of the Triangle Zone, overlying the antiformal stack and pop-up structures which involve Cretaceous rocks, bounded by upper and lower detachment faults. The base of the model is composed of Mississippian, Devonian and Cambrian horizons which are essentially planar with a gentle dip to the west.



| Layer<br>(Formation)      | P-wave velocity<br>(m/s) | S-wave velocity<br>(m/s) | Density<br>(kg/m <sup>3</sup> ) |
|---------------------------|--------------------------|--------------------------|---------------------------------|
| 1<br>(upper Tertiary)     | 3350                     | 1675                     | 2360                            |
| 2<br>(lower Tertiary)     | 3480                     | 1740                     | 2380                            |
| 3<br>(Edmonton Group)     | 3520                     | 1760                     | 2387                            |
| 4<br>(Belly River)        | 3760                     | 1880                     | 2420                            |
| 5<br>(Wapiabi)            | 3592                     | 1796                     | 2400                            |
| 6<br>(Belly River)        | 3975                     | 1987                     | 2460                            |
| 7<br>(Wapiabi)            | 3896                     | 1948                     | 2450                            |
| 8<br>(Belly River)        | 3831                     | 1915                     | 2430                            |
| 9<br>(Wapiabi)            | 3930                     | 1965                     | 2450                            |
| 10<br>(Cardium)           | 4050                     | 2025                     | 2470                            |
| 11<br>(Top Mississippian) | 5880                     | 2940                     | 2710                            |
| 12<br>(Wabamun)           | 6050                     | 3025                     | 2730                            |
| 13<br>(Leduc)             | 5900                     | 2950                     | 2716                            |
| 14<br>(Cambrian)          | 6200                     | 3100                     | 2750                            |

Table 5.1. Physical parameters of the numerical model shown in Figure 5.1.

It should be noted that the geologic model utilized in this modelling analysis was slightly modified from the final balanced cross-sections of the Triangle Zone shown in Figures 4.17 and 4.18. This was done for convenience and simplicity in model construction since the model segments had to be input by hand, and also due to some limitations of the UNISEIS software in handling complex models. However, the major geometry and velocity fields are essentially preserved.

The next step in model construction was to define the P-wave velocity, S-wave velocity and density for each layer. The P-wave velocity field was derived from sonic logs and velocity functions from velocity analysis during the processing of data from line 2B. Because the UNISEIS software does not allow for multiple velocity values within individual layers, all available P-wave velocity information was averaged to obtain an optimum value for each unit. Also, due to the unavailability of the complete full-waveform sonic log, a constant  $V_P/V_S$  value of 2.0 was assumed, a value which is an average for most rock types (Harrison, 1989). Formation densities were determined from the empirical relationship between velocity and density reported by Gardner et al. (1974) as follow :

$$\rho = 0.31V^{0.25} \quad (5.1)$$

where  $\rho$  is density in  $\text{g/cm}^3$ ,  $V$  is velocity in  $\text{m/s}$ . Table 5.1 gives a summary of the physical parameters used in this experiment.

### 5.2.3 Normal-Incidence Ray Tracing

It has been illustrated by many authors (e.g., Judson et al., 1985; Larner et al., 1985; Hatton et al., 1985) that, in the presence of significant lateral velocity variations, all time-migration algorithms currently used in the processing industry fail to image subsurface structures properly, even if correct velocity functions are used. The problem is especially obvious in the case of imaging structures associated with thrust faults or salt

domes because of their severe lateral velocity variation and vertical velocity inversion. The deficiencies of these time migrations are due mainly to the limitations and approximations of the wave equation used by each time-migration algorithm (Yilmaz, 1987).

The Triangle Zone is an interesting case on which to perform seismic imaging analysis since it may possess lateral velocity variations, velocity inversion and a range of geological dips. Moreover, abundant well information is available in the region, which provides good velocity control to the study.

The technique utilized to collect the data for this part of the study was normal-incidence ray tracing, which generates an output representing unmigrated, stacked data. In normal-incidence ray tracing, shot locations coincide with the receiver locations, and both are moved across the model. In this study, a constant spacing of 16.5 m was used, which is equal to the average CMP spacing of seismic line 2B. For simplicity, these numerical data contained no multiples and were noise free. Also, surface topography and station elevations were not taken into account, since the modelling results simulate field data processed to a fixed datum. The intermediate output from the ray tracing was a reflection coefficient series. This was subsequently convolved with a zero-phase Ricker wavelet having a central frequency of 30 Hz, which is the approximate central frequency of the field data from line 2B, to produce a zero-offset section, as displayed in Figure 5.2.

Inspection of this zero-offset section indicates that the juxtaposition of the antiformal stack, pop-up structure and younger Tertiary strata gives rise to velocity anomalies in the deeper horizons below them. The amount of pull-up ranges between 25 and 50 ms across the model, which matches fairly well that observed in the processed field data (Figure 4.6).

To further analyze the effects of the Triangle Zone structure on the image quality of deep seismic horizons, various migration tests on the zero-offset data were carried out.

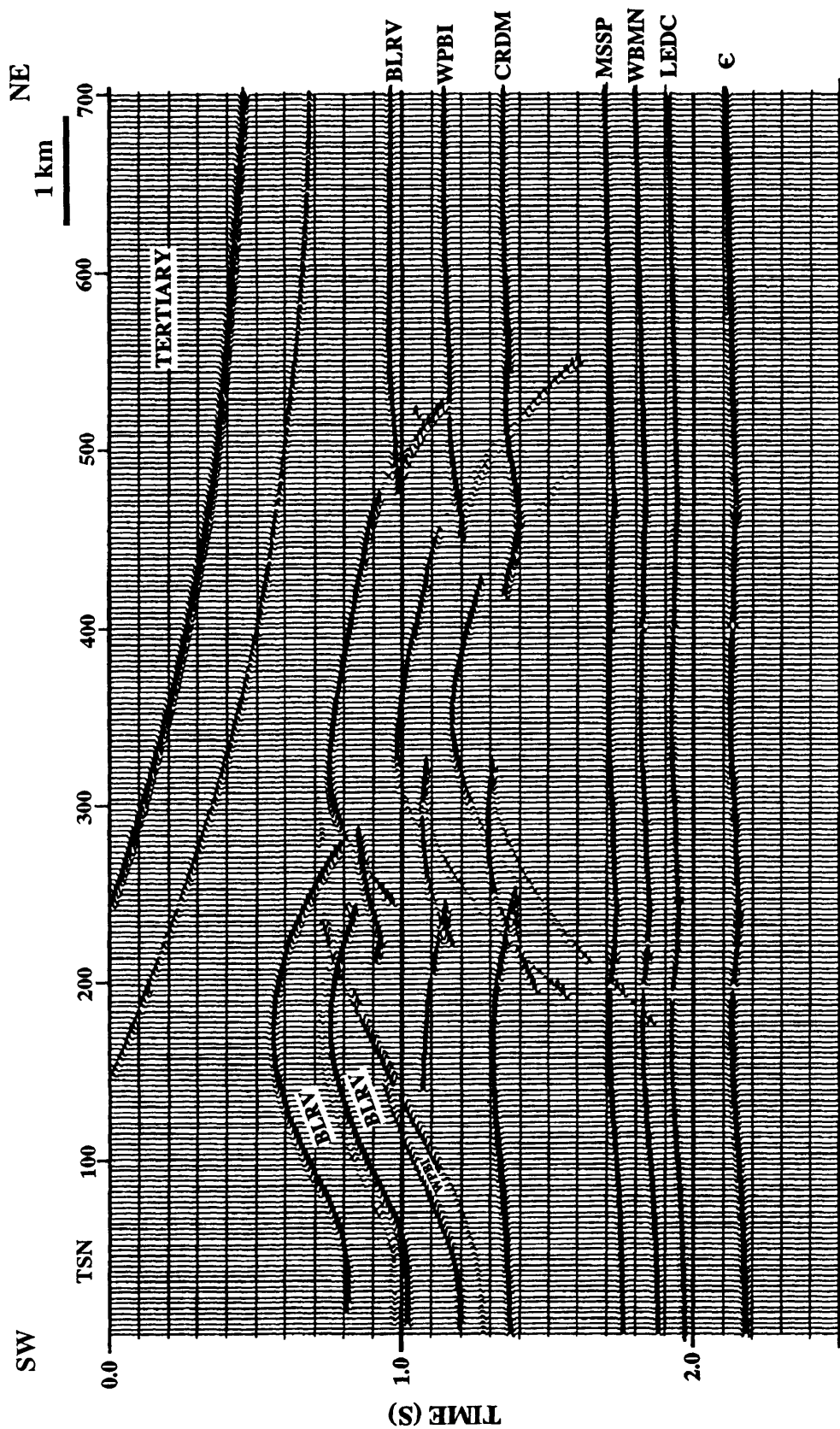


FIG. 5.2. Synthetic zero-offset section generated from the geologic model in Figure 5.1. A zero-phase Ricker wavelet with a central frequency of 30 Hz was used. The trace spacing is 16.5 m.

Three migration methods, namely Stolt ( $f-k$ ), phase-shift and finite difference (F-D) techniques were applied to the zero-offset data. Phase-shift and F-D migrations used in this test were performed in the depth domain, whereas the Stolt migration was applied in the time domain. The main goal of the tests was to evaluate collapse of diffractions situated along the edges and tips of the antiformal stack and pop-up structure.

True interval velocities (100%) of each formation were applied for the depth-migration cases, using a depth step size of 16.5 m (equal to the trace spacing of the field data). The maximum dip to migrate was specified as 85 degrees. The frequency bandwidth to be migrated ranged from 10-80 Hz in the shallow part and 7-70 Hz in the deep part of the section. In the Stolt-migration case, a series of constant velocities were tested; a medium velocity of 3500 m/s was found to yield the optimum result and was therefore applied. Figures 5.3, 5.4 and 5.5 show the results after application of these three migration techniques.

#### 5.2.4 Discussion

Examination and comparison of Figures 5.3 to 5.5 suggest that raypath distortion caused by lateral velocity variations and vertical velocity inversion, which was considered to be a major cause for the deterioration in reflection quality beneath the Triangle Zone core, may in fact not be too severe in this region. This was deduced from the observation that all of the migration methods yielded similar and comparatively reasonable results in terms of diffraction collapse and correct repositioning of events. However, some minor discrepancies between the time-and depth-migration results can be seen. The Stolt technique yielded inferior results in some areas, such as at the western edge of the pop-up structure, especially on the Wapiabi and Cardium horizons. The diffractions were not collapsed properly, resulting in blurry images of the steeply dipping portions when compared to the results from the other two techniques. These inferior

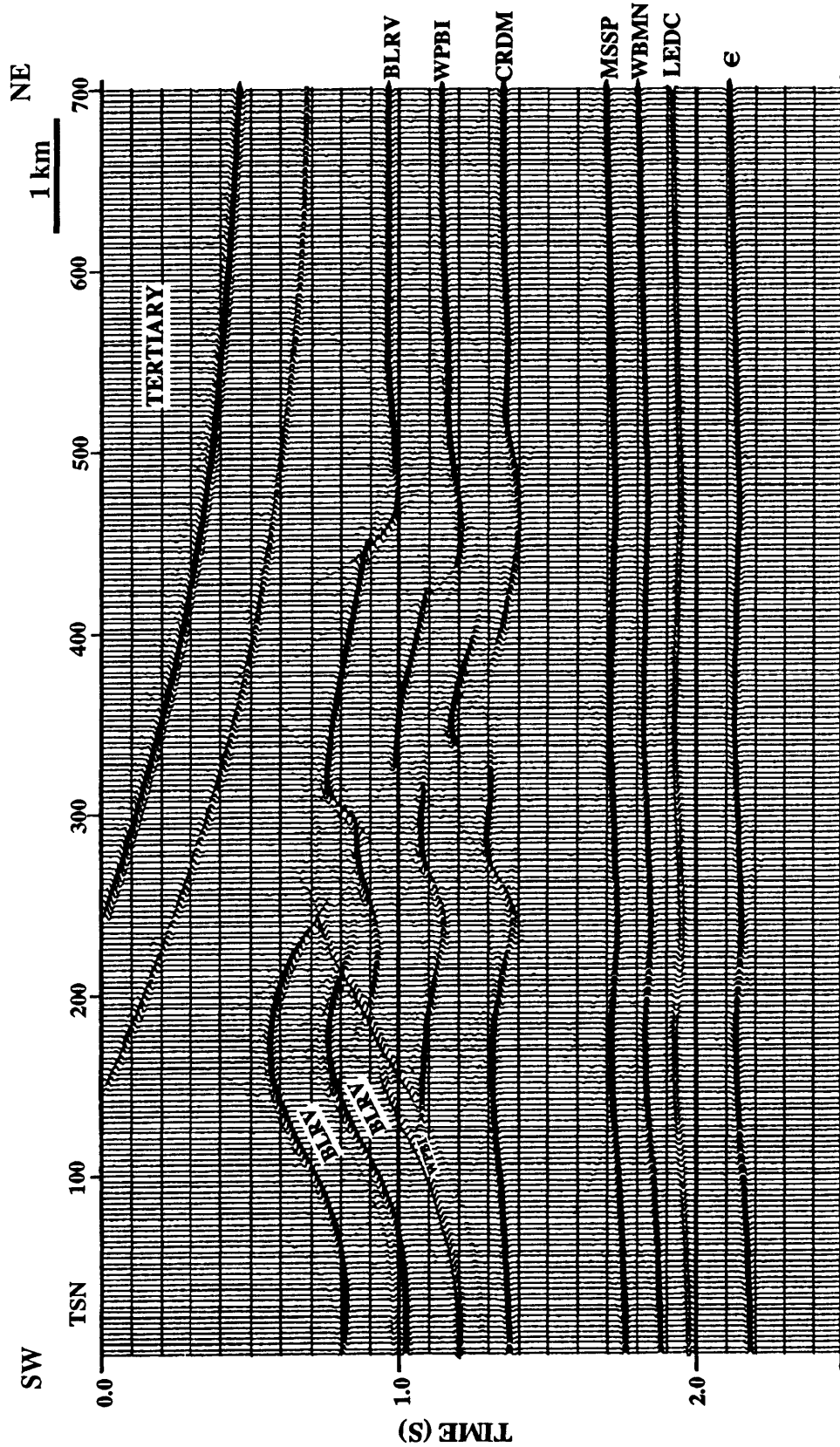


FIG. 5.3. Stolt ( $f-k$ ) migrated section of the zero-offset section assuming a constant velocity of 3500 m/s. The maximum dip to migrate was specified as 85 degrees. Note blurry images of the western edge of the pop-up structure.

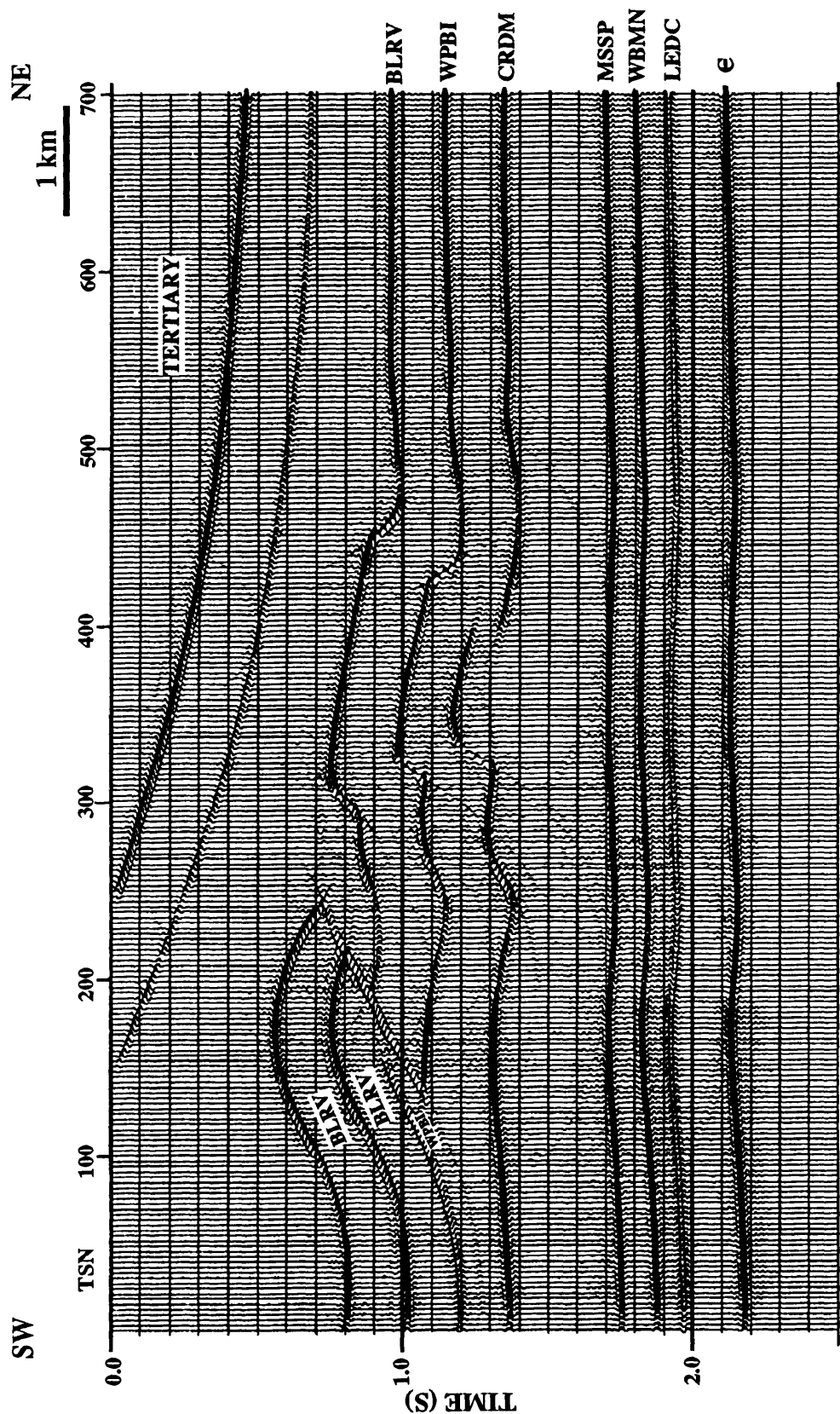


FIG. 5.4. Phase-shift migrated section of the synthetic zero-offset section using 100% interval velocity functions. The maximum dip to migrate was 85 degrees.

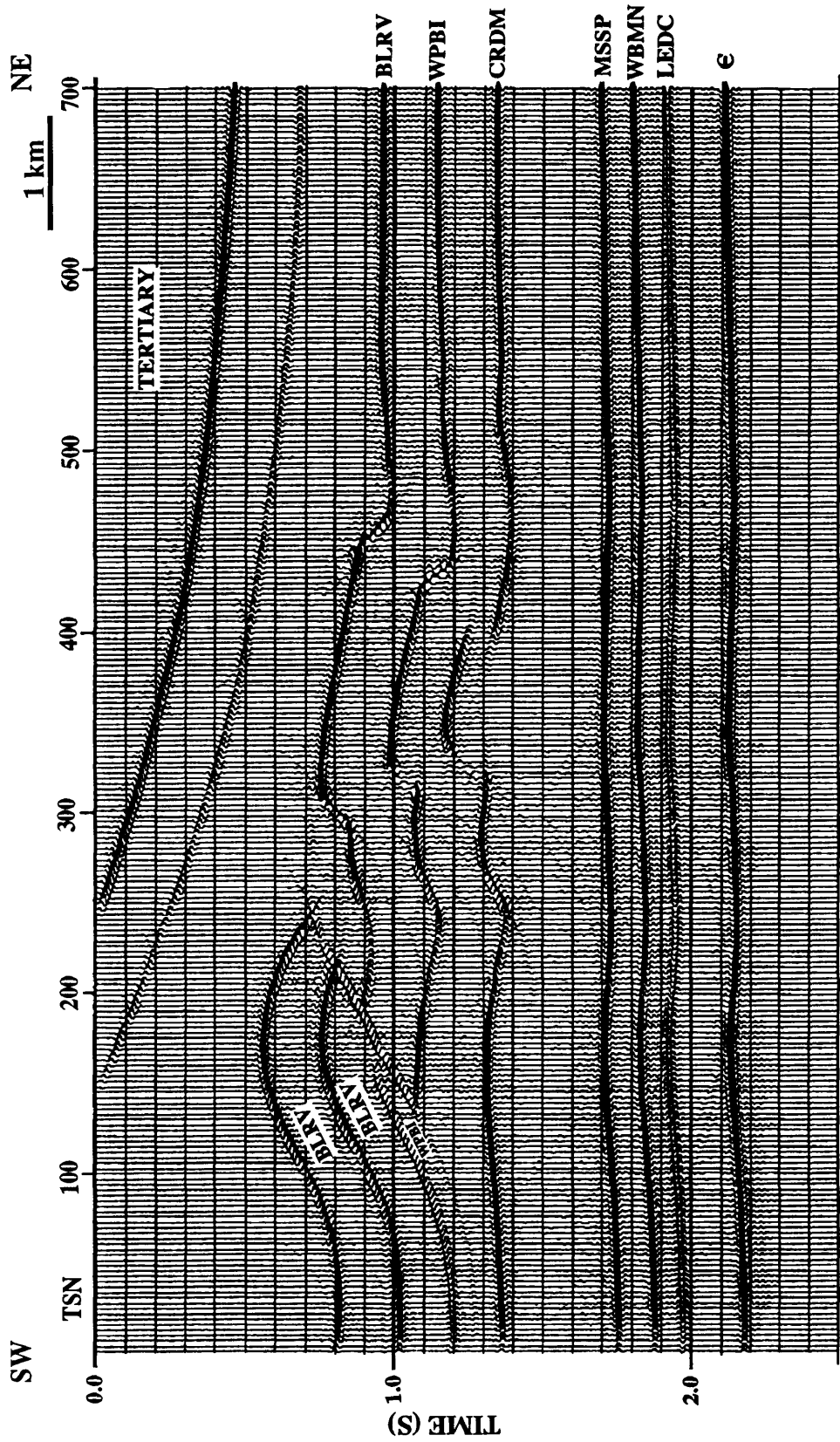


FIG. 5.5. Finite difference (F-D) migrated section using 100 % interval velocity functions.

results are, however, considered minor for this case. In real data, they may not be as easily observed due to the presence of background noise.

It should be emphasized that, for the migration tests described, it was assumed that the input data were perfectly zero-offset. However, this is not strictly valid for actual field data, since we can only mimic zero-offset data via the CMP stack. This means that the quality of the migration outputs depends largely on how well the CMP-stack method performs. Morse et al. (1991) performed a numerical modelling study of a fault-propagation fold and showed that there is a significant difference between the results from migration of zero-offset and of CMP-stacked data. One of their conclusions was that, although depth migration can correctly image the complex structures, limitations of the CMP-stack method reduce the effectiveness when applied poststack. This problem was also anticipated in this study because the model of Morse et al. (1991) appeared to be very similar to the Triangle Zone model, except for the lack of east-dipping layers in the shallow part of their model. Therefore, it was decided to undertake offset-modelling analysis to further investigate this and other problems that may arise during acquisition and processing of the field data.

### **5.2.5 Offset Ray Tracing**

Offset ray tracing has a wide variety of applications in seismic exploration. Generally, it is used to investigate the effectiveness of the processing steps and to evaluate new processing algorithms. As well, it can be used for data-acquisition design and to examine potential problems that can degrade field data quality. Offset modelling can be applied to simulate many types of seismic recording geometries, e.g., common-shot and CMP ray tracing, VSP ray tracing and side-scanning ray tracing. Compressional-wave, shear-wave and mode-converted (P-SV) data can all be generated. The technique is

regarded as being more realistic than the zero-offset ray tracing because it produces data that use a geometry similar to that used in recording conventional seismic data.

Common-shot ray tracing was used in this study to collect both synthetic P-P and P-SV data from the Triangle Zone model. The acquisition parameters applied in the experiment were essentially similar to the field acquisition parameters of seismic line 2B. As for the zero-offset case, assumptions made were that the data were free of noise, multiples and statics.

#### 5.2.5.1 P-P Modelling

Eighty-five shot gathers with a 240-channel split-spread geometry were acquired over the model. The receiver spacing was 33 m and the shot spacing was 99 m, producing a maximum subsurface fold of 40. Examples of P-P shot gathers from the core and eastern limb of the Triangle Zone model are displayed in Figures 5.6A and 5.6B respectively. Preliminary examination of the synthetic shot gathers indicates some potential acquisition problems associated with the shot gathers recorded over the Triangle Zone core. Firstly, it was observed that shadow zones are present in the Figure 5.6A on horizons below 1.0 s. The shadow zones are one of the common features observed in modelling structures containing velocity inversions (Fagin, 1991). These are areas of reflectors from which seismic raypaths do not return to surface because of critical incidence on overlying high-velocity layers. Secondly, conflicting dipping reflections are apparent, especially near the lower detachment. These reflections with conflicting dip are known to be one of the major causes in reducing the effectiveness of the NMO correction and stacking process (Hale, 1984).

The shot gathers were subsequently processed according to the flow summarized in Figure 5.7. Note that the processing flow for the synthetic data is less complicated than that of the field data since some processing steps, e.g., statics correction, velocity

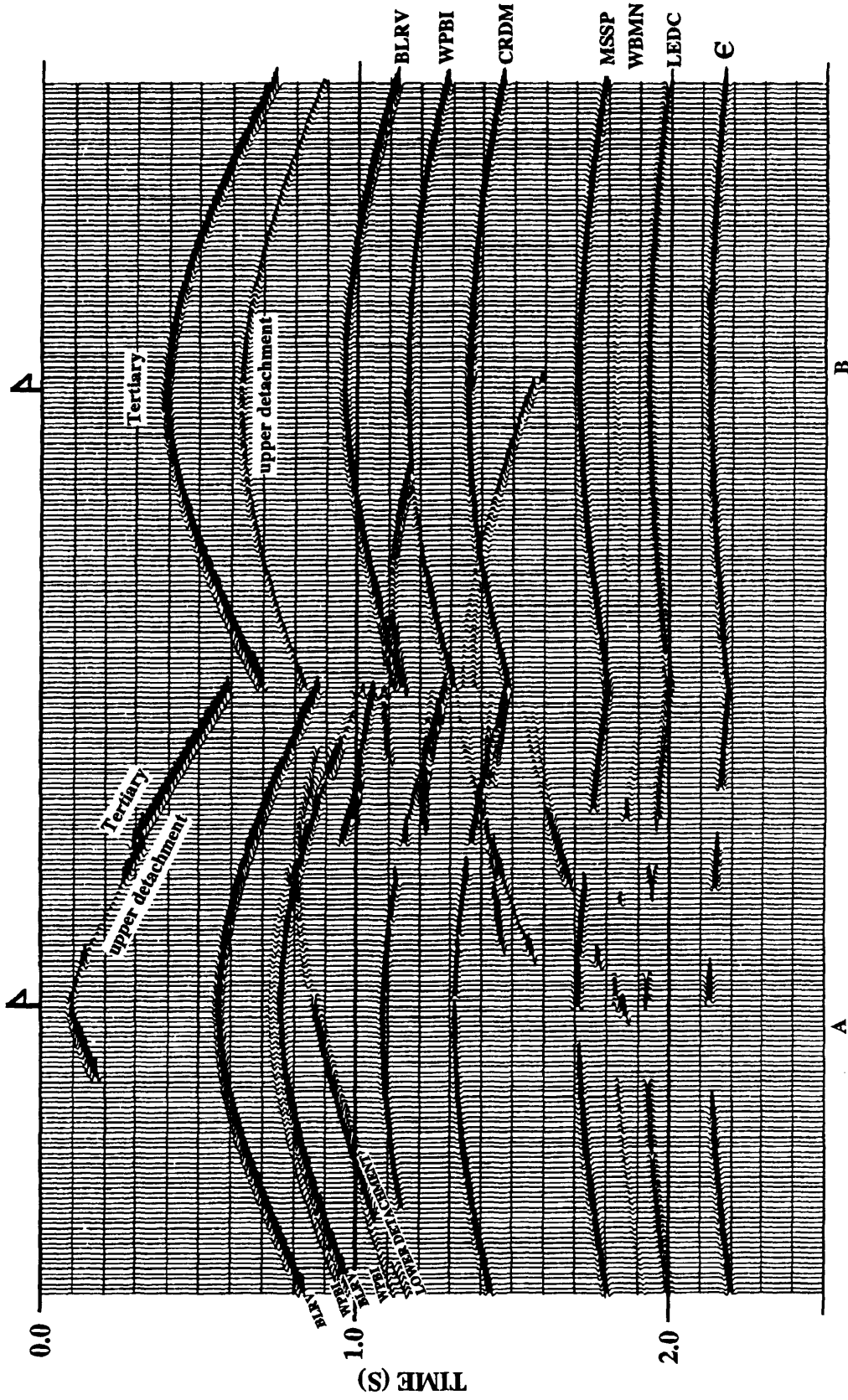


FIG. 5.6. Synthetic P-P shot gathers from the Triangle Zone core (A) and the eastern limb (B). A Ricker wavelet with a central frequency of 30 Hz was used. The trace spacing and maximum offset are 16.5 and 3993 m respectively. Dipping reflections present between 1.0-1.7 s which are not labelled are events from the steep edges of the pop-up structure.

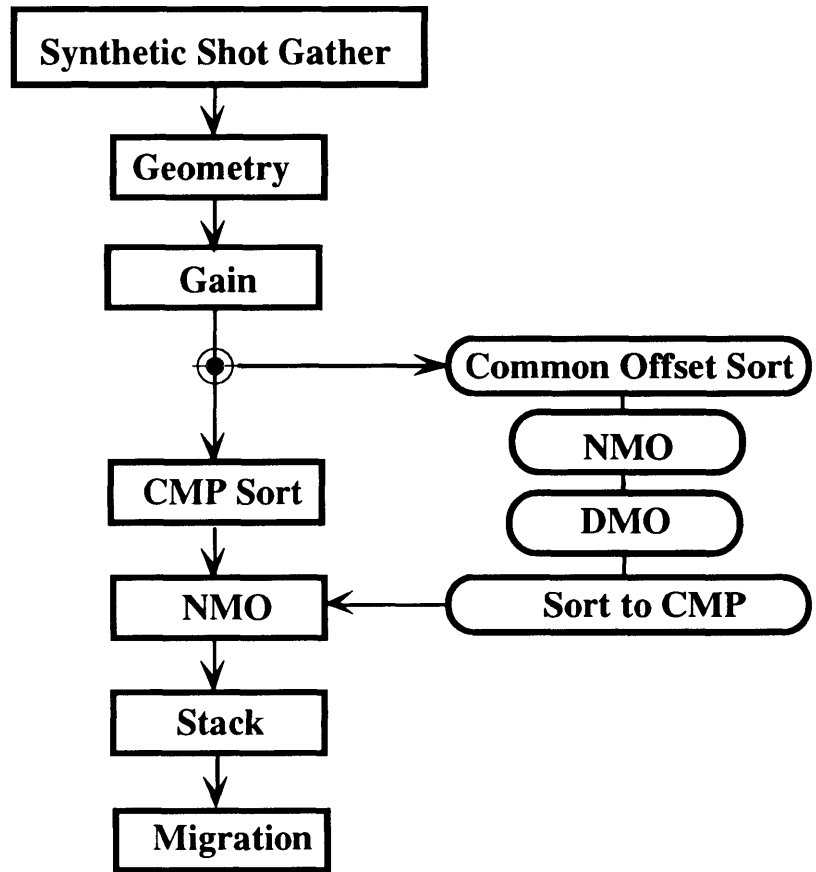


FIG. 5.7. Processing flow for the synthetic P-P data.

analysis, deconvolution, multiple and noise attenuation were not necessary. In processing synthetic seismic data, one of the major advantages is that the velocities are known. This enables the NMO correction to perform effectively which results in reliable stack qualities. The rms velocities applied to correct for NMO were calculated from Dix's equation :

$$V_{\text{rms}}^2 = \frac{\sum_{i=1}^N (V_i^2 t_i)}{\sum_{i=1}^N t_i} \quad (5.2)$$

where  $V_i$  and  $t_i$  are the interval velocity and interval transit time for the  $i$ th interval in a

sequence of N layers. Seventeen rms velocity functions across the model were computed and used to generate the stacked P-P section shown in Figure 5.8.

Comparison of the CMP-stacked section (Figure 5.8) and the zero-offset section (Figure 5.2) shows that the conventional CMP-stacking technique failed to correctly image some of the reflectors below the Triangle Zone core. Reflection smear due to incoherent stacking is seen on Mississippian, Devonian and Cambrian horizons between Trace 100 and 300 (Figure 5.8). This was expected as a result of ray-bending effects through the shallow velocity-inversion zone, along with the inability of the NMO process to correct far-offset traces. It is also noticed that the shallower horizons are less smeared than the deeper horizons. This is because the raypath aperture of deep horizons is larger than that of the shallower horizons, resulting in more deviation of the velocity field from that was applied to correct for NMO at that CMP location. This problem is particularly pronounced for complex models and far-offset traces. The deterioration of synthetic data below the Triangle Zone core is similar to that seen on processed field-seismic data, in that reflections below the Triangle Zone core are usually discontinuous and of lower quality than in other parts of the section.

To further evaluate the fidelity of the CMP-stack method, the stacked data were then migrated using the Stolt and the phase-shift methods. The F-D migration was excluded from this test because of its long processing time (it usually takes three or four times longer than the phase-shift method and about ten times longer than the Stolt method), and also because in the previous study it was found to produce results similar to those of phase-shift migration. All migration parameters were kept the same as those applied to the zero-offset case (see section 5.2.3). The results from the migration tests are shown in Figures 5.9 and 5.10, respectively, in which dispersion of events along the edge of the pop-up structure and synclines below antiformal stack are noticeable.

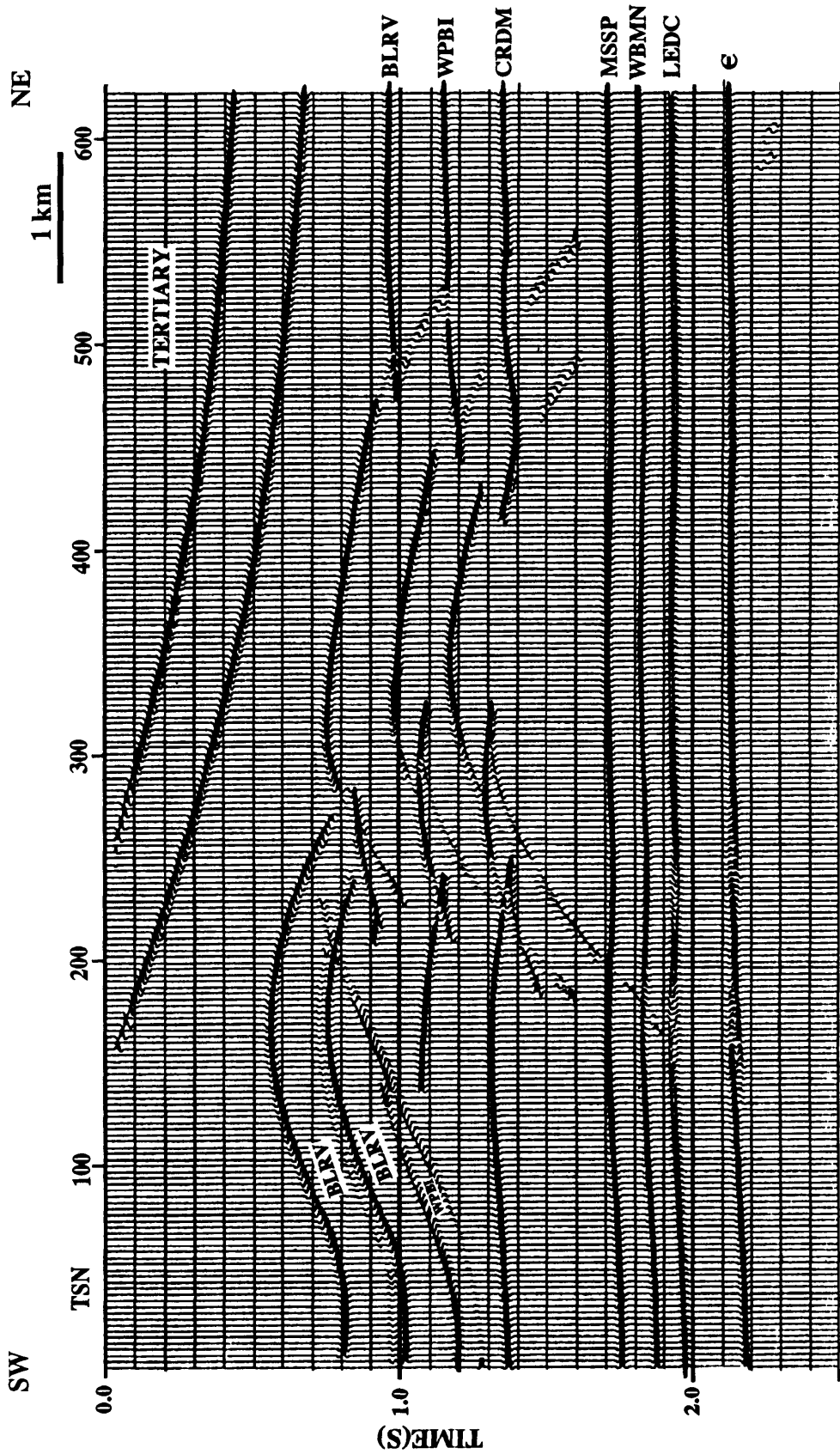


FIG. 5.8. Synthetic P-P stacked section generated from the processing flow in Figure 5.7. Full-offset traces were used. Note the smearing events below the Triangle Zone core, i.e., below 1.8 s. between trace 100 - 300.

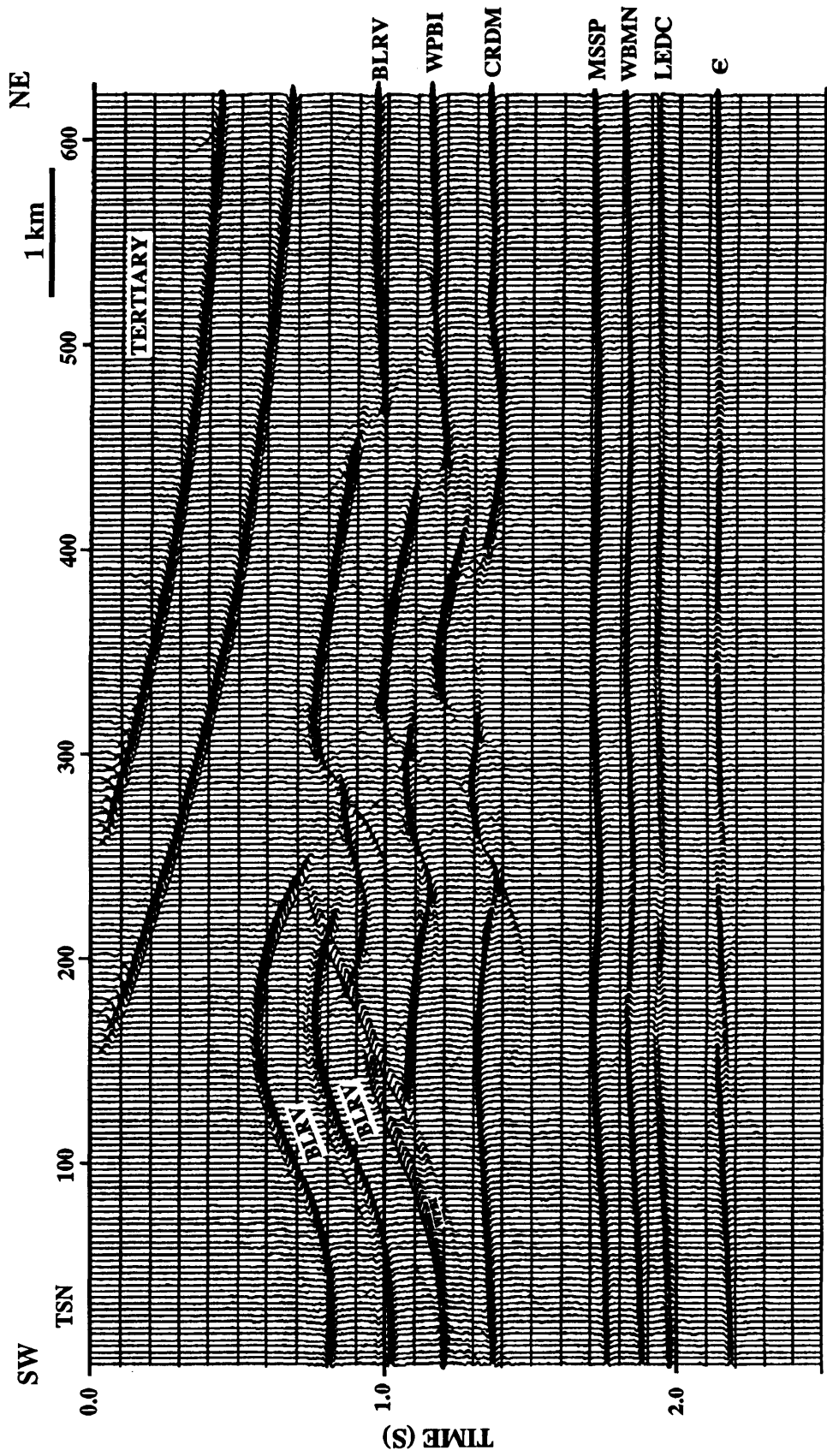


FIG. 5.9. Stolt ( $f-k$ ) migrated section of the full-offset stacked section in Figure 5.8. The events along the edges of the pop-up structure and synclines below the antiformal stack appear to be dispersed.

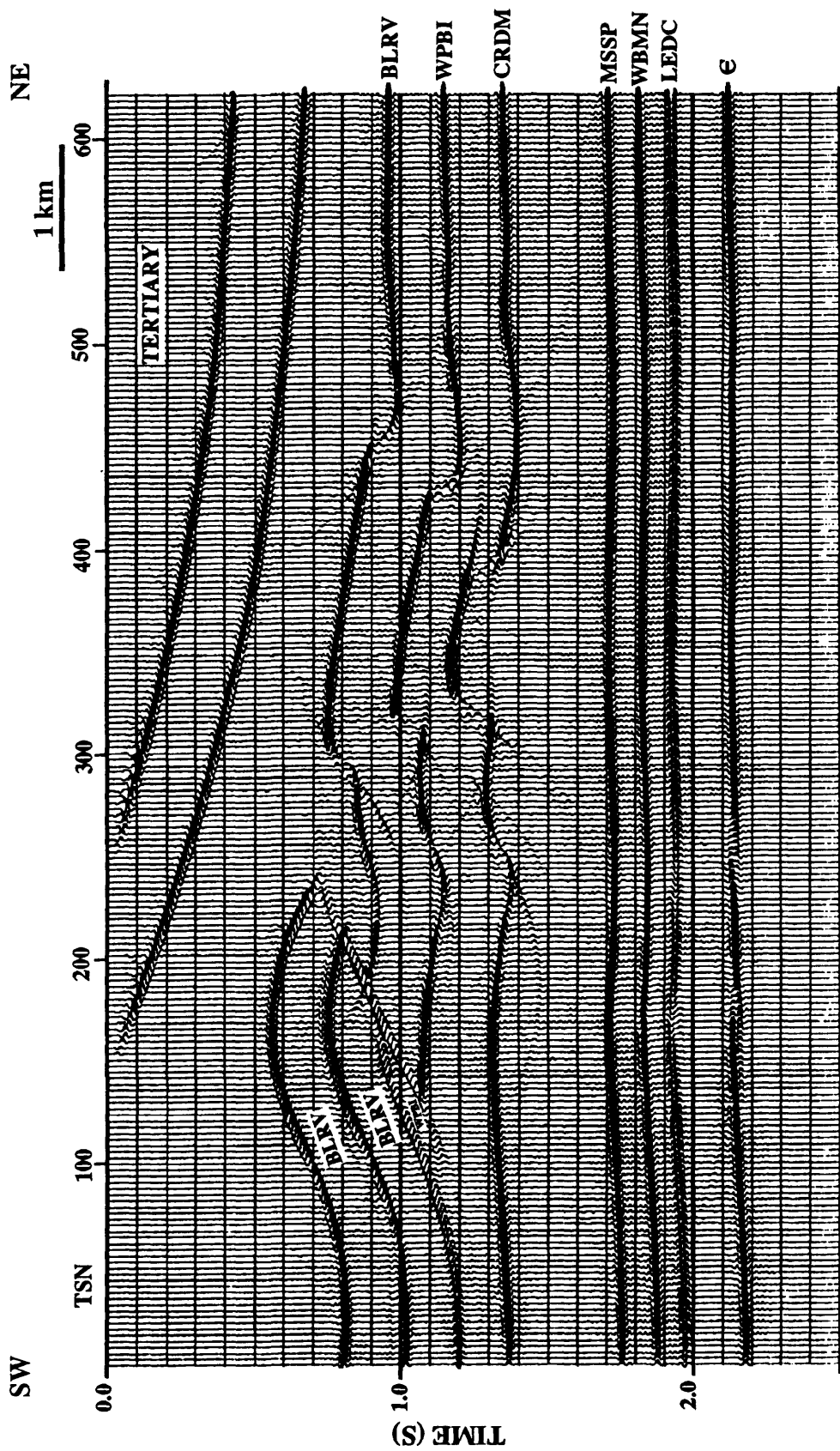


FIG. 5.10. Phase-shift migrated section of the full-offset stack. DMO was not included in the processing flow. Note dispersion of events at the western edge of the pop-up structure and synclines below the antiformal stack.

The migration results of the CMP-stacked section clearly show that, with the existence of significant vertical and lateral velocity variations, the conventional CMP-stack method not only failed to stack the events coherently but also may not be able to mimic the true zero-offset section, even though correct stacking velocities were applied. As a result of the latter failure, the effectiveness of poststack migration was reduced because the zero-offset assumption was violated. These observations substantiate the conclusion of Morse et al. (1991) in that depth migration, when applied poststack, can cause significant errors in repositioning stacked events and collapsing diffractions. Furthermore, the results from this modelling study also imply that zero-offset ray tracing, which is usually employed to aid in seismic interpretation, in some cases may not be applicable, as its output does not exactly simulate a stacked section of field data. It is then preferable that full-offset modelling should be performed.

#### 5.2.5.1.1 Dip-Moveout (DMO) Correction

DMO was tested on this data set, based on the modified processing flow in Figure 5.7. After applying DMO correction, the data were stacked and migrated using the phase-shift technique. It is apparent from the DMO-corrected migrated results, displayed in Figure 5.11, that the DMO technique yielded a significantly improved image of steeply dipping reflectors. This can be seen from the edges of the pop-up structure, particularly for the Belly River and Wapiabi events. Diffractions in these zones were collapsed to their original reflection points almost perfectly whereas those in the non-DMO-corrected migrated section (Figure 5.10) appeared to be dispersed. However, it is observed that the improvement of reflection continuity obtained from DMO correction is confined to zones of steeply dipping reflectors (e.g., the edges of the pop-up structure). The overall image of the DMO-corrected, migrated section is essentially similar to that of the non-DMO corrected, migrated section. This result is consistent with that observed in the field data

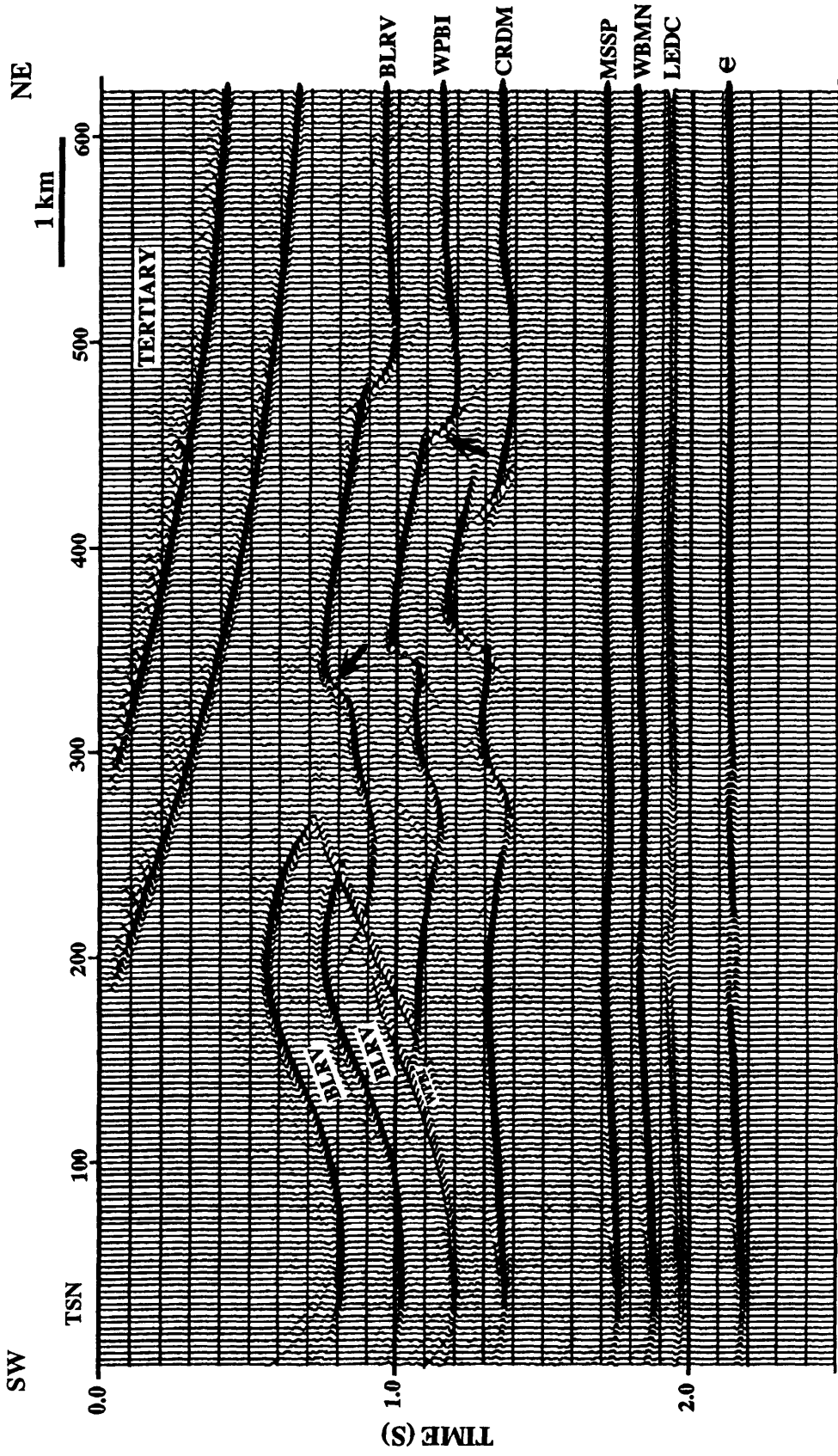


FIG. 5.11. DMO-corrected, phase-shift migrated section. Compare this figure with Figure 5.10 and note better imaging of steep dips, indicated by arrows, obtained from the DMO technique.

(line 2B) in that no obvious improved image of events in the Triangle Zone core was seen after application of DMO.

#### 5.2.5.1.2 Offset-Limited Stack

The DMO technique, although providing significant improvements in steep-dip imaging, did not address the problem of raypath distortion brought about by velocity inversions and lateral velocity variations. The coherency of events below the antiformal stack and pop-up structure was not improved after the correction for DMO, as indicated in Figure 5.11.

As illustrated in Chapter 3, in structurally complicated areas, a limited offset range of traces in the CMP stack can enhance reflection continuity. This is because the raypaths of a widely separated source and receiver can suffer complicated velocity distortions which may cause their corresponding NMO curves to deviate considerably from the hyperbolic approximation. Furthermore, the hyperbolic NMO assumption begins to break down when the source-receiver offset exceeds the reflector depth. All these effects, including others described in Chapter 3, contribute to the deficiency in performing NMO correction for large-offset data, which consequently deteriorate the stacked output.

Using only traces within a source-receiver offset between -2000 m and 2000 m with respect to the full-offset range of -3993 m to 3993 m, an offset-limited stacked section was generated and is displayed in Figure 5.12. The processing procedures and parameters used were the same as applied to generate the full-offset stacked section. Note that the DMO correction was not included in the processing flow as the effectiveness of this method had been determined previously, and also because it was found that the DMO process was very time-consuming. As expected, Figure 5.12 shows considerable improvement in continuity of the later events. Reflection smear present in the full-offset

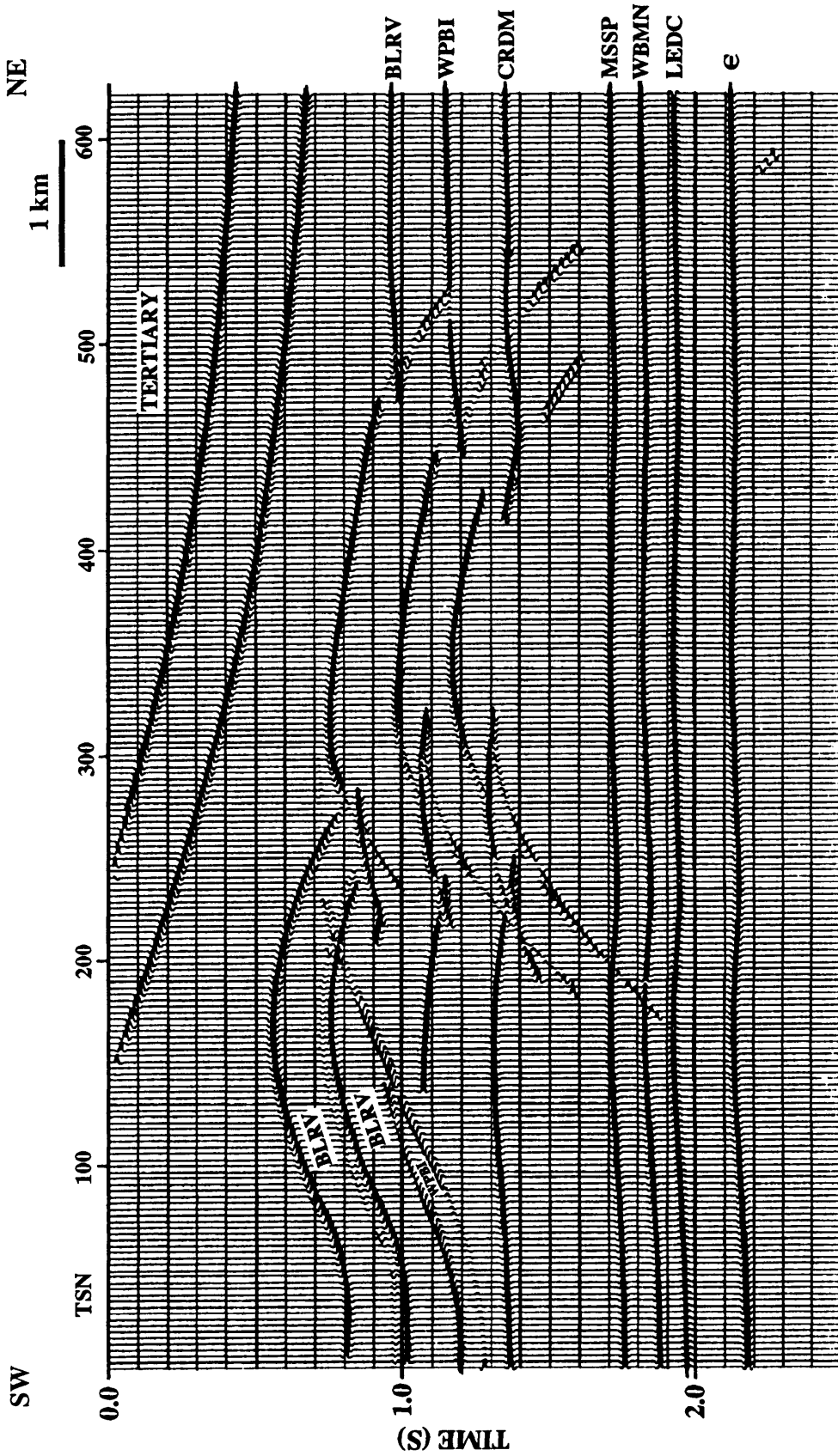


FIG. 5.12. Offset limited stack using traces within a window of -2000 to +2000 m with respect to the full-offset range of -3993 to 3993 m. The smeared events below 1.8 s seen on the full-offset stack (Figure 5.8) were eliminated.

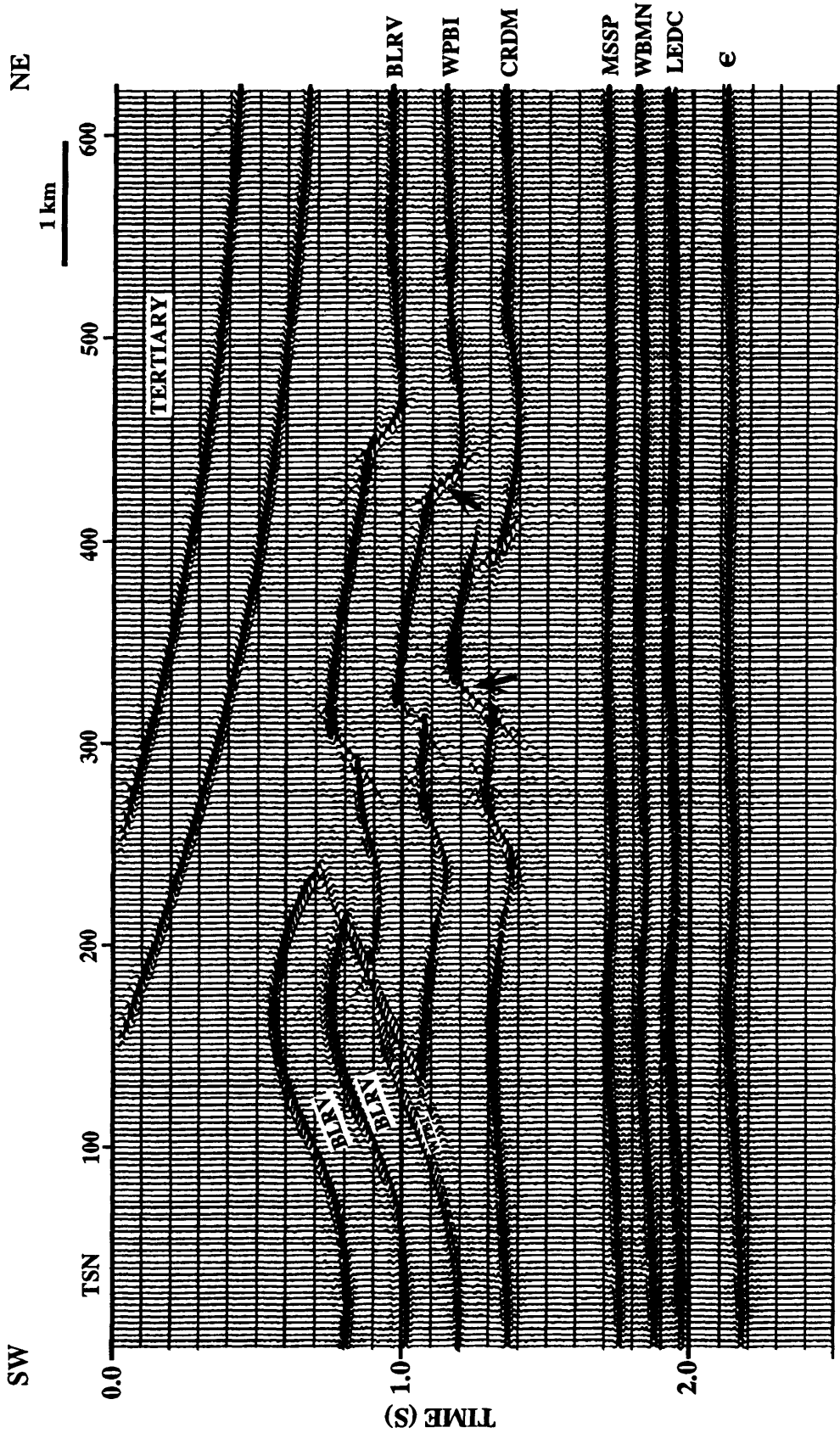


FIG. 5.13. Migrated section of the offset-limited stack in Figure 5.12 using phase-shift technique. Compare this Figure with the full-offset migrated stack in Figure 5.10 and note improvement of steep reflections indicated by arrows.

stacked section was eliminated almost completely by limiting the offset range. Furthermore, after the application of the phase-shift migration (Figure 5.13), the diffractions were also collapsed better, leading to a better overall image of the Triangle Zone when compared with the full-offset migrated section.

However, it should be remembered that in the field-data case, the value of this technique is limited by the correspondingly low fold (i.e., low signal-to-noise ratio characteristics). Also some processing steps, such as residual statics correction, require high-fold data for optimum performance.

#### 5.2.5.2 Discussion

Seismic modelling indicates the presence of seismic artifacts or velocity anomalies beneath the Triangle Zone and pop-up structures (Figure 5.9), which match fairly well the features observed in the processed field data (Figure 4.6). However, some remaining features in the field migrated section of line 2B cannot be explained. Firstly, seismic modelling depicts two zones of velocity pull-up beneath the antiformal stack and pop-up structure (Figure 5.9) but seismic line 2B shows that three time-structural anticlines are present in this zone (Figures 4.6 and 4.15b). Secondly, similar time-structural anticlines (with a much smaller magnitude) are observed to the northeast of the pop-up structure, i.e., at approximately the location of well 6-4-31-5W5 (Figure 4.8). Provided that these subtle features, which exist beyond the areas of complex velocity fields, are not the remaining long-wavelength statics as described by Yilmaz (1987), they might be real compressional structures formed during the last phase of the Laramide orogeny. Similar features were also found by Skuce et al. (1992) at approximately 30-40 km to the east of the Triangle Zone in their study area. Therefore, it is likely that both seismic artifacts and real compressional structures are associated in the zones beneath the

antiformal stack and pop-up structure, but these subtle structures are more noticeable in the seismic data because of the enhancement by velocity pull-up.

The results from seismic-modelling analyses suggest that raypath distortion through the central part of the Triangle Zone is not as severe as expected, since time migration yielded results similar to those of depth migrations. This is due mainly to the absence of high-velocity layers (i.e., carbonate rocks of Mississippian or Devonian age) in the antiformal stack. It is therefore concluded that smearing of reflection events, commonly found below the Triangle Zone core, is attributed to prestack or problems related to data acquisition. A synthetic P-P shot record collected over the central part of the Triangle Zone substantiates this as shadow zones are found to occur below the lower detachment (Figure 5.6 A). These, including severe statics in this part of the Triangle Zone, contribute to deterioration of data quality which consequently causes poor imaging of the Triangle Zone structure.

The current trends of seismic data acquisition are towards large number of seismic channels, with relatively large shot intervals (Lawton and Spratt, 1991). This may not be appropriate for exploration in Triangle Zones, since large source-receiver offsets were found to be detrimental in generating the highest-quality stacked sections. The modelling results indicate that better images can be achieved by using only near-offset traces in the stack. This, in turn, can be obtained by limiting the far offsets during data acquisition. It can therefore be concluded that the key in optimum imaging of the Triangle Zone is high-fold data with relatively small shot intervals and small offsets (i.e., offsets up to 2.5 km for imaging targets at approximately 3.0 to 3.5 km deep). These will ensure optimal static solutions, effectively cover the shadow zones, and optimize NMO and stacking process.

### 5.2.5.3 P-SV Modelling

The existence of seismic artifacts below the Triangle Zone may lead to difficulties in delineating structure, lithology and reservoir properties of formations in this region, based on the conventional P-P data only. This means that without adequate well control and high-quality well-log data, interpretation of the P-P seismic sections collected across the Triangle Zone may be ambiguous. Thus, in order to better understand the Triangle Zone geometry, other supporting information or integrated techniques are necessary.

One of the most promising techniques is to use conventional P-wave data in conjunction with S-wave data. This technique has been reported to successfully applied in many exploration and engineering problems. In seismic exploration, the technique is mainly used to identify rock lithology, stratigraphy and anisotropy; e.g., Domenico and Danbom (1987), Tatham and Stofa (1976), Tatham (1982), and McCommark and Tatham (1986). However, applications in structural mapping and interpretation have also been reported (e.g., Suyama et al., 1987; Fix et al., 1987).

In the Triangle Zone of the Canadian Rocky Mountain Foothills, Lawton and Harrison (1991) utilized converted shear-wave (P-SV) data integrated with P-P data to successfully map the eastern flank and the upper detachment of the Triangle Zone in the Springbank area, near Jumping Pound gas field in Alberta. However, their study did not cover the Triangle Zone core or its western limb. Thus, it was decided to evaluate the applicability of P-SV data for imaging a more complicated part of the Triangle Zone. Currently, shear-wave field data have not been collected and therefore the study was conducted by means of seismic modelling instead.

By using the same geologic model and physical parameters as were used for the P-P modelling, ninety synthetic P-SV shot gathers were collected from the model. Each shot gather comprised a 120-trace split-spread along with a 99-m shot spacing and a 33-m receiver spacing. This acquisition configuration produced a maximum fold of 20 over the

antiformal stack and the Triangle Zone core. The number of traces per record in this case was reduced from 240 (used in the P-P modelling) to 120 following preliminary acquisition tests which showed that significant phase distortions occurred in reflections on traces with large source-receiver offsets, due in part to directivity effects (Hatton et al., 1988).

Figures 5.14 demonstrates examples of the P-SV shot gathers from the eastern limb and the Triangle Zone core, in which polarity reversal of data on traces from opposite sides of the shot location is apparent. The P-SV data set underwent processing steps as outlined in Figure 5.15. Due to differences in raypath geometry and particle motion of the P-SV data with respect to P-P data, additional processing steps were required and are discussed as follows.

When acquiring the P-SV data using a split-spread geometry, all the radial-component geophone sensors are oriented in the same direction along the entire line. However, the SV waves arriving at the receivers on one side of the shot position possess initial particle motion opposite to that at receivers on the other side of the shot (Figure 5.16). This gives rise to the polarity reversal across the shot locations seen on P-SV records. Moreover, unlike the raypaths of conventional P-P waves, the P-SV raypaths are asymmetric, hence they cannot be sorted using the conventional CMP gathering method directly (Schafer, 1993).

In this study, the asymptotic gathering technique was used to sort the data. The asymptotic value was derived by Fromm et al. (1985) and is defined as :

$$x_p = \frac{x}{1 + \left(\frac{V_p}{V_s}\right)^{-1}}, \quad (5.3)$$

where  $x_p$  is the offset from the source to an asymptotic value which was used instead of the CMP or the actual common conversion points (CCP);  $x$  is the source-receiver offset,

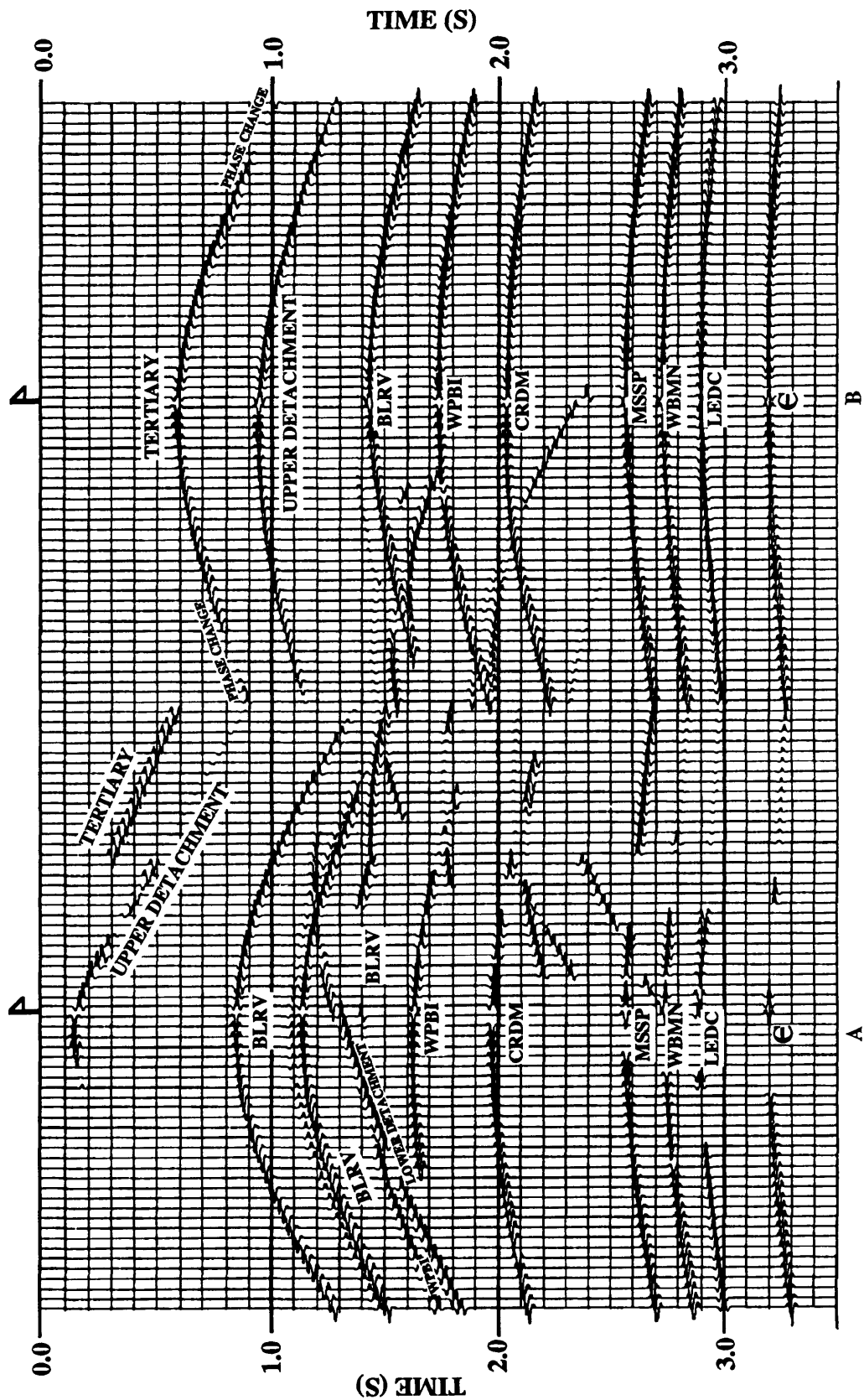


FIG. 5.14. Synthetic P-SV shot gathers from the Triangle Zone core (A) and eastern limb (B). A Ricker wavelet with a central frequency of 25 Hz was used. Polarity reversal on one side of the spread is present. Also, phase changes on the far-offset shallow events begin to appear.

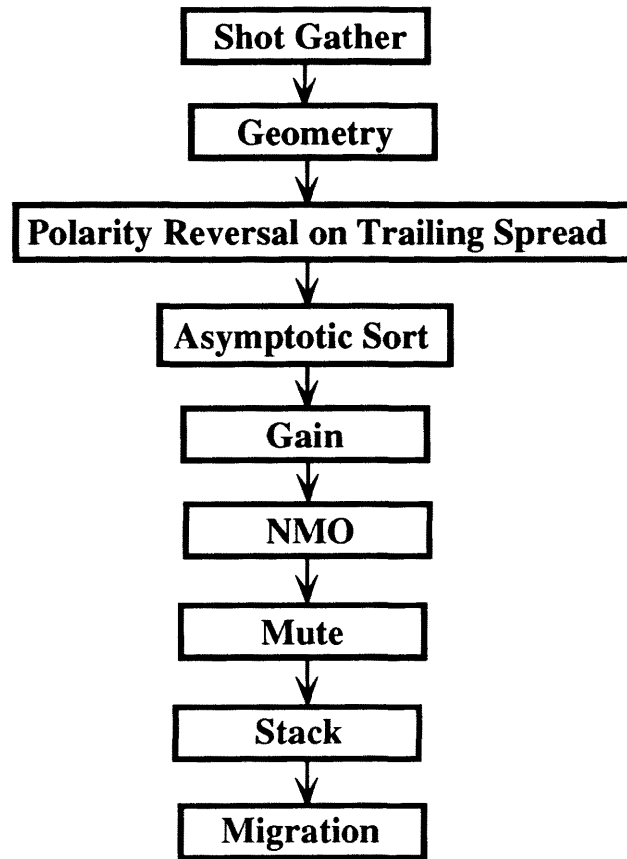


FIG. 5.15. Processing flowchart for synthetic P-SV data.

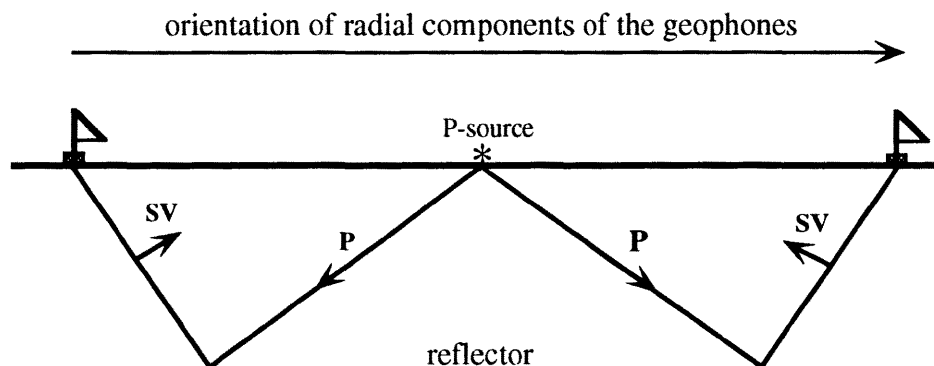


FIG. 5.16. P and SV particle-motion directions with respect to the orientation of radial-component geophone sensors.

and  $V_P/V_S$  is an average P-wave to S-wave velocity ratio. The P-SV raypath geometry as well as the geometry of parameters in equation 5.3 is shown in Figure 5.17.

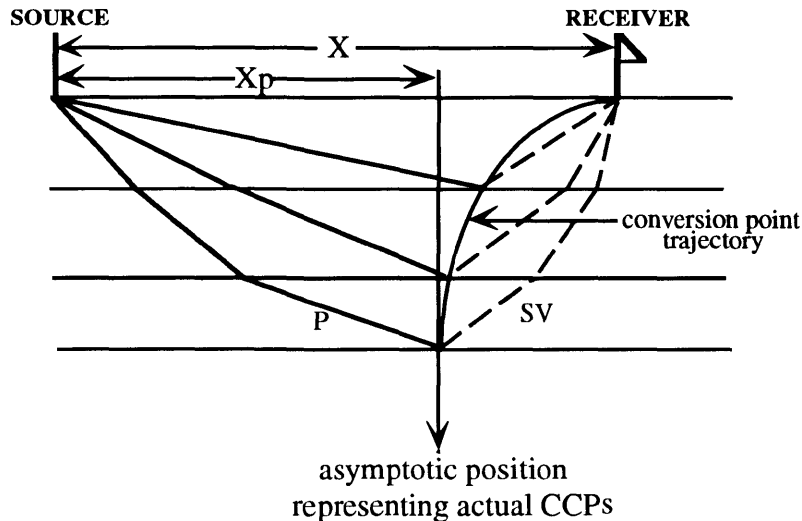


FIG. 5.17. P-SV raypath geometry showing the asymptotic position and the actual common conversion points along the conversion trajectory curve (from Eaton et al., 1990).

As portrayed in Figure 5.17, the asymptotic gathering method only approximates the actual P-SV common conversion points (CCP) by using a constant position ( $x_p$ ) obtained from equation 5.3 regardless of the lateral variation in position of the conversion point with depth. This technique will be detrimental to stacked data in cases when the CCP locations deviate significantly from the asymptotic position, especially in the shallow parts of the section. Eaton et al. (1990) showed that to gather the P-SV data properly, a depth-variant mapping technique should be used. However, in this analysis, the asymptotic gathering technique was employed due to its simple operation and effective run time. The results were examined carefully to determine if the depth-variant mapping technique would, in fact, make a significant difference. It was found that the

quality of the P-SV stacked section (Figure 5.18), based on the asymptotic sort, was reasonable when compared with the P-P stacked section. No severe reflection smear appears to occur from incoherent stacking, and the major segments of the model were well delineated. The stacked data were then migrated using the conventional phase-shift technique. The P-SV interval velocities applied in migration were calculated from equation 5.4 (Iverson et al., 1989) :

$$V_i^2 = V_{Pi}V_{Si} \quad (5.4)$$

where  $V_{Pi}$  and  $V_{Si}$  are the P-wave and S-wave interval velocities, respectively. The P-SV migrated section is displayed in Figure 5.19 with major events annotated. It is seen that the image of the model is similar to that obtained from the P-P data (Figure 5.10).

#### 5.2.5.4 Discussion

The results from P-SV modelling demonstrate good potential for using P-SV data to aid in complex structural interpretation. All the major components of the Triangle Zone, i.e., the antiformal stack, and the upper and lower detachment faults were well delineated in the processed P-SV data. These observations are very encouraging in that, in a complex structural environment, the P-SV data may convey information similar to that of the conventional P-P data. This, in turn, means an integrated P-P and P-SV technique can be a very useful tool in elucidating the Triangle Zone, and provide more accurate interpretations of its geometry, because the interpreted model has to fit both data types. In addition, lithology and stratigraphy of the formations below the Triangle Zone, which are of exploration interest, can also be obtained by analyzing the  $V_P/V_S$  variation between these horizons.

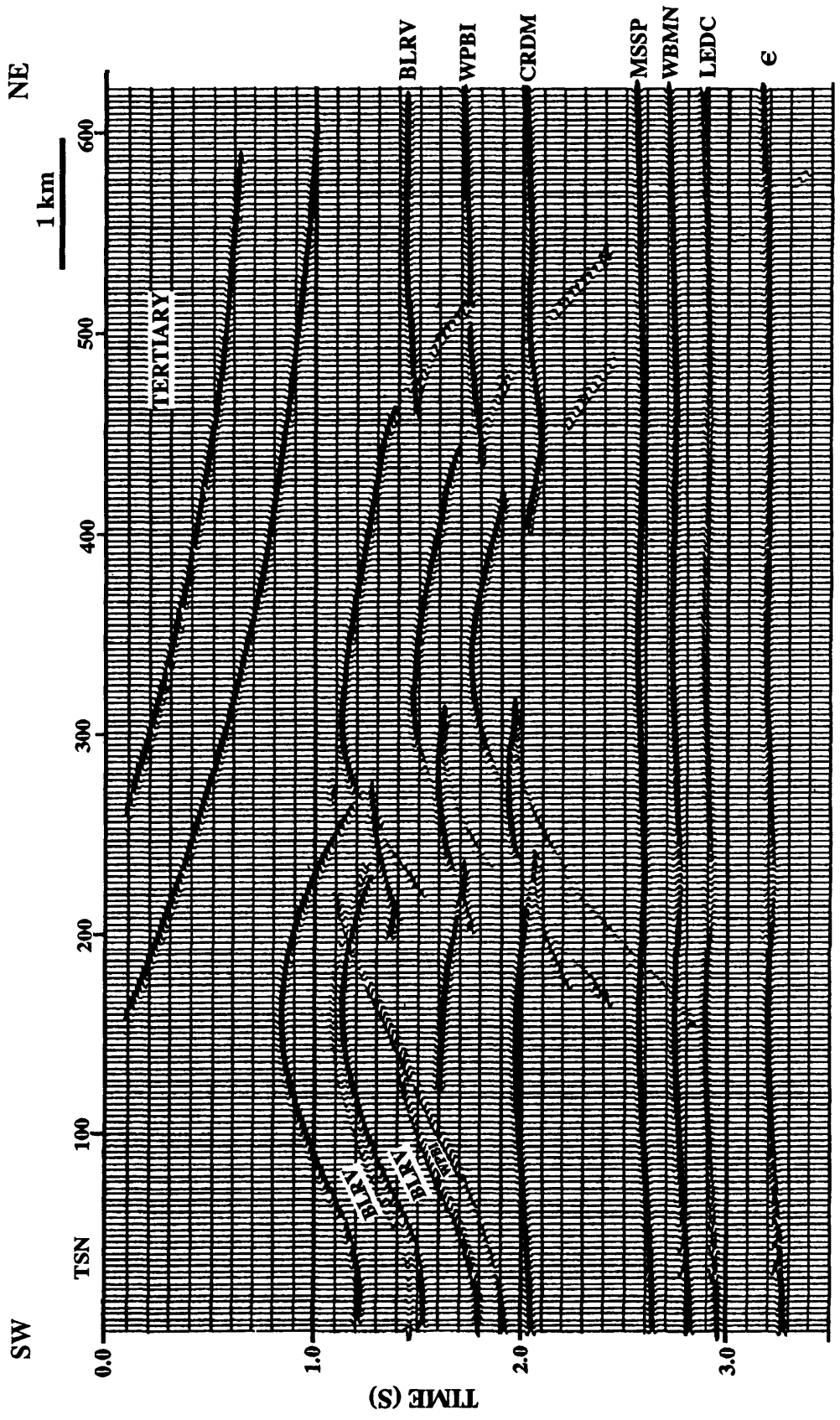


FIG. 5.18. Synthetic P-SV stacked section generated from the processing flow in Figure 5.15.

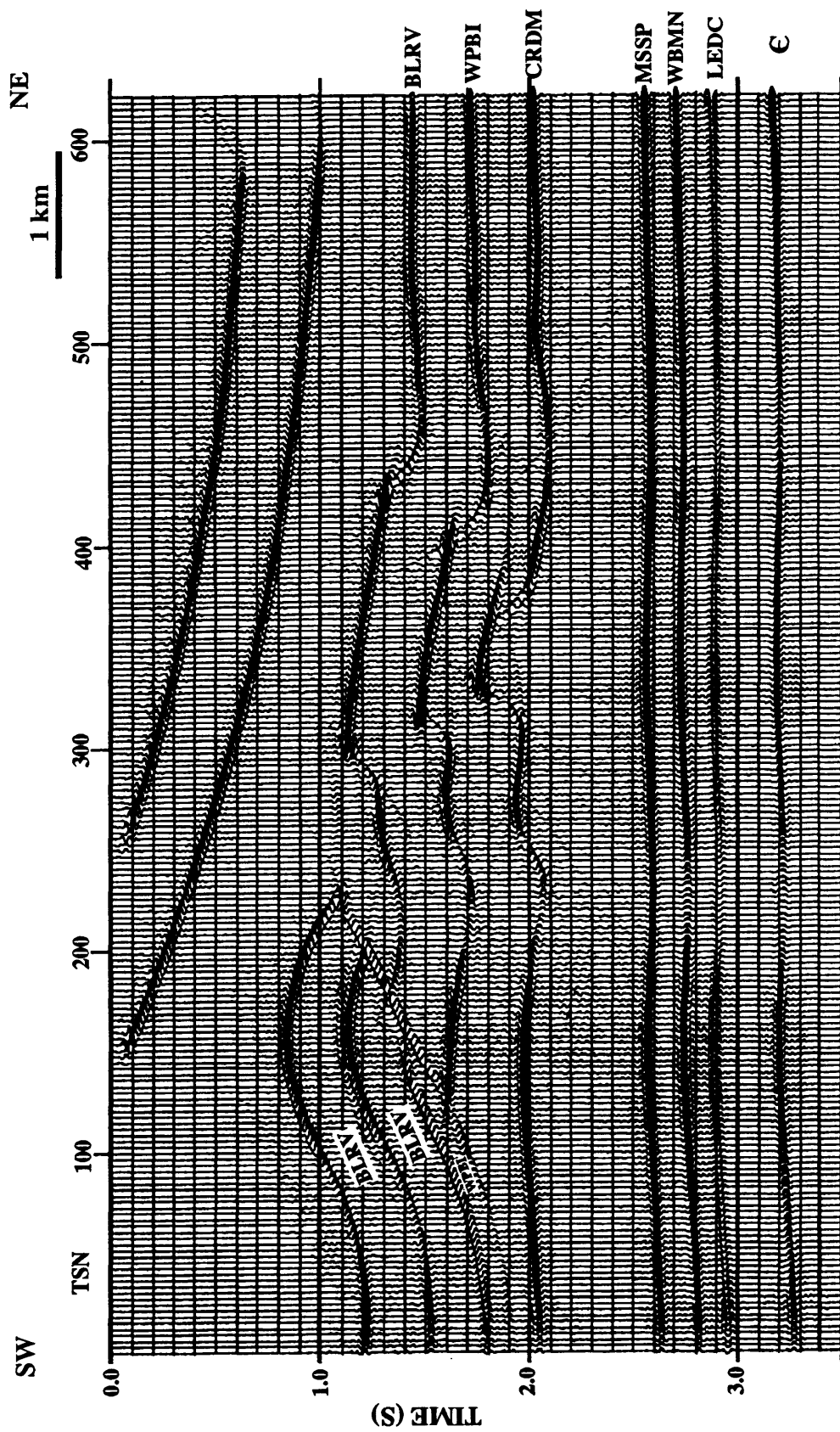


FIG. 5.19. Phase-shift migrated section of the P-SV stack in Figure 5.18 using 100 % interval velocities.

## 5.3 Physical Seismic Modelling

### 5.3.1 Background

Physical seismic modelling has been employed by researchers to investigate seismic wave propagation since the early part of the century (Terada and Tsuboi, 1927; Zimmerman, 1991). The method involves generating and collecting full-waveform seismic data over scaled geologic models using laboratory apparatus. In practice, geological structures are scaled down using scaling factors chosen to keep the size of the physical model manageable, while maintaining the desired seismic resolution. The scaling factors are dependent upon the frequency bandwidth of the model sensors and limitations in model construction (Zimmerman, 1991). The scaling factors are related to the field velocity, distance and time as follows.

In a field situation, a particular wave travels a distance  $S$  in time  $T$  through a medium of velocity  $V$ . Therefore,

$$S = VT. \quad (5.5)$$

In the laboratory modelling situation, all distances and lengths are scaled by a factor  $a$ ; all velocities by a factor  $b$ ; and all times by a factor  $c$ , such that:

$$s = vt,$$

where,

$$s = aS, \quad (5.6)$$

$$v = bV, \quad (5.7)$$

and

$$t = cT. \quad (5.8)$$

Therefore,

$$aS = bVcT, \quad (5.9)$$

and

$$a = bc. \quad (5.10)$$

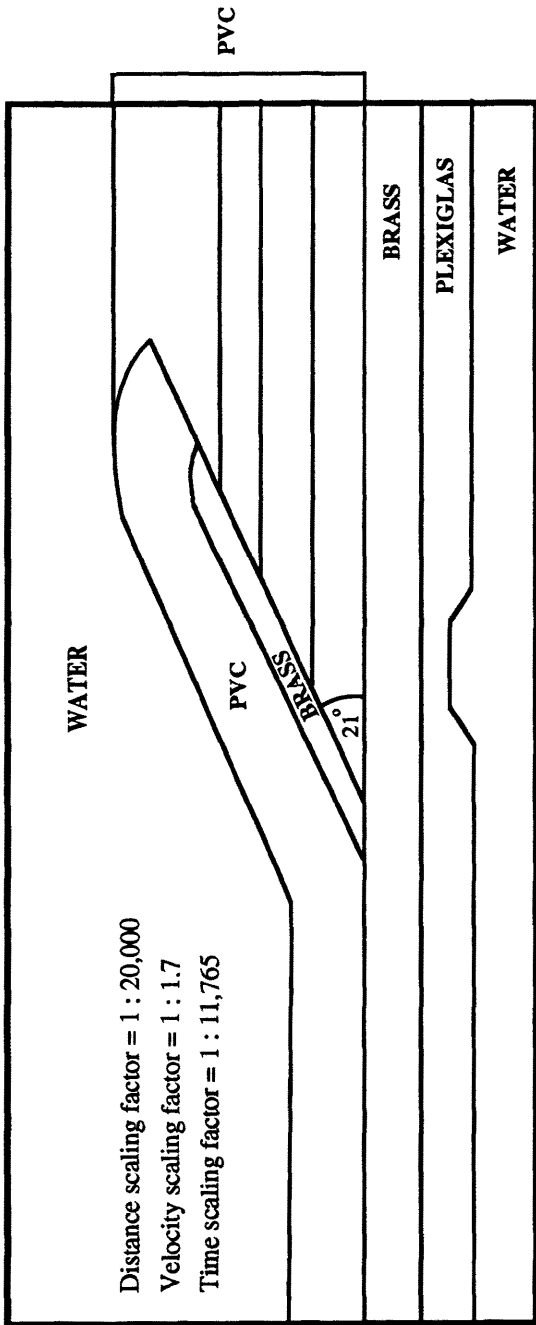
Typically, the distance-and time-scaling factors are chosen such that the scaled frequency bandwidth is in the same range as that of the field data, while velocity is usually left unscaled, i.e.,  $b = 1$  (Zimmerman, 1991). However, to accommodate large

geologic models or very high-velocity components of models, the model velocity can also be scaled (Chow, 1989; Edwards, 1992; Hrabí and Lawton, 1992). Normally, the velocity scaling factors are within the range  $1 < b < 3$  for rock formations in the Alberta basin (Chow, 1989).

The physical modelling system at the University of Calgary, developed and described by Cheadle (1988), is currently equipped with spherical piezoelectric transducers having a central frequency of 250 kHz. The sampling intervals available on the digital oscilloscope are 50, 100, 200 and 500 ns. Hence, if the time scaling factor is selected as 1:10,000, along with a 100-ns sampling rate, then the scaled central frequency of the corresponding field data is 250 kHz/10,000 (= 25 Hz, as the frequency scaling factor is the reciprocal of the time scaling factor); and the scaled sample interval is 100 ns x 10,000 (=1 ms) respectively.

### 5.3.2 Model Construction and Data Collection

A generic model of thrust fault in the Alberta Foothills, characterized by high-velocity carbonate layers thrust over lower-velocity clastic rocks, was constructed out of PVC, brass and Plexiglas. Figure 5.20 shows a cross-section of the physical model along with the physical parameters, i.e., P-wave velocity, S-wave velocity, density and thickness of each layer. PVC, representing the clastic layers, was used to form the bulk of both the hanging-wall and footwall sheets of the model, with a 1.3-cm thick brass sheet inserted at the base of the hanging wall of the thrust fault to simulate a high-velocity carbonate layer. The ramp angle is approximately 21 degrees. The lower part of the thrust model is composed of brass and Plexiglas planar layers representing undeformed Mississippian and Devonian rocks. Also included in the Plexiglas layer is a simulated Devonian reef situated beneath the ramp at approximately the middle part of the model.



| Materials         | Thickness (cm) | Vp (m/s) | Vs (m/s) | Density (Kg/m <sup>3</sup> ) |
|-------------------|----------------|----------|----------|------------------------------|
| Water             | —              | 1480     | 0        | 1000                         |
| PVC (hangingwall) | 3.5            | 2300     | 1030     | 1400                         |
| PVC (footwall)    | 11.75          | 2300     | 1030     | 1400                         |
| Brass (ramp)      | 1.3            | 4300     | 1990     | 2200                         |
| Brass (planar)    | 2.7            | 4300     | 1990     | 2200                         |
| Plexiglas         | 2.25           | 2750     | 1375     | 1190                         |

FIG. 5.20. A cross-section of a thrust fault model and material parameters.

The distance and velocity scaling factors were chosen to be 1:20,000 and 1:1.7 respectively, which results in a time scaling factor of 1:11,765. This time scaling factor leads to a scaled central frequency of about 21 Hz which is slightly lower than the average central frequency of the surface-seismic data used in this study, i.e., 30 Hz. However, the acoustic-impedance contrasts at each layer interface, which are of interest in this experiment, are similar to those of the real geological structure.

Initially an acoustic experiment was undertaken for which the model was placed on a table base in the water-filled seismic modelling tank. A pseudo 2-D zero-offset seismic line was recorded using a receiver and source spacing of 16.5 m (after scaling) which is equivalent to the trace spacing of the field-seismic data used in this thesis. The line contained 700 traces and was recorded to 6 s (two-way time).

### 5.3.3 Results and Discussion

Figures 5.21 and 5.22 illustrate unprocessed and processed data from this experiment with the major events annotated. The processing procedures applied were predictive deconvolution, AGC (with a 0.6 s window) and mute. It is seen that the recorded data are of rather poor quality, i.e., very little seismic energy was recorded from layers beneath the ramp, and the events are essentially masked by multiples across the section. The ringy signals in the shallow part, i.e., between 0.35 and 1.2 s (Figure 5.21) are interpreted to be reverberations between source and receiver. Some diffractions generated from surface discontinuities of the model can as well be observed, e.g., at the middle of the section between time 1.6 and 2.0 s.

Predictive deconvolution effectively suppressed the multiple energy especially for the dipping and shallow, flat events on the footwall of the model, resulting in significantly improved vertical resolution of the data. Data gaining was found to be mandatory in obtaining images of later events below the ramp since only very low-

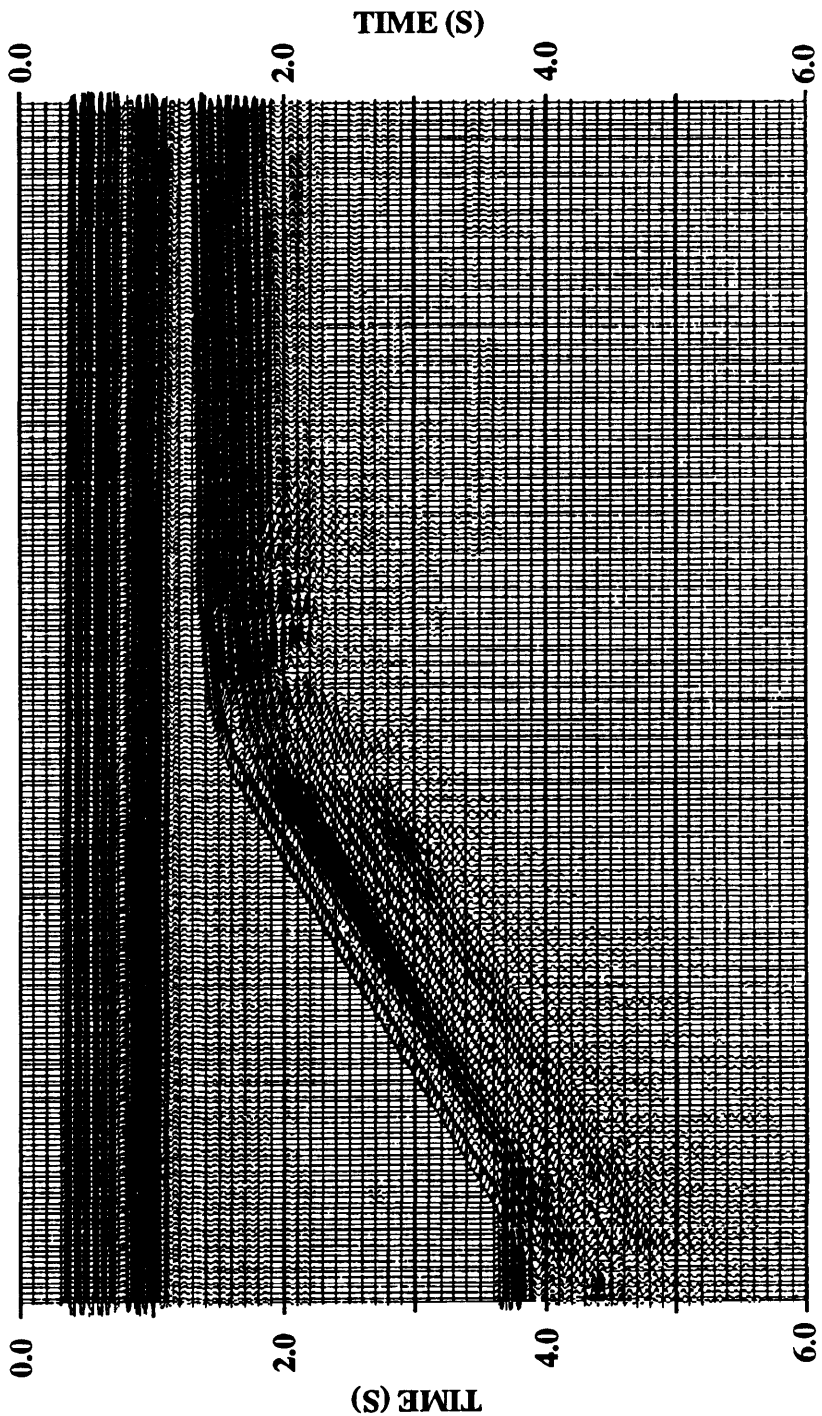


FIG. 5.21. A zero-offset physical modeling record from the thrust fault model in Figure 5.20.

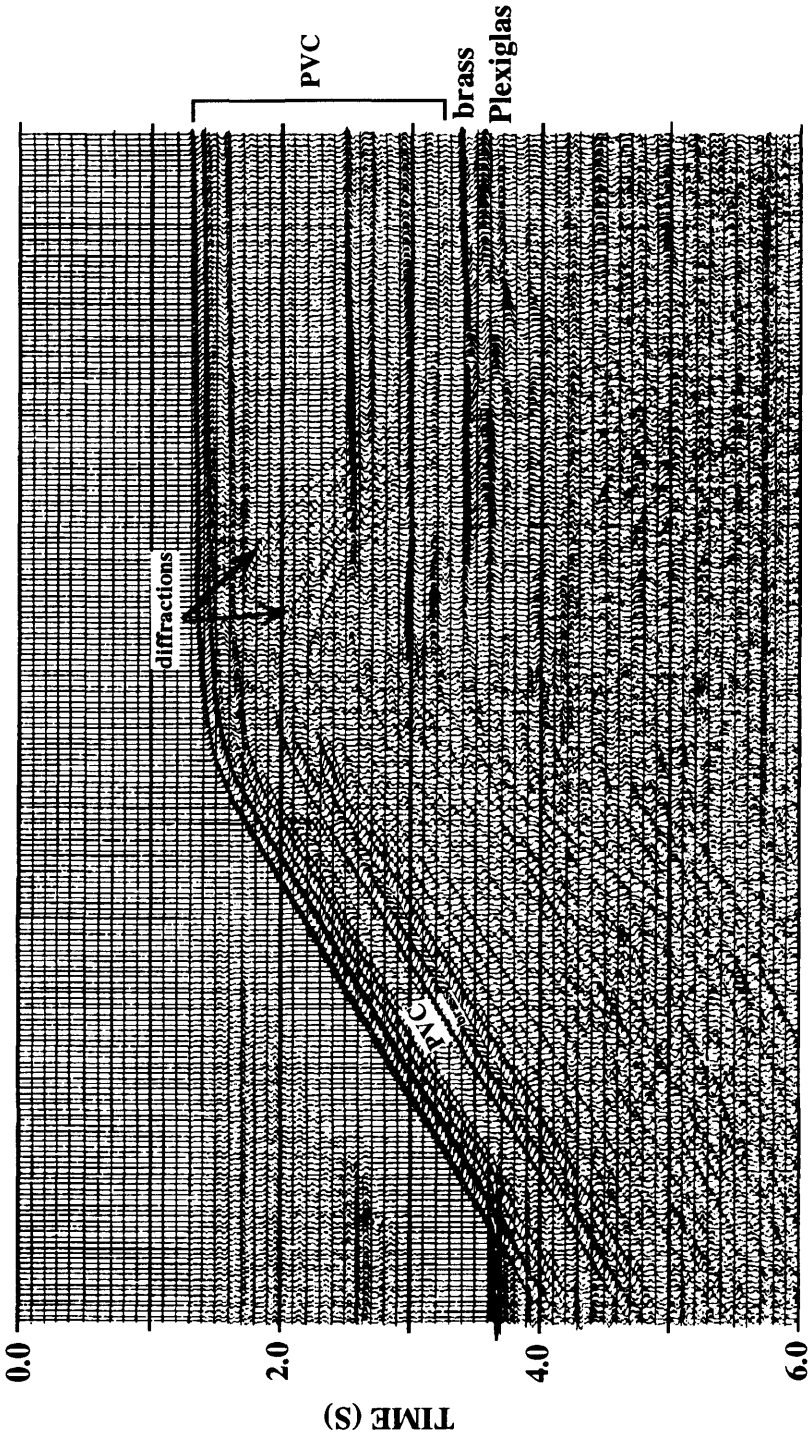


FIG. 5.22. The same record as in Figure 5.21 after Predictive Deconvolution, AGC with a window of 0.4 s, and mute.

amplitude signals are present in this zone. Following deconvolution and gain, mute was applied to eliminate the reverberations in the shallow part of the section.

It is obvious that although the basic processing steps, as described above, partially improved the overall image of the recorded section, most of the improvements are in the zones of flat or dipping events in the early part of the model. Later events still appear to be very chaotic and no clear reflections from the simulated Devonian reef can be determined in the processed section. This poor image is considered to be an effect of the high-velocity dipping layer (brass) which prevented a significant amount of the seismic energy from penetrating through it.

To verify these results, a numerical modelling analysis was undertaken based on the same model geometry, velocities and densities as that used for the physical model. A zero-offset data set was recorded across the model using a trace spacing of 16.5 m. Figure 5.23 shows a numerical record from this thrust-fault model. As expected, the numerical-modelling result exhibits characteristics similar to those of the physical modelling results in that amplitudes of the horizons below the ramp are very low and no reflections from the reef model can be determined. It was further found that in order to image the events below the ramp a very small AGC window (i.e., 0.2 s in this case) had to be applied (Figure 5.24). This small AGC window is not applicable in the processing of real seismic data as all events will be significantly equalized and noise will as well be enhanced.

This physical modelling study demonstrates some important characteristics of seismic reflection data collected over zones with a severe velocity inversion. These include low signal-to-noise ratio, low signal coherency and severe multiples. This suggests that delineation of subtle structures below this structural feature is difficult and will require a very high-fold data to both improve signal-to-noise ratio and to suppress multiple energy effectively. Another implication from this study is that AVO analysis of

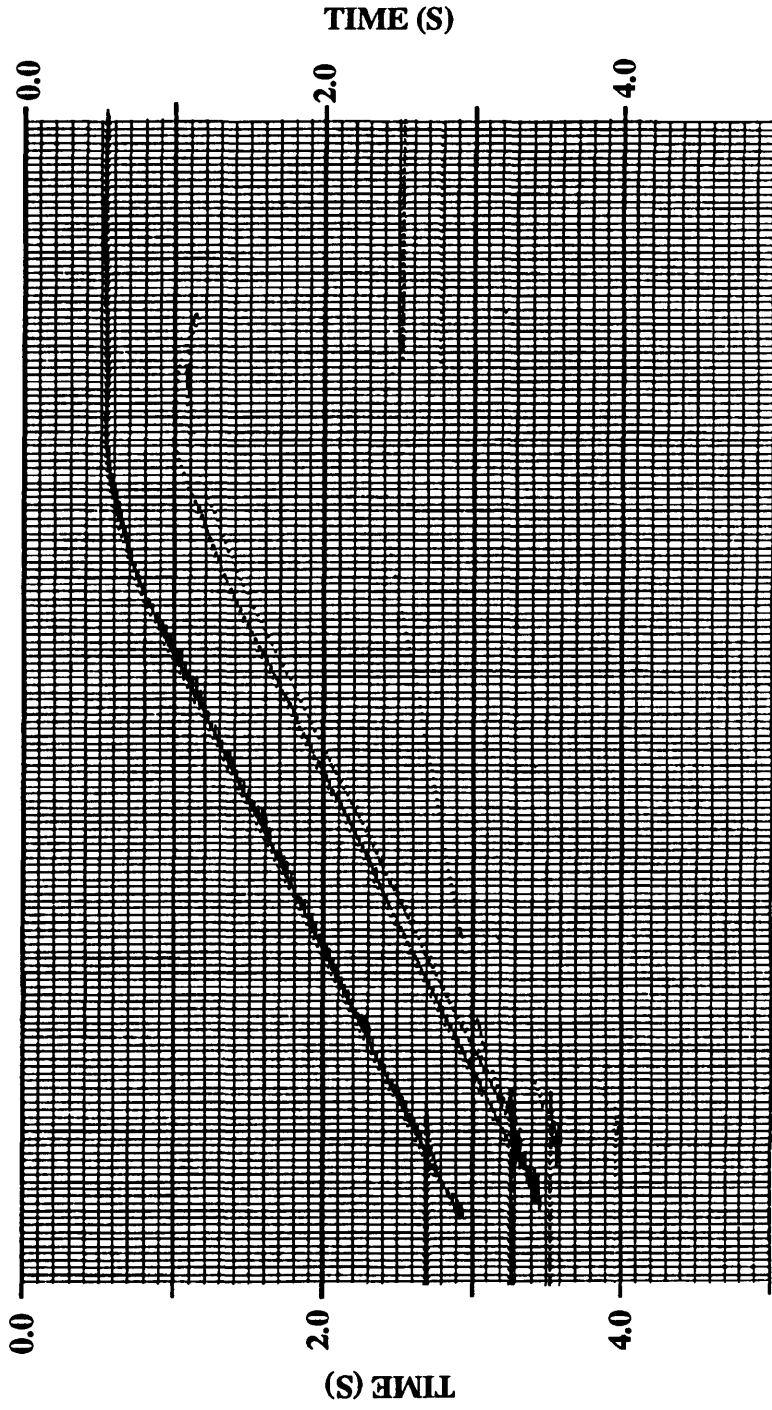


FIG. 5.23. A zero-offset numerical modelling record from the thrust fault model in Figure 5.20.

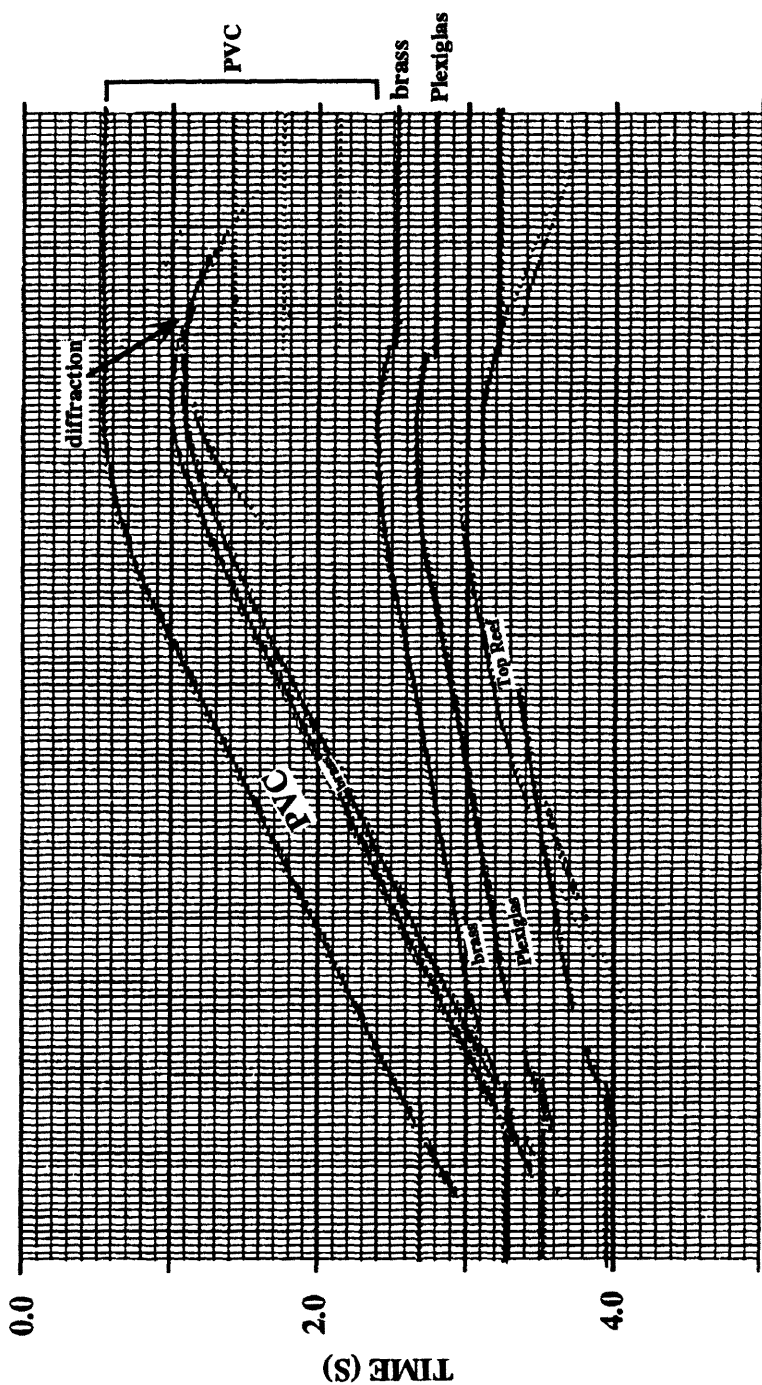


FIG. 5.24. The same record as in Figure 5.23 after AGC with a window length 0.2 s.

deep events or other true-amplitude processing techniques may not be applicable, as significant amplitude decay is present due to severe transmission losses.

## **Chapter 6 - CONCLUSIONS AND RECOMMENDATIONS**

In this thesis, reflection seismic data, acquired across the leading edge of the Canadian Rocky Mountain Foothills, have been processed, interpreted and used to construct balanced cross-sections to show geometries of frontal structures in the Triangle Zone. Seismic modelling was used to aid in the interpretation and to evaluate the effectiveness of data processing algorithms and parameters as applied to the field data.

The major conclusions drawn from this study are :

- 1) The main culmination of the Triangle Zone in this region is interpreted to be a NW-SE trending antiformal stack of Upper Cretaceous rocks that has been driven into the foreland basin between upper and lower detachments. The upper detachment, lying within Edmonton Group rocks, exhibits a listric trajectory and dips towards the foreland at an angle of approximately 10 degrees in the west, decreasing to zero degrees in the east. The lower detachment is interpreted as being blind. It has a staircase geometry with a lower flat detached within the Jurassic Fernie Group. It is connected to a forethrust that cuts up-section through Cretaceous sequences, then becomes a long upper flat parallel to the bedding planes within Edmonton Group rocks.
  
- 2) Due to an ambiguity in the geometrical relationship between the upper detachment and the upper flat of lower detachment, two interpretations of the Triangle Zone geometry are presented in this thesis. The first model shows the upper flat of the lower detachment being parallel to the upper detachment, indicating that strain extends eastward into the foreland, whereas an alternative model shows merging of these faults, suggesting a rapid decrease in strain in this interval.

- 3) A pop-up structure involving Upper Cretaceous rocks is interpreted to form in the footwall of the lower detachment, approximately 2 km east of the antiformal stack. The pop-up structure is bounded by a forethrust on its eastern side, and by back thrusts on its western side. Its presence not only provides an insight into an evolution mechanism of an antiformal stack but it also indicates that the current lower detachment was about to be abandoned and replaced by a fault surface below the pop-up structure.
- 4) An undulating geometry of later events on the seismic sections below the central part of the Triangle Zone is found to be caused mainly by velocity anomalies caused by the juxtaposition of the antiformal stack with younger strata (i.e. Upper Cretaceous and Tertiary rocks). However, subtle compressional structures of Paleozoic rocks were also found to be associated with these time-structural anomalous zones. Therefore, it is important to exercise caution when delineating prospects in Paleozoic rocks below the Triangle Zone, and seismic modelling should be incorporated into the interpretation to verify the location and magnitudes of these velocity anomalies.
- 5) It has been shown by this study that velocity variations and inversions across the Triangle Zone in this region are mild to moderate since time migration yielded similar results to those of depth migration in terms of diffraction collapse and correct repositioning of events. Thus, smearing of deep seismic events below the Triangle Zone core was due mainly to the failures of prestack processing (e.g., NMO and stack) and problems related to shadow zones below fault planes.

- 6) The results from seismic modelling and the processing of field data show that excessively large source-receiver offsets can be detrimental to generating high-quality stacked sections due to overlying velocity structures across the Triangle Zone, along with the inefficiency of conventional NMO to correct far-offset traces. One possible method to overcome this problem is to use limited-offset traces in CMP gathers to stack (e.g., offsets up to 2.5 km for imaging targets at approximately 3.0 to 3.5 km deep). However, a drawback of this approach is a correspondingly lower signal-to-noise ratio in the stacked data. Therefore, it is recommended that in acquiring seismic data over the Triangle Zone structure, limited source-receiver offset distances be used along with relatively small shot intervals. This acquisition geometry will limit far offsets, while maintaining high fold, which should provide optimum imaging of both the Triangle Zone and later events below the Triangle Zone core.
- 7) This study demonstrates good potential for the use of P-SV data in structural imaging since it was found from modelling that P-SV data conveyed similar information to that of the conventional P-P data in a complex structural environment. This in turn means integrated P-P and P-SV reflection seismology could be a very useful tool in elucidating the Triangle Zone geometry as the interpretation has to fit with both data types. In addition, lithologic and stratigraphic information can be obtained by analyzing  $V_p/V_s$  between various horizons of interest.
- 8) The results from physical seismic modelling experiments show some important characteristics of reflection seismic data acquired over structures containing a severe velocity inversion. These include low signal-to-noise ratio, low signal

continuity and strong multiples. This indicates that delineation of subtle prospects below this inversion zone is difficult and will require high-fold data to produce reliable stacks and to suppress multiples effectively.

Although structural geometries of individual frontal structures in the Triangle Zone in this region have been well-delineated, the relationship between the upper detachment and upper flat of lower detachment in the foreland remains inconclusive. To resolve this geometrical relationship, a series of NE-SW seismic profiles across the Triangle Zone and extended into the structured part of the foreland basin is required and recommended. Interpretation of these data would indicate whether strain in rocks, bounded by the upper detachment and the upper flat of the lower detachment, extends into the foreland, and establish a tie between geometry of foreland duplexes with that of the core of the Triangle Zone.

In summary, this thesis provides a description and structural analysis of a pop-up structure in the southern Alberta Foothills which has not previously been documented. The results from this study are significant as the pop-up structure is regarded as one possible initial stage of the development of an antiformal stack, a major component of the Triangle Zone, thus providing insight into the mechanism of how this frontal structure forms. In addition, a concept that strain extends east of the Triangle Zone, put forward by this thesis, is different from various, previous publications (e.g., Jones, 1982; Charlesworth et al., 1987; McMechan; 1985). This has an implication for future work in the Alberta Foothills in that strain in the foreland should be taken into account when interpreting frontal structures in the Triangle Zone.

## References

- Bally, A. W., Gordy, P. L., and Stewart, G.A., 1966, Structure, seismic data and orogenic evolution of the Southern Canadian Rocky Mountains, *Bull. Can. Petrol. Geol.*: 14, 337-381.
- Banks, C. J., and Warburton, J., 1986, "Passive roof" duplex geometry in the frontal structures in the Kirthar and Sulaiman mountain belts, Pakistan, *J. Struct. Geol.*: 8, 229-237.
- Beach, H.H., 1942, Bearberry, Alberta, G.S.C. Map 670A 1" = 1 mile.
- Beach, H.H., 1943, Moose Mountain and Morley Map area, Alberta, G.S.C. Memoir 236, 74 p.
- Butler, R.W.H., 1982, The terminology of structures in thrust belts: *J. Struct. Geol.*, 4, 239-245.
- Charlesworth, H. A. K., and Gagnon, L. G., 1985, Intercutaneous wedges, the triangle zone and structural thickening of the Mynheer coal seam at Coal Valley in the Rocky Mountain Foothills of central Alberta: *Bull. Can. Petrol. Geol.*: 33, 22-30.
- Charlesworth, H. A. K., Johnston, S.T., and Gagnon, L.G., 1987, Evolution of the triangle zone in the Rocky Mountain Foothills near Coalspur, central Alberta: *Can. J. Earth Sci.*: 24, 1668-1678.
- Cheadle, S.P., 1988, Applications of Physical Modelling and Localized Slant Stacking to a Seismic Study of Subsea Permafrost: Ph.D. Thesis, The University of Calgary, Calgary, Alberta, Canada.
- Chow, T.Y.N., 1989, Physical Seismic Modelling of Pinnacle Reefs: M.Sc. Thesis, The University of Calgary, Calgary, Alberta, Canada.
- Claerbout, J. F., and Doherty, S. M., 1972, Downward continuation of moveout corrected seismograms: *Geophysics*, 37, 741.
- Dahlstrom, C.D.A, 1969, Balanced cross-sections: *Can. J. Earth Sci.*: 6, 743-757.
- Dahlstrom, C.D.A, 1970, Structural geology in the eastern margin of the Canadian Rocky Mountains: *Bull. Amer. Assoc. Petrol. Geol.*, 43, 992-1025.
- Deregowski, S.M., 1986, What is DMO ? : *First Break*, 4, 7-24.
- Dobrin, M.B., and Savit, C.H., 1988, *Introduction to Geophysical Prospecting*: McGraw-Hill International Editions.
- Domenico, S.N., and Danbom, S.H., 1987, shear-wave technology in petroleum exploration-past, current, and future : *in* Danbom, S.H., and Domenico, S.N., Eds., *Shear-wave Exploration, Geophysical Development*, No. 1, Society of Exploration

Geophysicists, 3-18.

- Eaton, D.W.S., and Stewart, R.R., 1989, Aspects of seismic imaging using P-SV converted waves: The CREWES Project Research Report, Volume 1, 68-92.
- Eaton, D.W.S., Slotboom, R.T., Stewart, R.R., and Lawton D.C., 1990, Depth-variant converted-wave stacking: 60th Ann. Internat. Mtg. Soc. Expl. Geophys., Expanded Abstracts, 1107-1110.
- Edwards, D.J., 1992, 3-D Modelling of a reef-fault block structure: The CREWES Project Research Report, Volume 4, 4-1 - 4-33.
- Fagin, S.W., 1991, Seismic Modeling of Geologic Structures: Applications to Exploration Problems: Geophysical Development Series, No. 2, Society of Exploration Geophysicists.
- Fix, J.E., Robertson, J.D., and Pritchett, W.C., 1987, Shear-wave reflections in three west Texas basins with high-velocity surface rocks: *in* Danbom, S.H., and Domenico, S.N., Eds., Shear-wave Exploration, Geophysical Development, No. 1, Society of Exploration Geophysicists, 180-196.
- Fromm, G., Krey, T., and Wiest, B., 1985, Static and dynamic corrections: *in* Dohr, G., ed., Seismic Shear Waves: Handbook of Geophysical Exploration, Volume 15a, Geophysical Press, 191-225.
- Gallup, W.B., 1975, A brief history of the Turner Valley oil and gas field: *in* Foothills Field Trip Guidebook, Can. Soc., Petrol. / Can. Soc. Expl. Geoph., Calgary, 12-17.
- Gardner, G.H.F., Gardner, L.W., and Gregory, A.R., 1974, Formation Velocity and Density - The Diagnostic Basics of Stratigraphic Traps : Geophysics, 39, 770-780.
- Gazdag, J., 1978, Wave equation migration with the phase shift method: Geophysics, 43, 1342-1351.
- Gordy, P.L., Frey, F.R., and Norris, D.K., 1977, Geological guide for the Canadian Society of Petroleum Geologists and the 1977 Waterton-Glacier Park Field Conference: C.S.P.G., Calgary, 93 p.
- Hale, D., 1984, Dip-Moveout by Fourier Transform, Geophysics, 49, 741-757.
- Harrison, M.P., 1989, Three-component seismic data processing: Carrot Creek Alberta: The CREWES Project Research Report, Volume 1, 6-26.
- Hatton, L., Larner, K., and Gibson, B.S., 1985, Migration of seismic data from inhomogeneous media: *in* Gardner, G.H.F., ed., Migration of seismic data, Geophysics reprint series, No. 4, Society of Exploration Geophysicists, 397-413.
- Hatton, L., Worthington, M.H., and Makin, J., 1988, Seismic Data Processing Theory and Practice: Blackwell Scientific Publications.

- Hiebert, S.N., 1992, Deformation Styles Near the Leading Edge of the Fold-and-Thrust Belt, Pincher Creek, Alberta: M.Sc. Thesis, The University of Calgary, Calgary, Alberta, Canada.
- Hrabi, K.D., and Lawton, D.C., 1992, 3-D physical modelling study of a lower Cretaceous channel in central Alberta: The CREWES Project Research Report, Volume 4, 5-1 - 5-23.
- Hume, G.S., and Beach, H.H., 1944, Bragg Creek, Alberta, G.S.C. Map 654A, 1" = 1 mile.
- Hume, G.S., and Hage, C.O., 1941, Wildcat Hills (East Half) Alberta, G.S.C. Map 652A, 1" = 1 mile.
- Inverse Theory and Applications Inc., 1992, Insight/1: Prestack and Poststack Reference Guide.
- Iverson, W.P., Fahmy, B.A., and Smithson, S.B., 1989,  $V_p/V_s$  from mode-converted P-SV reflections: *Geophysics*, 54, 843-852.
- Jones, P. B., 1982, Oil and Gas beneath east-dipping underthrust faults in the Alberta Foothills Canada: in R.B. Powers, ed., *Geological studies of the Cordilleran thrust belt: Denver, Rocky Mountain Assoc. Geol.*, 1, 61-74.
- Jones, P. B., Schink, E.A., and Downey, M.E., 1992, Winchell Coulee, case history of an integrated structural-stratigraphic play using computer-balanced cross-section: *Bull. Can. Petrol. Geol.*, 40, 60-68.
- Jones, P.B., and Workum, R.H., 1978, Geological guide to the Central Foothills and Rocky Mountains of Alberta: *Can. Soc. Petrol. Geol.*, 3-16.
- Judson, D.R., Lin, J., Schultz, P.S., and Sherwood, J.W.C., 1985, Depth Migration after stack: in Gardner, G.H.F., ed., *Migration of seismic data, Geophysics reprint series, No. 4, Society of Exploration Geophysicists*, 347-361.
- Keary, P., and Brooks, M., 1984, *An Introduction to Geophysical Exploration: Blackwell Scientific Publications.*
- Krebs, E., 1989, *Geophysics 557, course notes: The University of Calgary.*
- Landmark Uniseis, 1988, *User Guide.*
- Larner, K.L., Hatton, L., Gibson, B.S., and Hsu, I-Chi, 1985, Depth Migration of imaged time sections, in Gardner, G.H.F., ed., *Migration of seismic data, Geophysics reprint series, No. 4, Society of Exploration Geophysicists*, 380-396.
- Lawton, D.C., and Harrison, M.P., 1991, A two-component seismic survey, Springbank, Alberta: The CREWES Project Research Report, Volume 2, 123-146.

- Lawton, D. C., and Spratt D.A., 1991, Geophysical and geological aspects of the triangle zone, Rocky Mountains Foothills: C.S.E.G. Continuing Education Field Trip, 33 p.
- MacKay, B.R., 1939, Fallen Timber (West Half), West of Fifth Meridian, Alberta, G.S.C. Map 548A, 1" = 1 mile.
- MacKay, P. A., 1991, A geometric, kinematic and dynamic analysis of the structural geology at Turner Valley, Alberta: Ph.D. thesis, University of Calgary, Calgary, Alberta, Canada, 138 p.
- McClellan, B., Johnson, J., Whitney, S., and Bryan, R., 1991, Seismic Depth Conversion and Migration-Techniques and Applications: *in* Fagin, S.W., ed., Seismic Modeling of Geologic Structures Applications to Exploration Problems: Geophysical Development, No. 2, Society of Exploration Geophysicists, 99-110.
- McCormack, M.D., and Tatham, R.H., 1986, Shear-wave exploration seismology, course notes: SEG continuing education series.
- McMechan, M.E., 1985, Low-taper triangle zone geometry: an interpretation for the Rocky Mountain Foothills, Pine Pass - Peace River area, British Columbia: Bull. Can. Petrol. Geol., 33, 31-38.
- McQuillin, R., Bacon, M., and Barclay, W., 1984, An Introduction to Seismic Interpretation: Gulf Publishing Company.
- Morley, C. K., 1986, A classification of thrust fronts: Bull. Amer. Assoc. Petrol. Geol., 70, 12-25.
- Morse, P.F., Purnell, G.W., and Medwedeff, D.A., 1991, Seismic Modeling of Fault-Related Folds: *in* Fagin, S.W., ed., Seismic Modeling of Geologic Structures Applications to Exploration Problems: Geophysical Development, No. 2, Society of Exploration Geophysicists, 127-152.
- Newman, P., 1973, Divergence effects in a layered earth: Geophysics, 38, 481-488.
- Notfors, C.D., and Godfrey, R.J., 1987, Dip moveout in the frequency-wavenumber domain: Geophysics, 52, 1718-1721.
- Ollerenshaw, N. C., 1967, Geology Wildcat Hills (West Half) West of Fifth Meridian, Alberta, G.S.C. Map 1351A, 1:50000.
- \_\_\_\_\_, 1974, Geology, Fallen Timber Creek, Alberta. G.S.C. Map 1387A, 1:50000.
- \_\_\_\_\_, 1975, Cretaceous Exposures along the Sheep and Elbow Rivers, Field Trip: Can. Soc. Petrol. Geol.
- \_\_\_\_\_, 1978, Geology of Calgary, west of Fifth Meridian, Alberta-British Columbia, G.S.C. Map 1457A, 1:250000.

- Price, R.A., 1986, The southeastern Canadian Cordillera: thrust faulting, tectonic wedging, and delamination of the lithosphere: *Jour. Struct. Geol.*, 8, 239-254.
- Sanderson, D.A., and Spratt, D.A., 1992, Triangle zone and displacement transfer structures in the Eastern Front Ranges, Southern Canadian Rocky Mountains: *Bull. Amer. Assoc. Petrol. Geol.*, 76, 828-839.
- Schafer, A.W., 1993, Binning, Static Correction, and Interpretation of P-SV Surface-Seismic Data: M.Sc. Thesis, The University of Calgary, Calgary, Alberta, Canada.
- Skuce, A. G., Goody, N. P., and Maloney, J., 1992, Passive-roof duplexes under the Rocky Mountain Foreland Basin, Alberta: *Bull. Amer. Assoc. Petrol. Geol.*, 76, 67-80.
- Slotboom, R.T., 1992, Geophysical Investigation of the Triangle Zone structure in Jumpingpound-Wildcat Area, Southern Alberta Foothills: M.Sc. Thesis, The University of Calgary, Calgary, Alberta, Canada.
- Soule, G.S., 1993, The Triangle Zone and Foothills Structures in the Grease Creek Syncline Area, Alberta: M.Sc. Thesis, The University of Calgary, Calgary, Alberta, Canada.
- Stolt, R.H., 1978, Migration by Fourier transform: *Geophysics*, 43, 23-48.
- Stott, D. F., 1963, The Cretaceous Alberta Group and equivalent rocks, Rocky Mountain Foothills, Alberta: *Geol. Surv. Canada Memoir*, 317, 306 p.
- Suyama, K., Imai, T., Ohtomo, H., Ohta, K., and Takahashi, T., 1987, Delineation of Structures in Alluvium and Diluvium using SH-wave reflection and VSP methods: *in* Danbom, S.H., and Domenico, S.N., Eds., *Shear-wave Exploration, Geophysical Development*, No. 1, Society of Exploration Geophysicists, 165-179.
- Tatham, R.H., 1982,  $V_p/V_s$  and lithology: *Geophysics*, 47, 336-344.
- Tatham, R.H., and Stoffa, P.L., 1976,  $V_p/V_s$  - A potential hydrocarbon indicator : *Geophysics*, 41, 837-849.
- Teal, P. R., 1983, The triangle zone Cabin Creek, Alberta, *in* A. W. Bally, ed., *Seismic expressions of structural styles: AAPG Studies in Geology* 15, 3, 3.4.1-48-3.4.1-53.
- Terada, T., and Tsuboi, C., 1927, Experimental studies on elastic waves (Parts I and II): *Tokoyo Imperial University, Bull. Earthquake. Res. Inst.*, 3, 55-65, 4, 9-20.
- Vann, I. R., Graham, R. H., and Hayward, A. B., 1986, The structure of mountain fronts: *J. Struct. Geol.*, 8, 215-227.
- Workum, R. H., 1978, Stratigraphy of the Central Foothills, *in* Jones, P. B., and Workum, R. H., eds., *Geological guide to the central Foothills and eastern Rockies, Field Trip Guide Book*, CSPG, 61 p.

Yilmaz, O., 1987, Seismic data processing, Series: Investigations in geophysics, Volume 2, Society of Exploration Geophysicists, Tulsa, Oklahoma, 526 p.

Zimmerman, L.J., 1991, Modeling the Seismic Response of Geologic Structures with Physical Models: *in* Fagin, S.W., ed., Seismic Modeling of Geologic Structures: Applications to Exploration Problems: Geophysical Development, No. 2, Society of Exploration Geophysicists, 189-195.